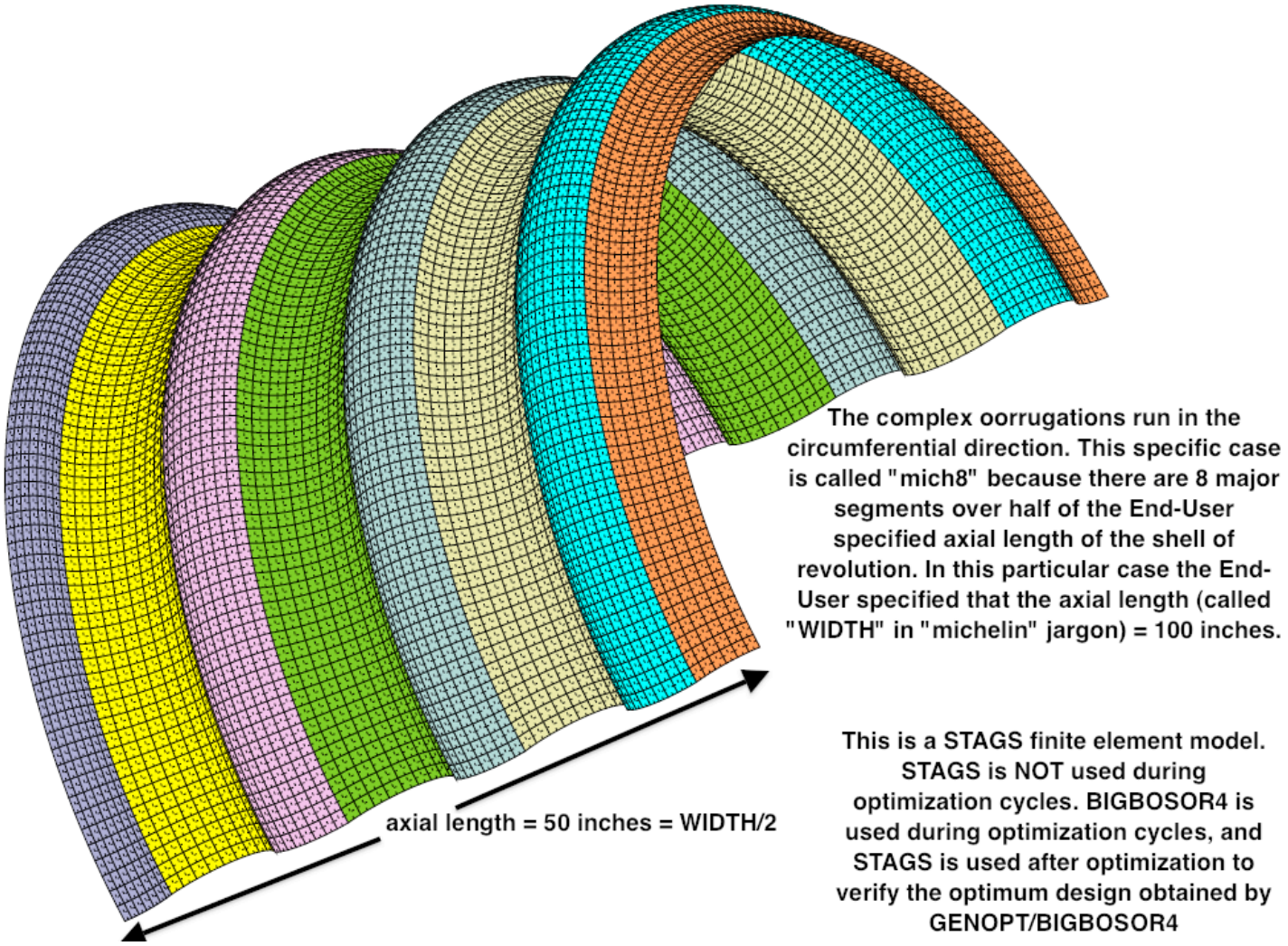

Fig. 1 The subject of this paper is **circumferentially complexly corrugated shells of revolution subject to uniform external normal pressure**. In the text the loading is called "uniform external **lateral** normal pressure" because this pressure does NOT give rise to any applied axially compressive stress resultant equal to pr/2. The GENOPT/BIGBOSOR4 computer program is used to obtain minimum-weight designs of shells like the one shown here. Then, after the optimized design has been obtained by GENOPT/BIGBOSOR4, the STAGS general-purpose finite element computer program is used to validate the predictions of local buckling, general buckling, and maximum effective stress predicted by BIGBOSOR4. (NOTE: "Smoothing" segments are not included in this particular STAGS so-called "half-module" model.)

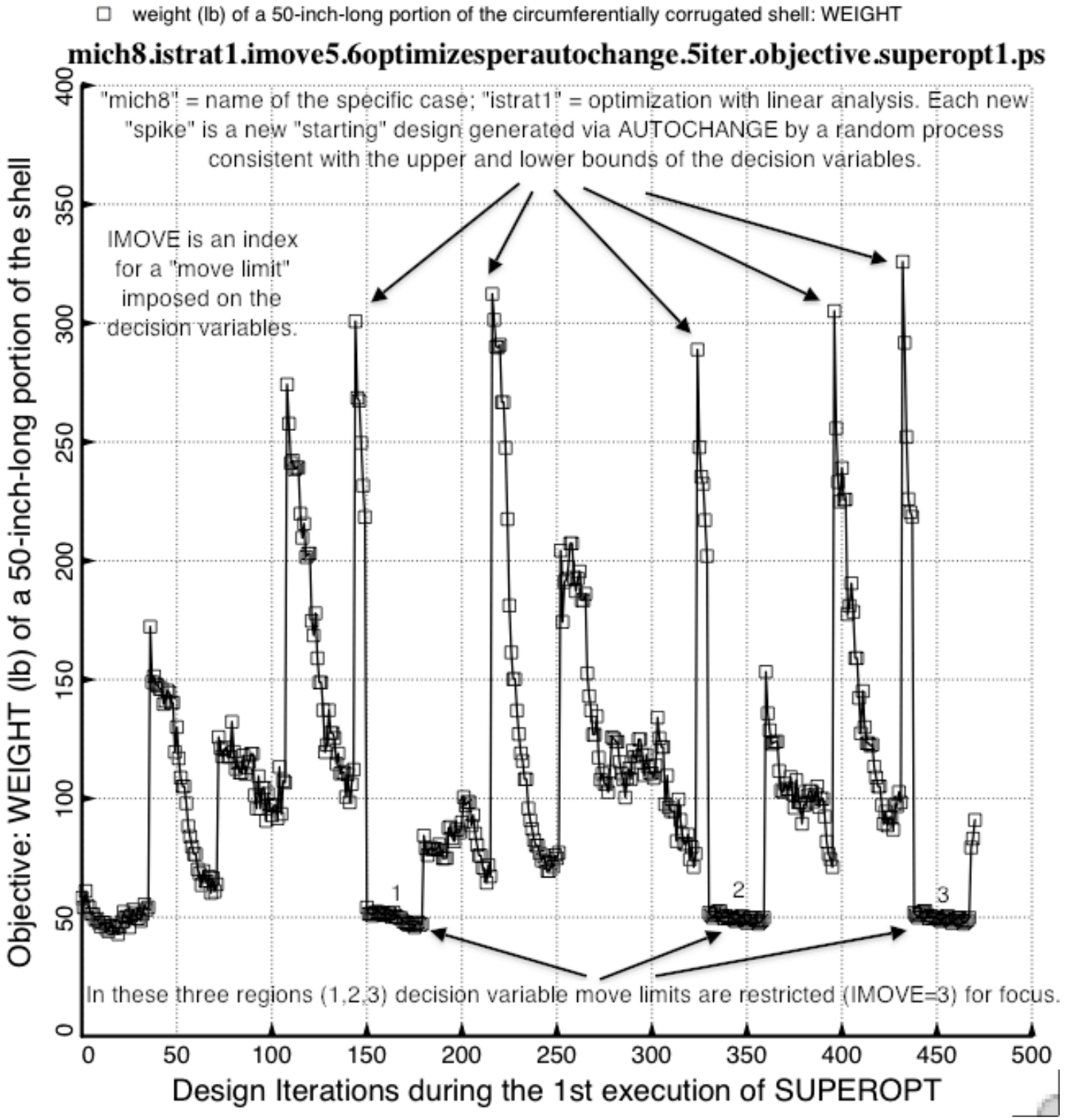

Fig. 2a. **Linear optimization of the specific case called "mich8" via the GENOPT processor called "SUPEROPT"**. It is difficult to find a "global" minimum-weight design because some of the "behavioral" constraint gradients, especially those associated with general buckling, are extremely high. (See Fig. 17.)

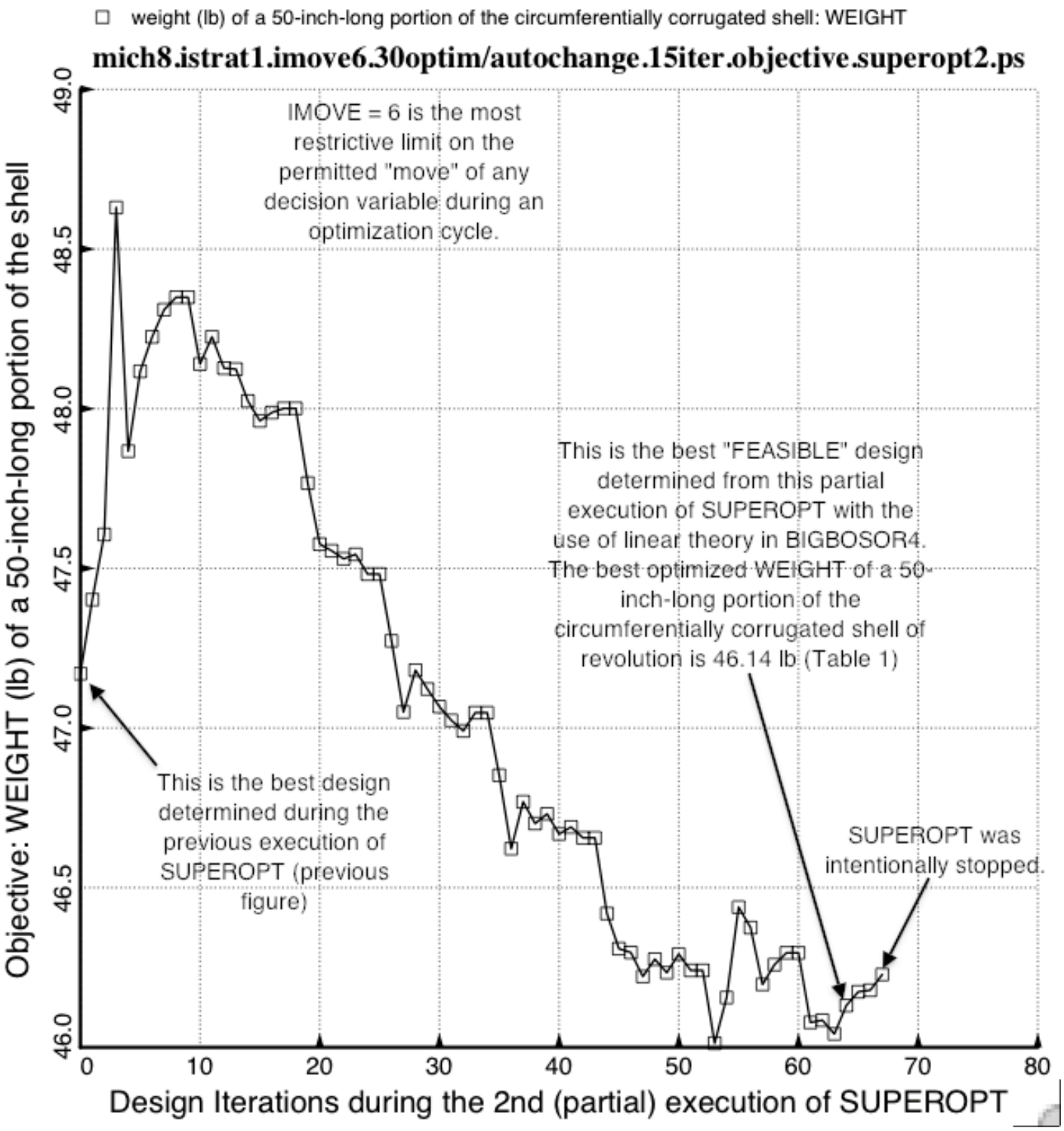

Fig. 2b **Continuing linear optimization of the specific case called "mich8"**. In the presence of very high behavioral constraint gradients, in order to "home in" on a minimum-weight design in the neighborhood of that determined from the previous execution of SUPEROPT, the decision variables here are permitted to change by only 0.5 per cent during each design iteration. (Notice the fine scale on the vertical axis.)

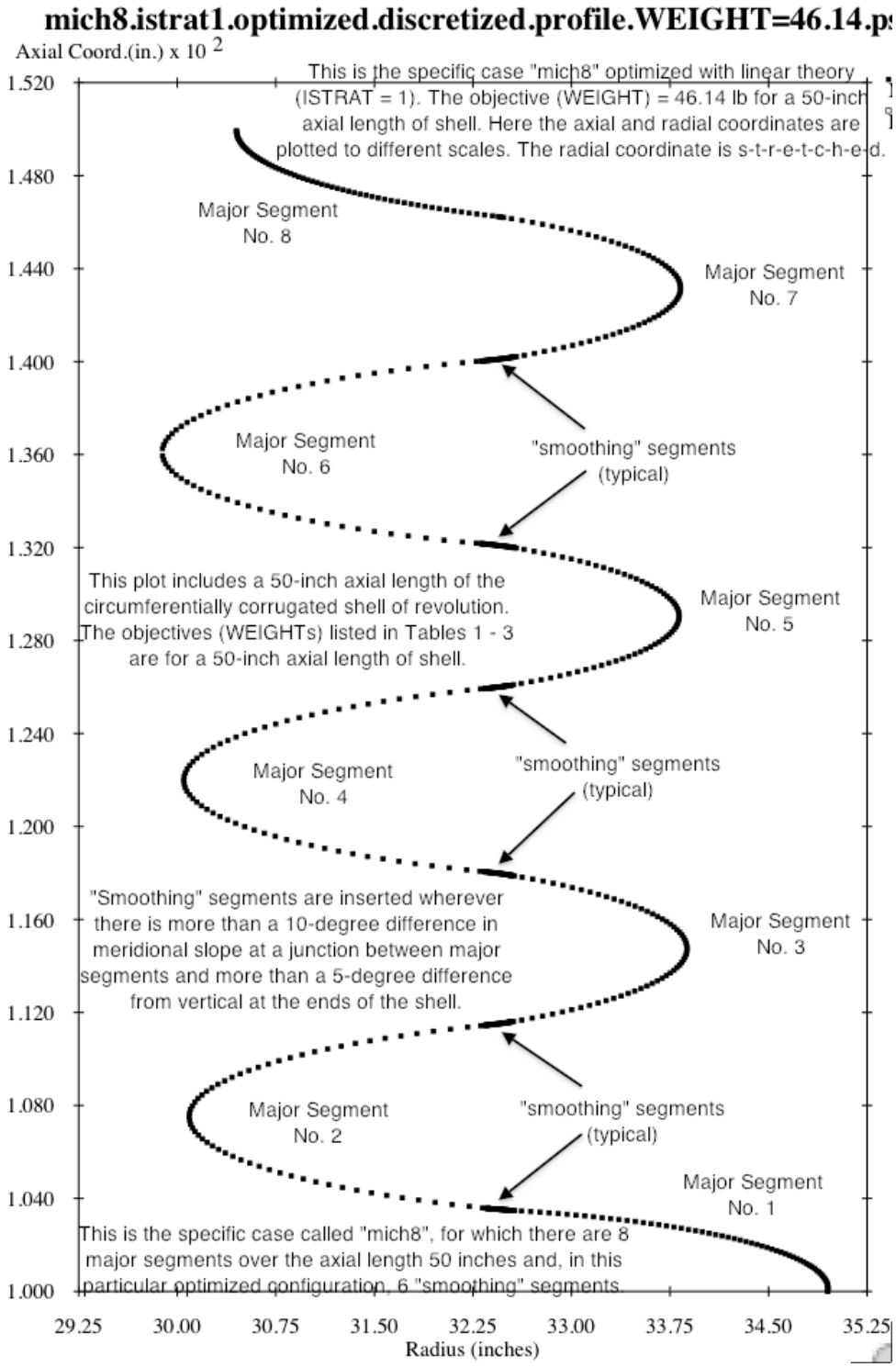

Fig. 2c **The profile of the linearly optimized specific case called "mich8"**, showing the discretization used in the BIGBOSOR4 model and showing where additional "smoothing" segments have automatically been inserted by GENOPT/BIGBOSOR4 in order to eliminate "corners" (discontinuities of meridional slope) between major segments. In this figure the radial coordinate has been s-t-r-e-t-c-h-e-d better to show the discretization.

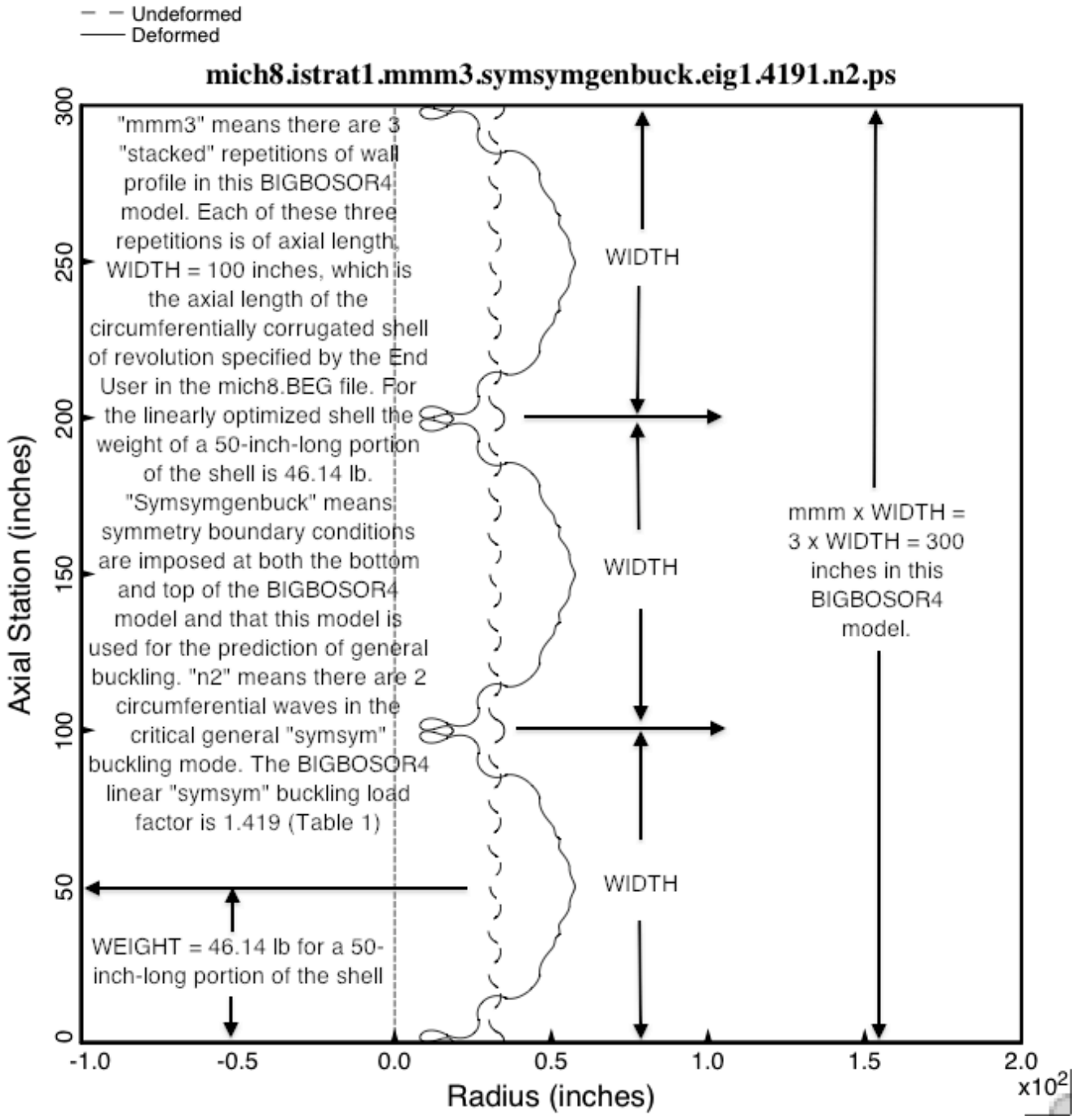

Fig. 3a **Symmetric linear general buckling ("symsymgenbuck") from BIGBOSOR4 of the linearly optimized specific case called "mich8"**. The length of circumferentially corrugated shell displayed here (300 inches) is six times that included in the previous figure. This 300-inch-long shell is one of the three BIGBOSOR4 models ("symsymgenbuck", "symantigenbuck" and "antiantigenbuck") used during optimization cycles for the prediction of general buckling. The discretized model of axial length, WIDTH/2 = 50 inches, shown in the previous figure, is first reflected to produce a portion of shell of axial length, WIDTH = 100 inches, then repeated three times to generated the BIGBOSOR4 model used for general buckling.

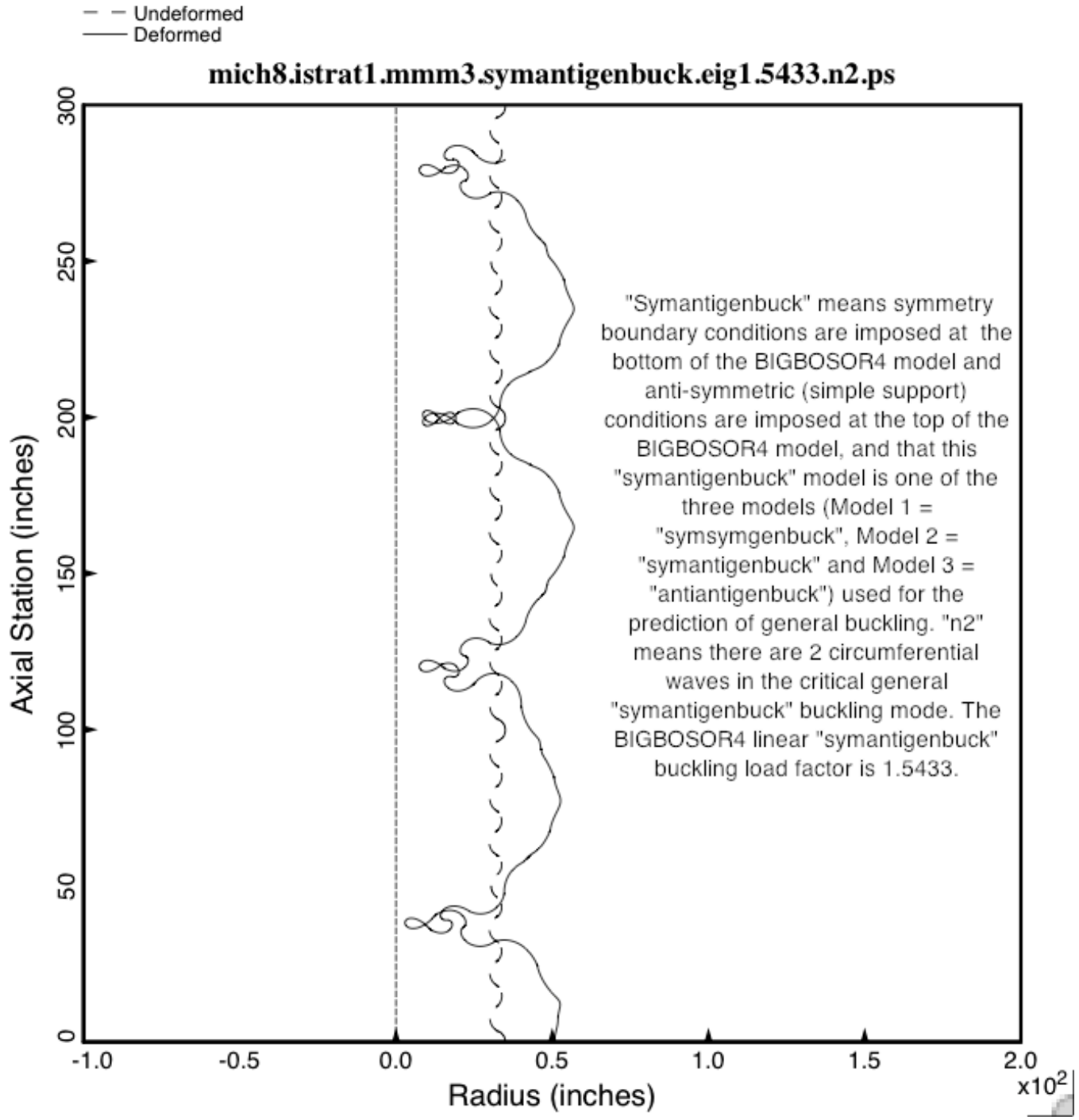

Fig. 3b **"Symantigenbuck" from BIGBOSOR4 of the linearly optimized specific case called "mich8"**. The buckling load factor, 1.5433, is not listed in Table 1 because the general "antisymmetric" buckling load factor called "BUKASY" listed in Table 1 is the lowest buckling load factor computed from the two BIGBOSOR4 general buckling models, "symantigenbuck" and "antiantigenbuck", and the "antiantigenbuck" model shown in the next figure happens to yield the more critical "antisymmetric" general buckling load factor in this particular case.

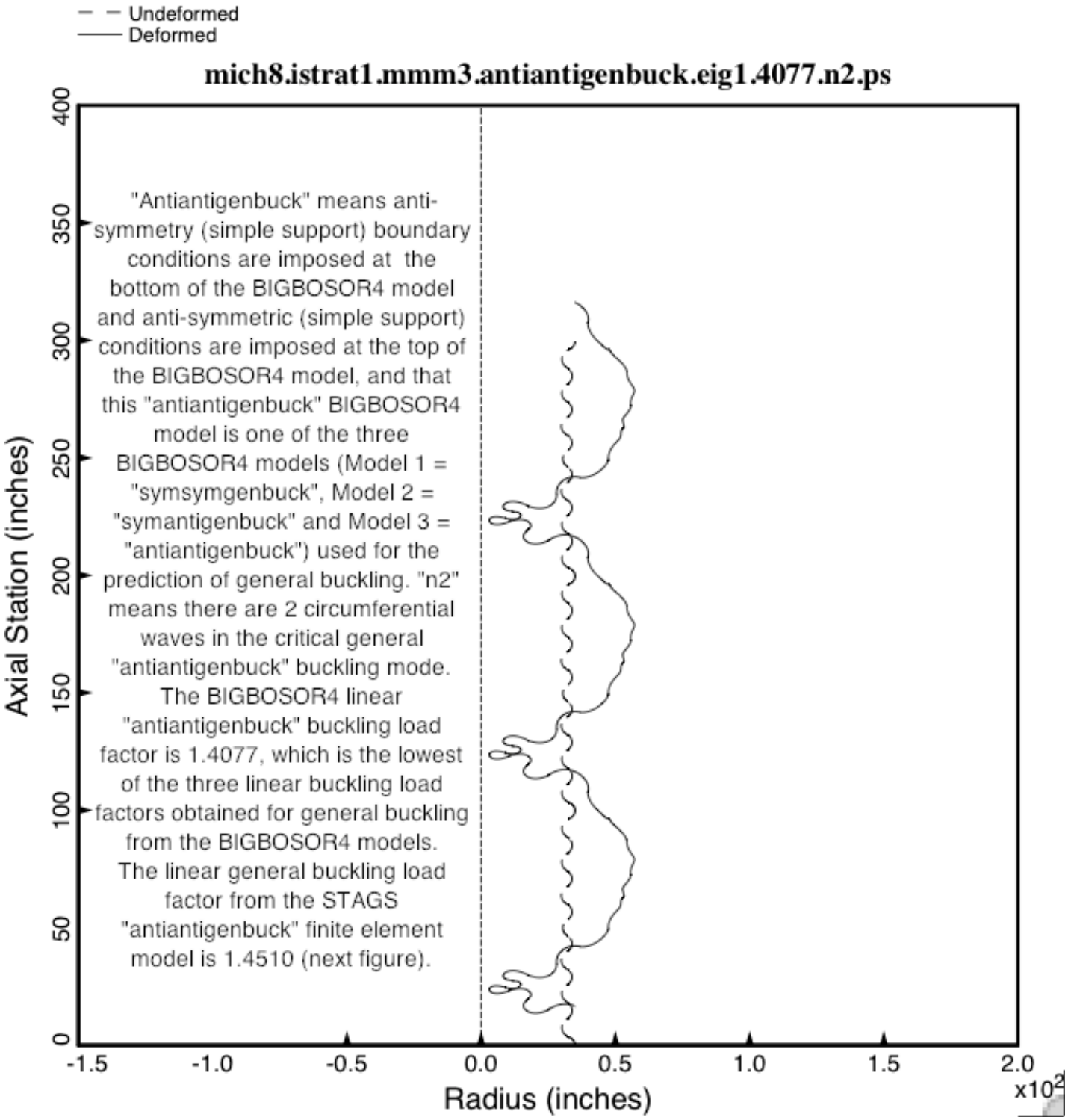

Fig. 3c **"Antiantigenbuck" from BIGBOSOR4 of the linearly optimized specific case called "mich8"**. The "antiantigenbuck" linear general buckling load factor, 1.4077, is the load factor listed for "BUKASY" in Table 1 because it is the more critical (lowest) load factor computed from the two BIGBOSOR4 general buckling models, "symantigenbuck" (previous figure) and "antiantigenbuck" (this figure).

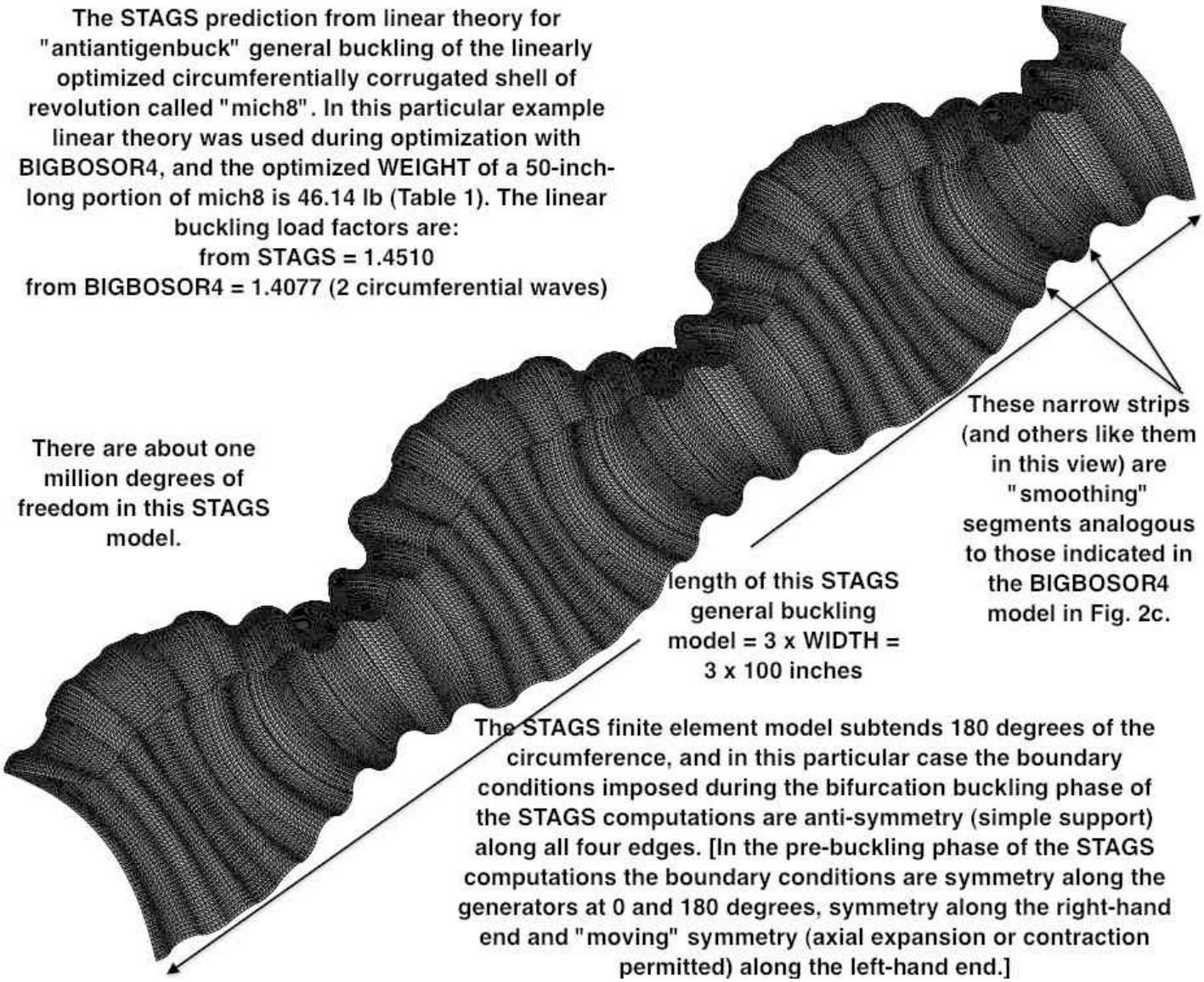

Fig. 4 **The prediction from STAGS of linear general buckling for the linearly optimized specific case called "mich8"**. Two STAGS models were analyzed: "symantigenbuck" and "antiantigenbuck". In this particular case the "antiantigenbuck" STAGS model yields the more critical (lowest) general buckling load factor. The corresponding "antiantigenbuck" general buckling mode is shown here.

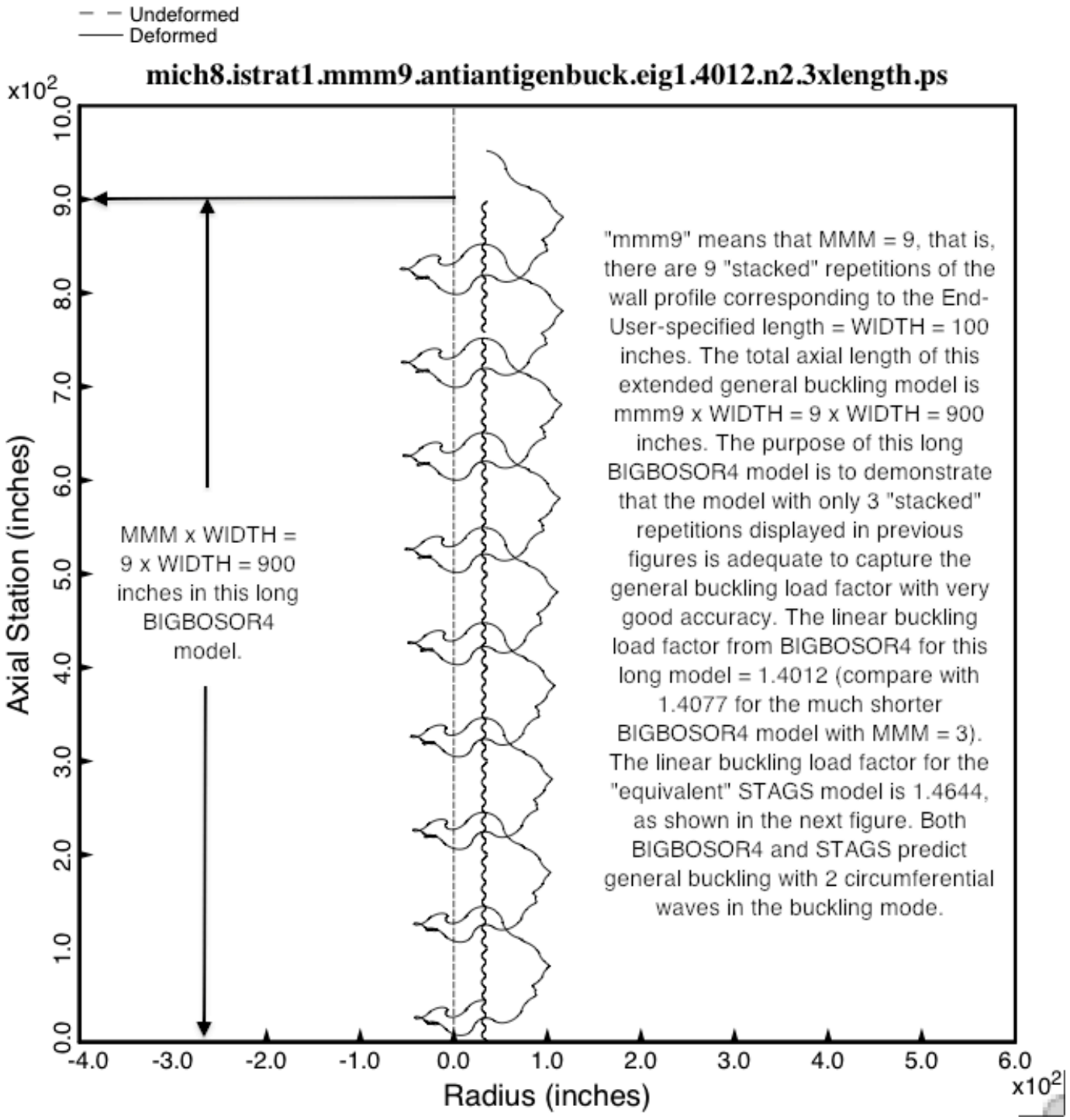

Fig. 5 **"Antiantigenbuck" from BIGBOSOR4 of the linearly optimized specific case called "mich8"**. The purpose of this very long general buckling BIGBOSOR4 model is to prove that the much shorter BIGBOSOR4 model displayed in Fig. 3c is long enough to predict with reasonable accuracy general buckling of the linearly optimized "mich8" configuration, and that therefore it is not necessary to use such a long BIGBOSOR4 model for optimization.

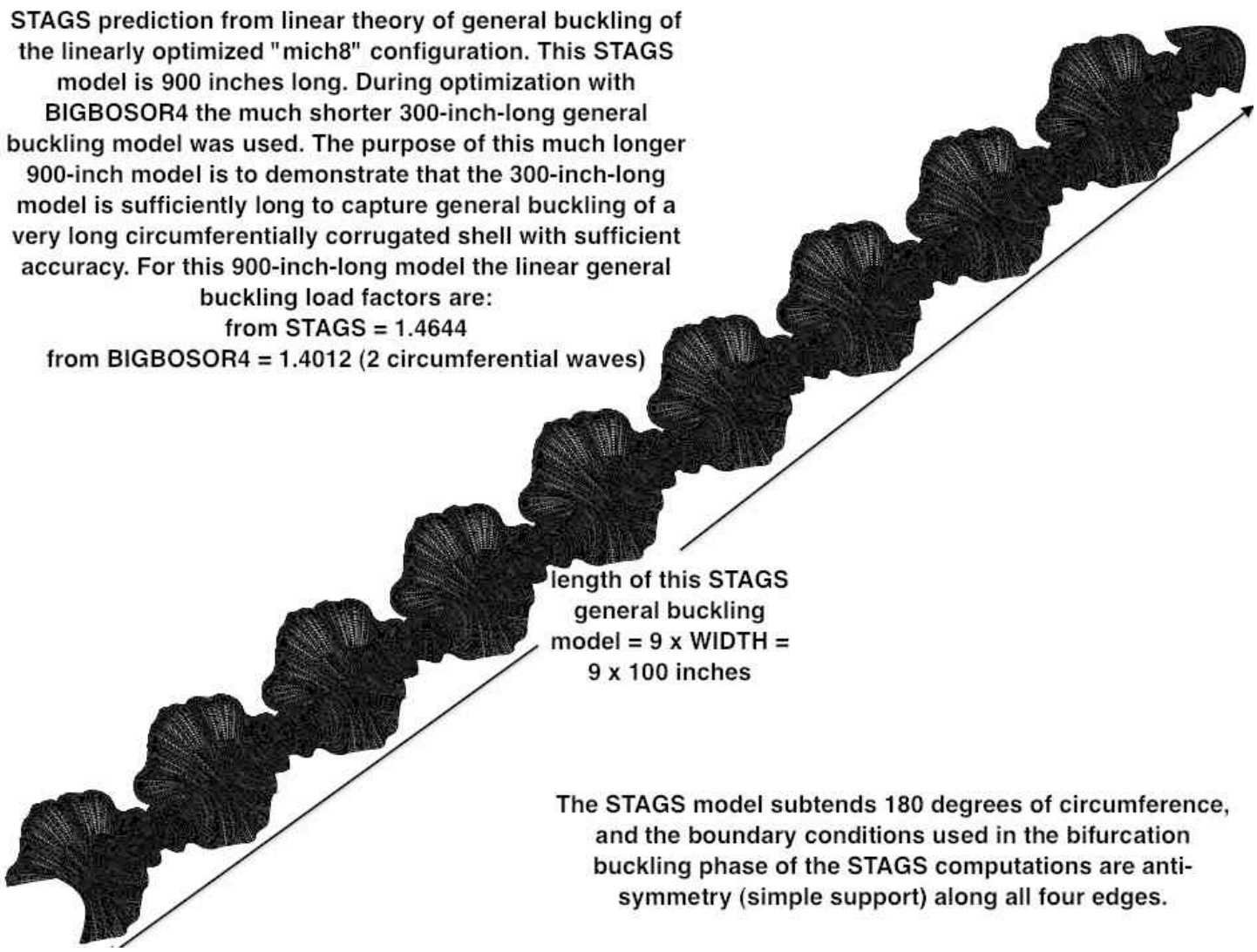

Fig. 6 **The prediction from STAGS of linear general buckling for the linearly optimized specific case called "mich8"**. Compare the general buckling mode displayed here with that predicted by BIGBOSOR4 and shown in the previous figure.

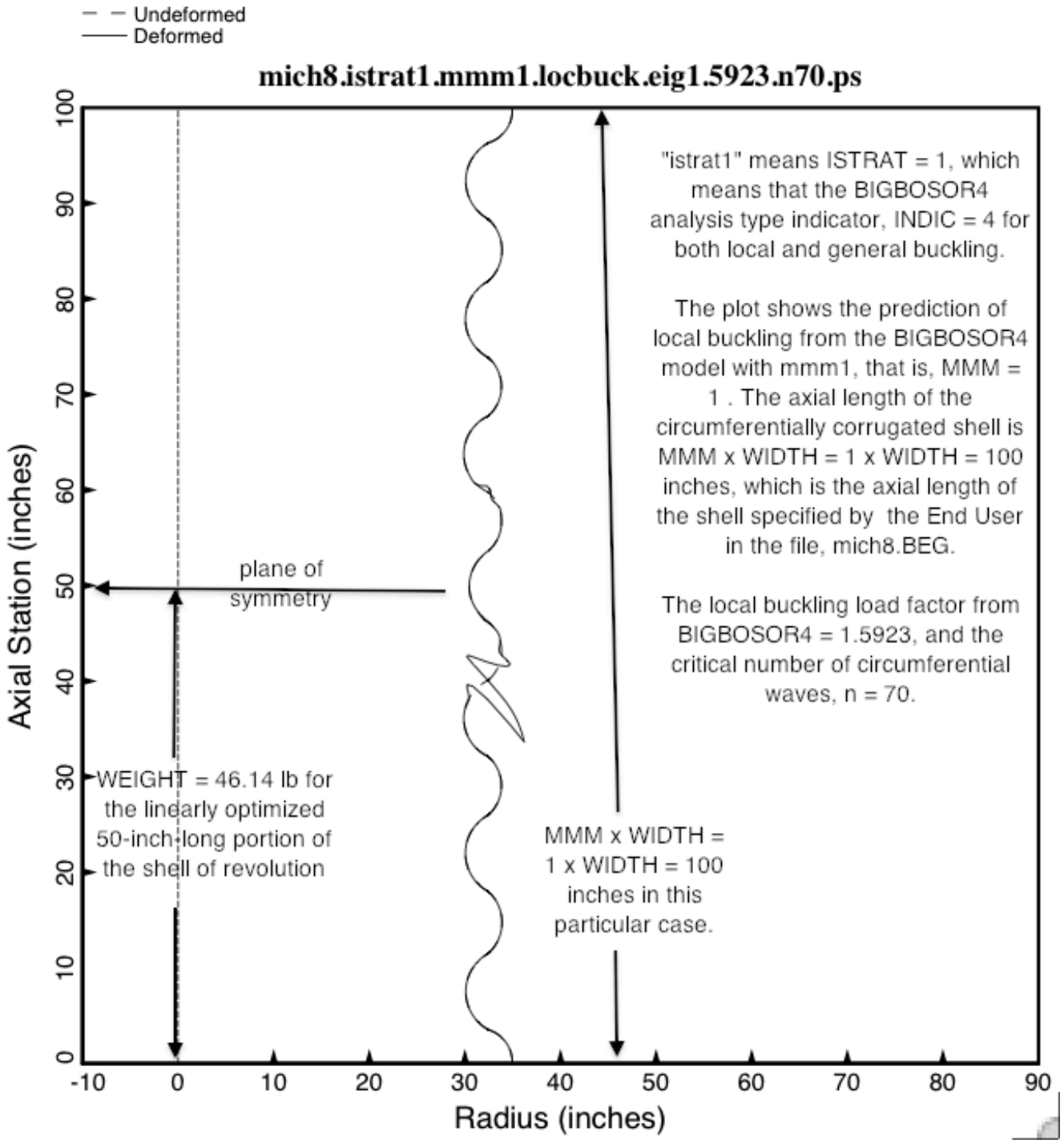

Fig. 7a **Linear local buckling from BIGBOSOR4 of the linearly optimized specific case called "mich8"**. The BIGBOSOR4 model used for **linear** local buckling is that of axial length = 50 inches displayed in Fig. 2c plus a portion of equal axial length and discretization reflected about the plane of symmetry located at the top of the model shown in Fig. 2c. In this particular case there happen to be two critical linear local buckling modes, the one shown here with 70 circumferential waves and the one shown in the next figure with 140 circumferential waves.

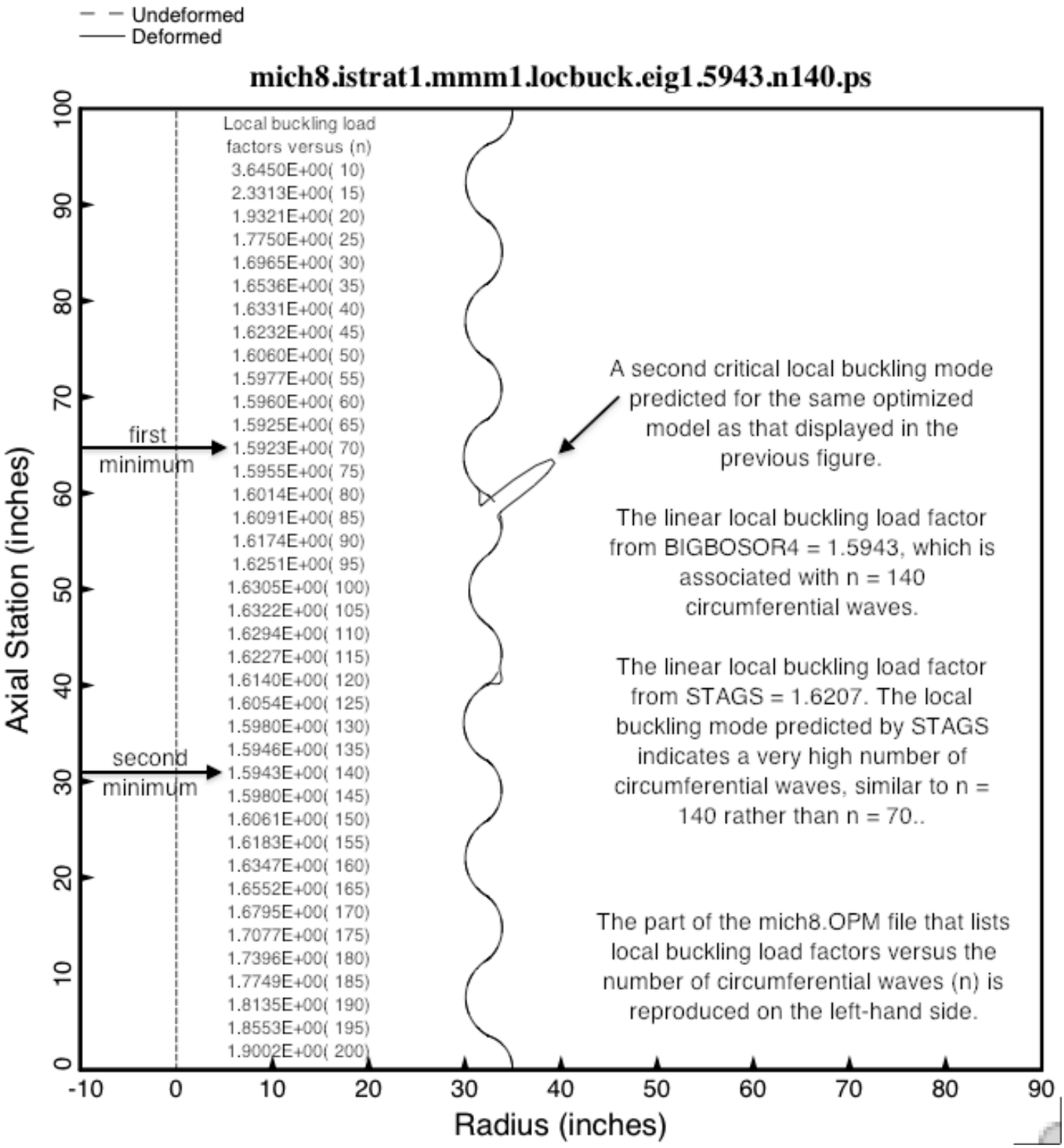

Fig. 7b **A second critical linear local buckling mode and load factor from BIGBOSOR4 of the linearly optimized specific case called "mich8".** Compare with the prediction of linear local buckling from STAGS shown in the next figure.

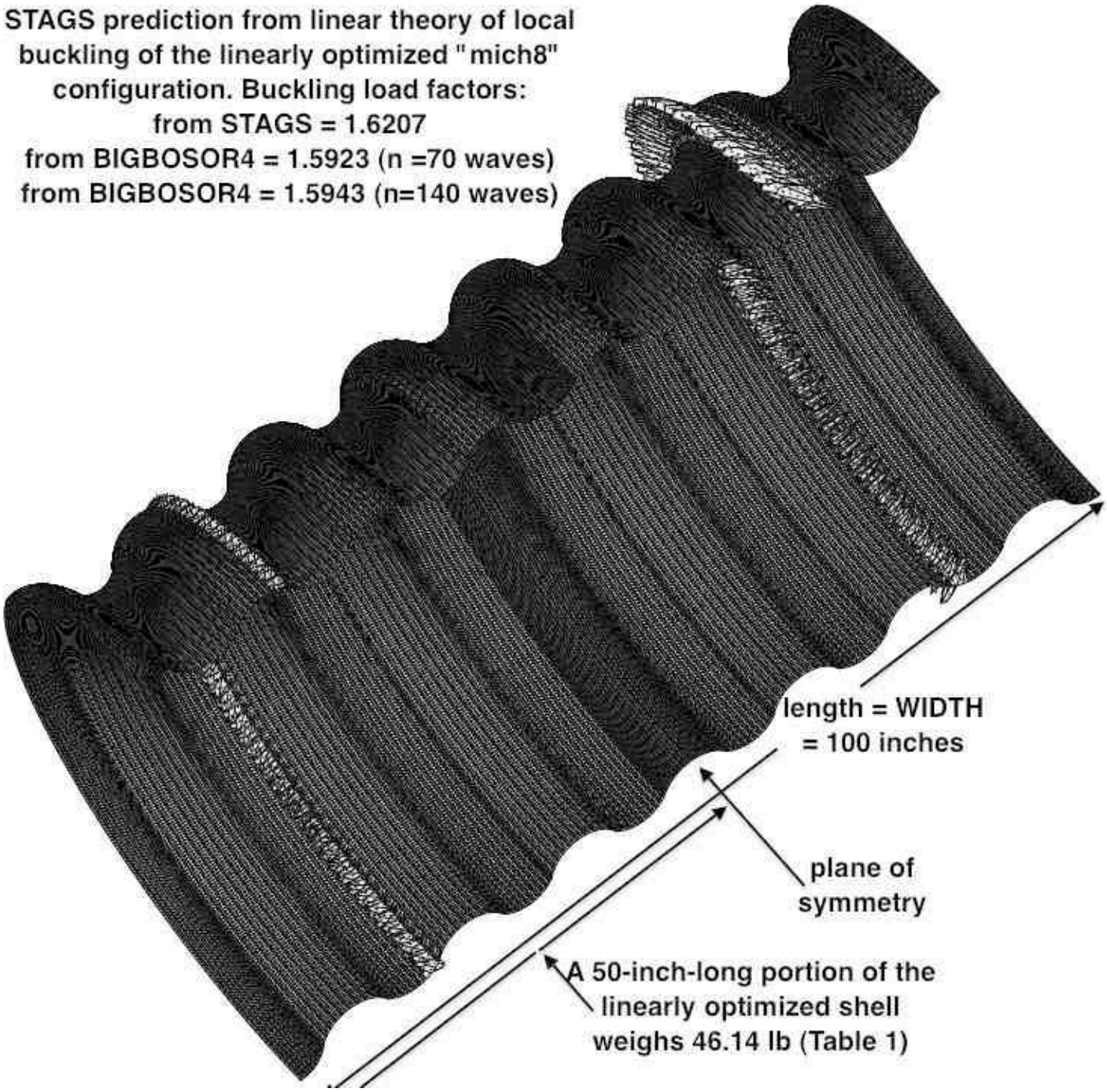

Fig. 8 **STAGS model of linear local buckling of the linearly optimized specific case called "mich8"**. This STAGS model has 1.6 million degrees of freedom because many, many 480 finite elements are required in the circumferential direction in order accurately to capture local buckling modes with many, many circumferential waves over 180 degrees of circumference.

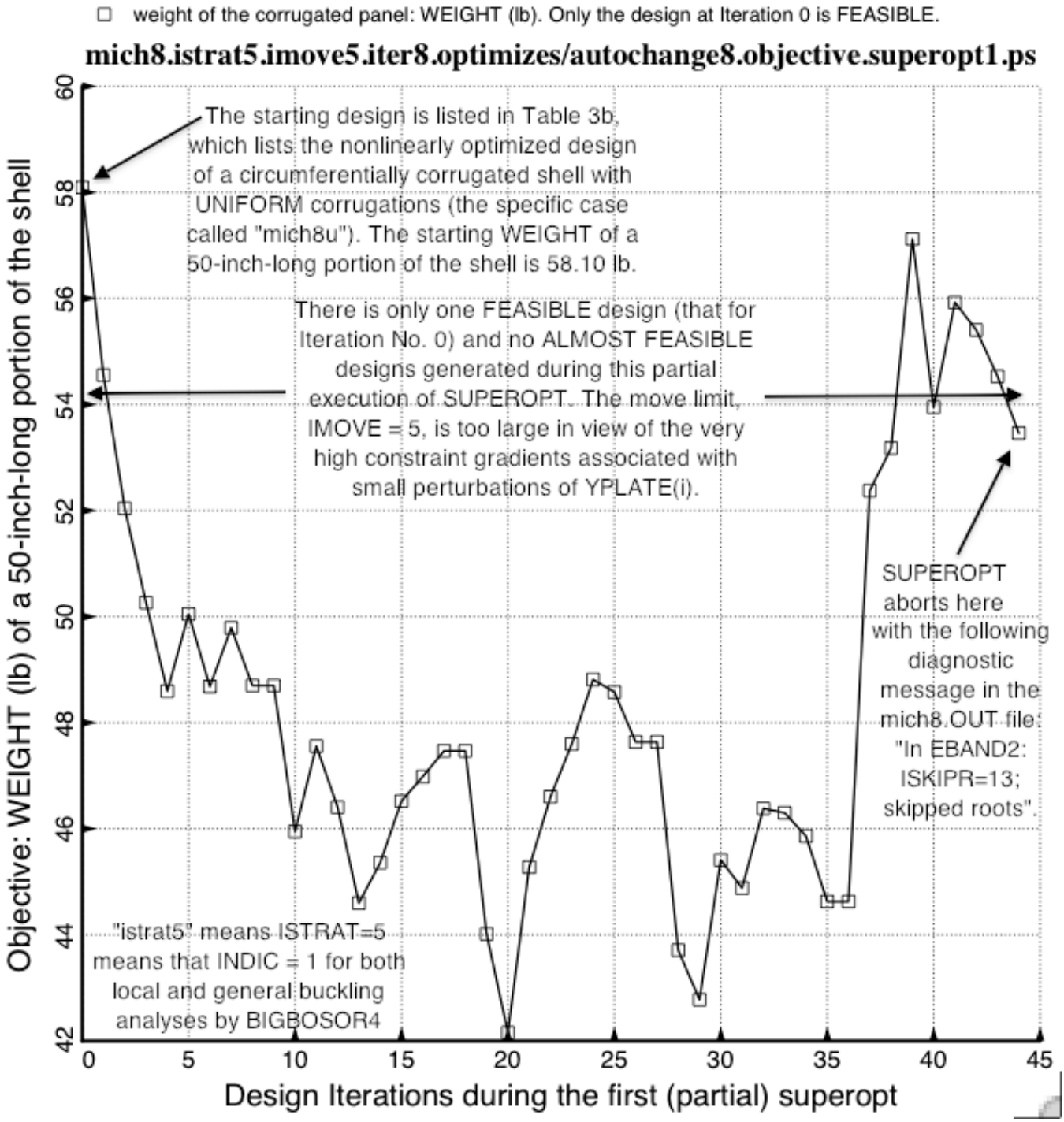

Fig. 9a **Nonlinear optimization of the specific case called "mich8" with use of the mildest nonlinear strategy, that specified by ISTRAT = 5**. The GENOPT processor, SUPEROPT, "bombs" during Iteration No. 45 because of "skipped roots". This figure shows an example in which the move limit imposed on the decision variables during each optimization cycle is too liberal in view of the presence of very high behavioral constraint gradients, especially those associated with general buckling. (See Figs. 17 and 18.) (IMOVE=5 means that the decision variables may change by no more than 5 per cent during a single optimization cycle.)

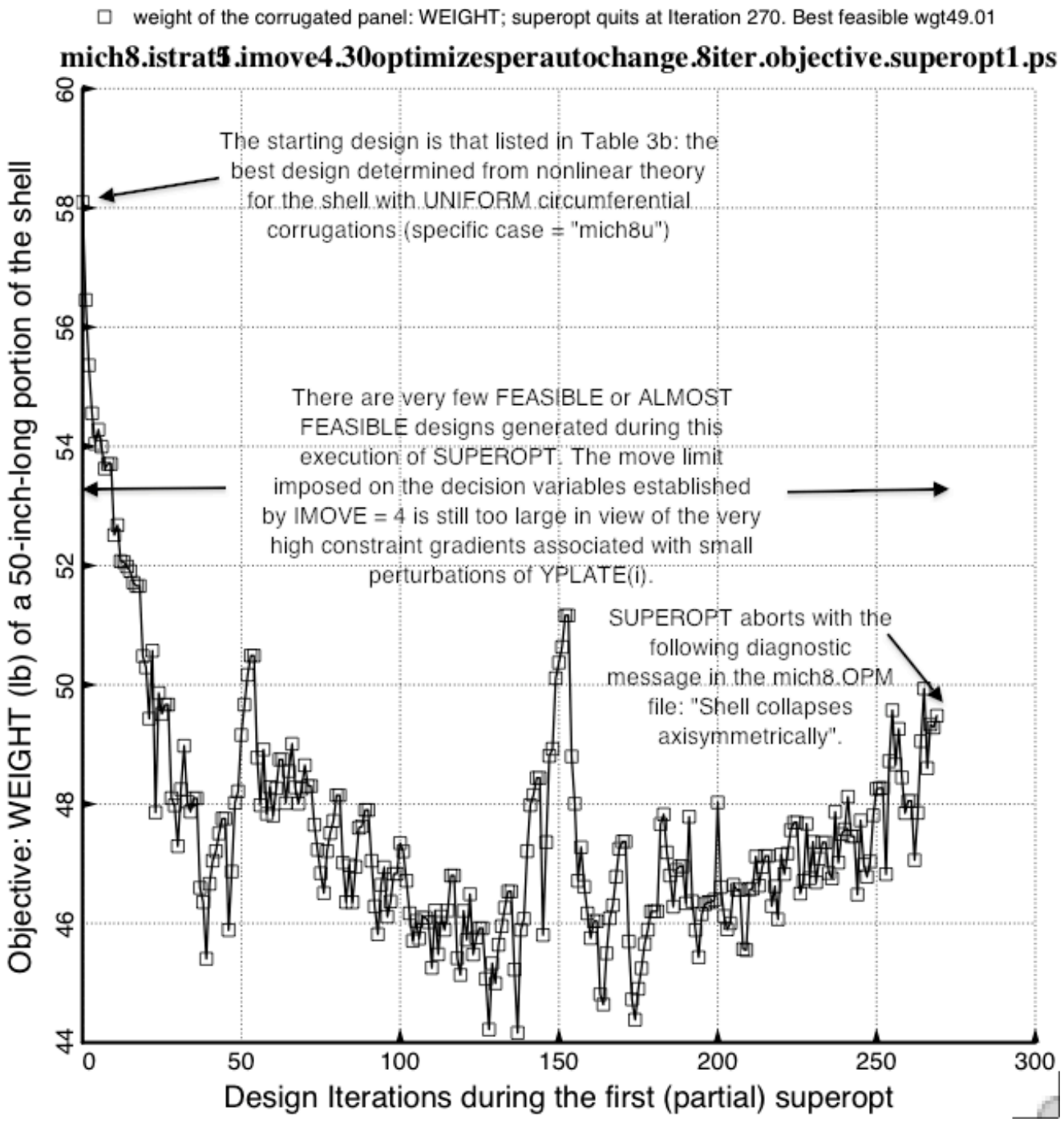

Fig. 9b **Nonlinear optimization of the specific case called "mich8"** with use of the mildest nonlinear strategy, that specified by ISTRAT = 5, and with use of a more restrictive move limit (IMOVE=4) on the decision variables. (IMOVE = 4 means that decision variables may change by no more than 2 per cent per optimization cycle.) The more restrictive move limit imposed by IMOVE = 4 is still too liberal. Again, SUPEROPT "bombs", this time at about Iteration No. 270 and with a different diagnostic message: ("Shell collapses axisymmetrically") than that given in the previous figure.

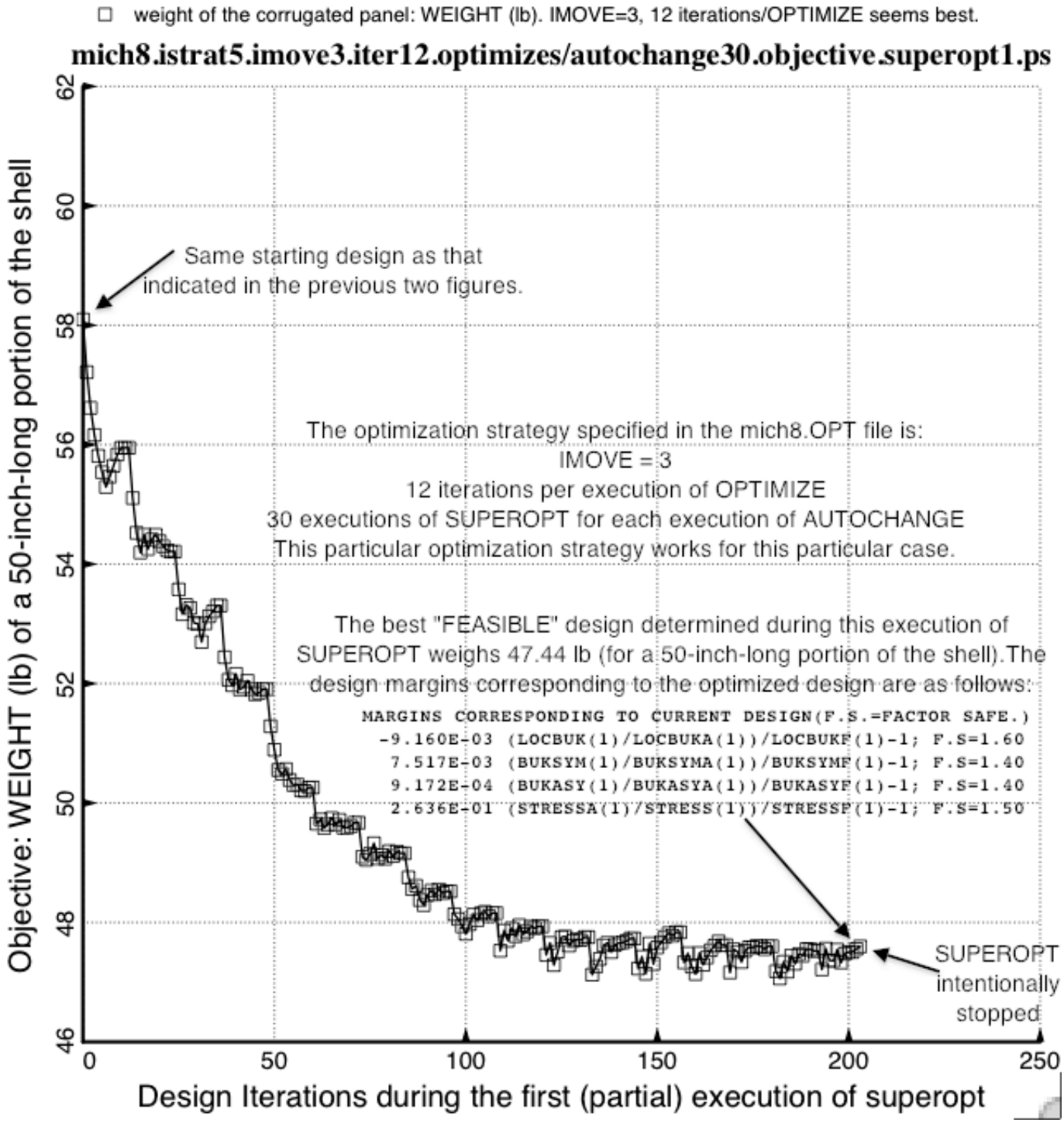

Fig. 9c **Nonlinear optimization of the specific case called "mich8" with use of the mildest nonlinear strategy, that specified by ISTRAT = 5 and with a yet more restrictive move limit**. (IMOVE = 3 means that decision variables may change by no more than one per cent during each optimization cycle.) In this computer run the GENOPT processor, SUPEROPT, did not "bomb" but was terminated intentionally to avoid another 12 hours of waiting for SUPEROPT to finish naturally.

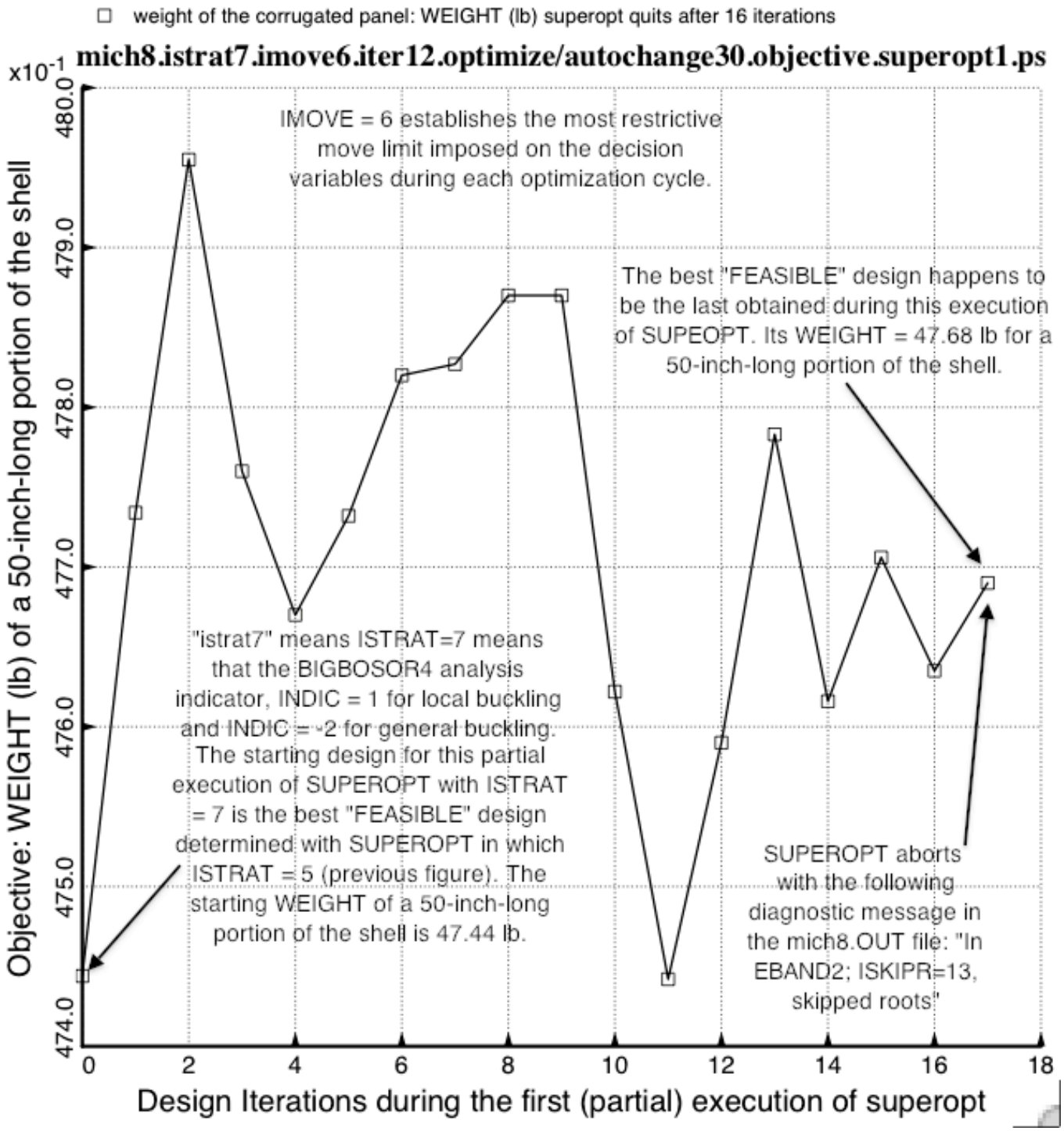

Fig. 9d **Nonlinear optimization of the specific case called "mich8" with use of a less mild nonlinear strategy, that specified by ISTRAT = 7 and with a yet more restrictive move limit**. (IMOVE = 6 means that decision variables may change by no more than 0.5 per cent during each optimization cycle.) The SUPEROPT execution "bombed" during computations for Iteration No. 18 because of "skipped roots". A FEASIBLE design was found. However, that FEASIBLE design was deemed unacceptable for the reason given in the next figure.

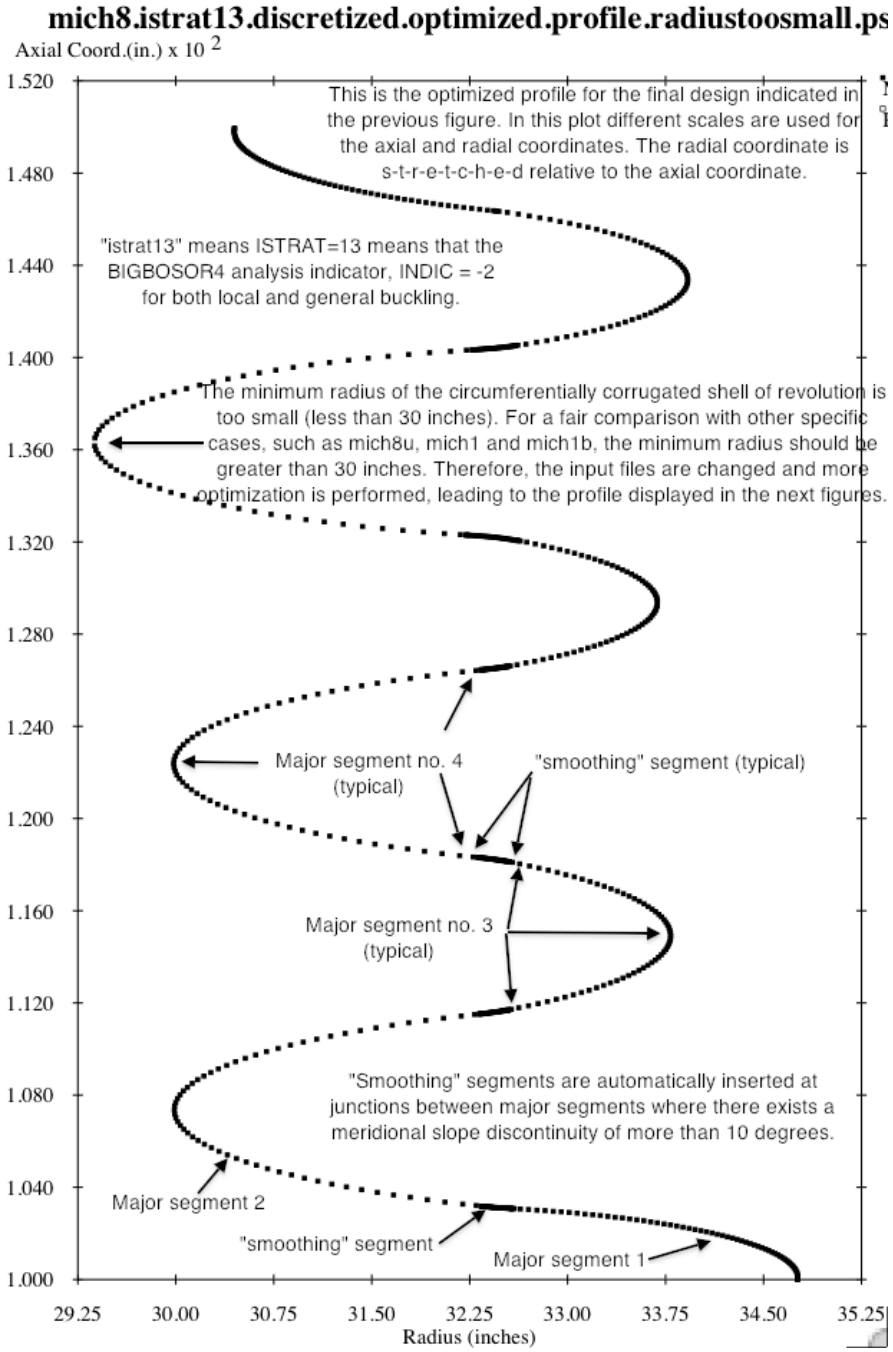

Fig. 9e **Profile of the "final" nonlinearly optimized design of the specific case called "mich8"** obtained by the multi-step process illustrated in the previous several figures. This nonlinearly optimized design was deemed unacceptable because the minimum radius from the axis of revolution to the shell wall reference surface is less than 30 inches. This minimum radius cannot be controlled directly by appropriate specification of a lower bound of YPLATE(i), i=1, 2, …, NSEG because YPLATE(i) are the radii from the axis of revolution to the shell wall reference surface at the junctions of major segments, not the minimum radii between those junctions. The shell had to be re-optimized with the use of a higher lower bound imposed on YPLATE(i), i=1, 2, …, NSEG than that previously specified in the GENOPT processor called "DECIDE".

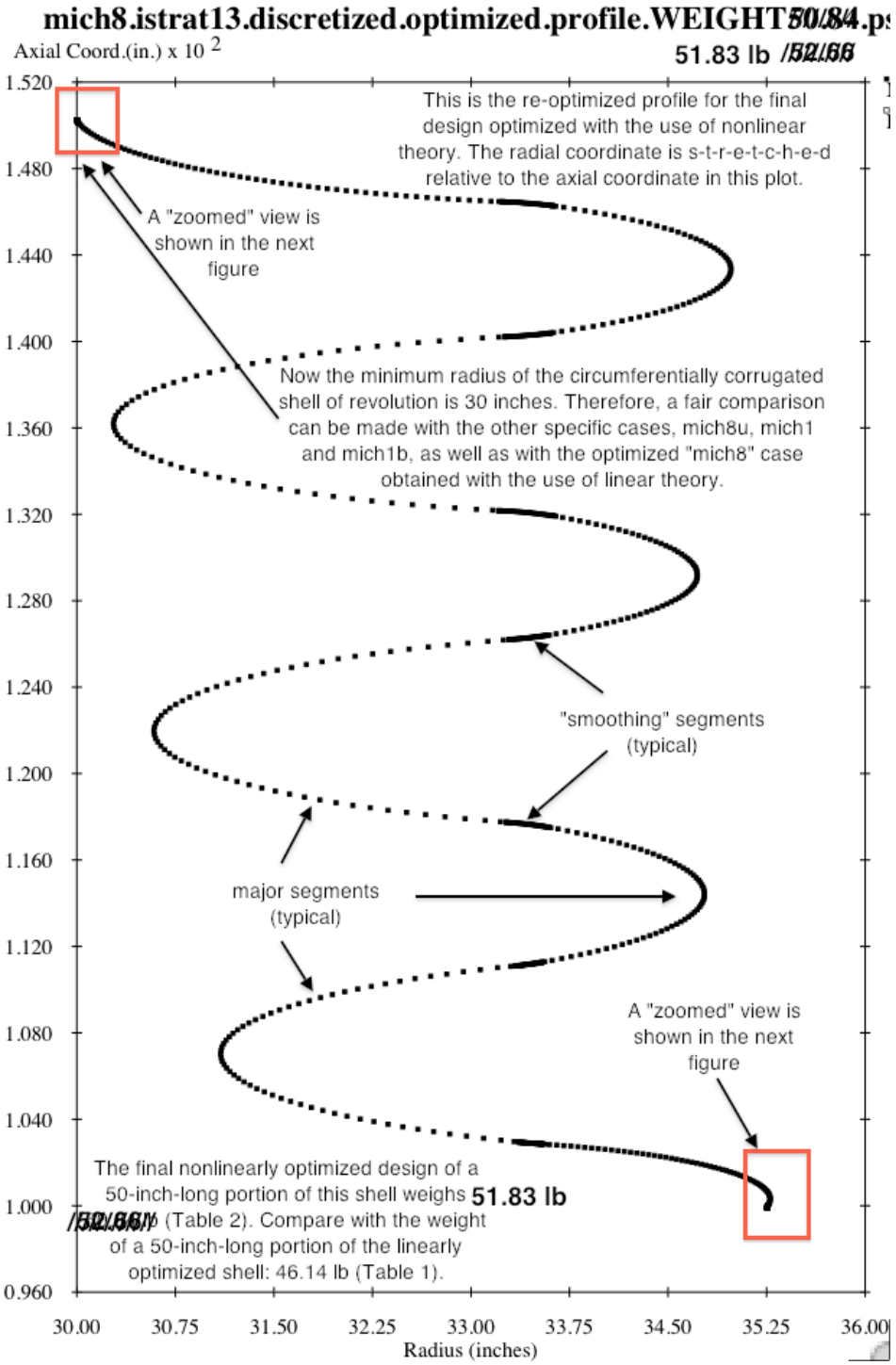

Fig. 9f **Profile of the final nonlinearly optimized design of the specific case called "mich8".** Because of frequent "bombings" of SUPEROPT with use of the most rigorous nonlinear strategy specified by ISTRAT = 13, this final nonlinearly optimized design was developed in the final stages of optimization by increasing the thickness, THICK(1), step-wise until the most critical design margin (that for local buckling, LOCBUK, listed in Table 2) qualified the optimum design as being "FEASIBLE". This is probably not a "global" optimum.

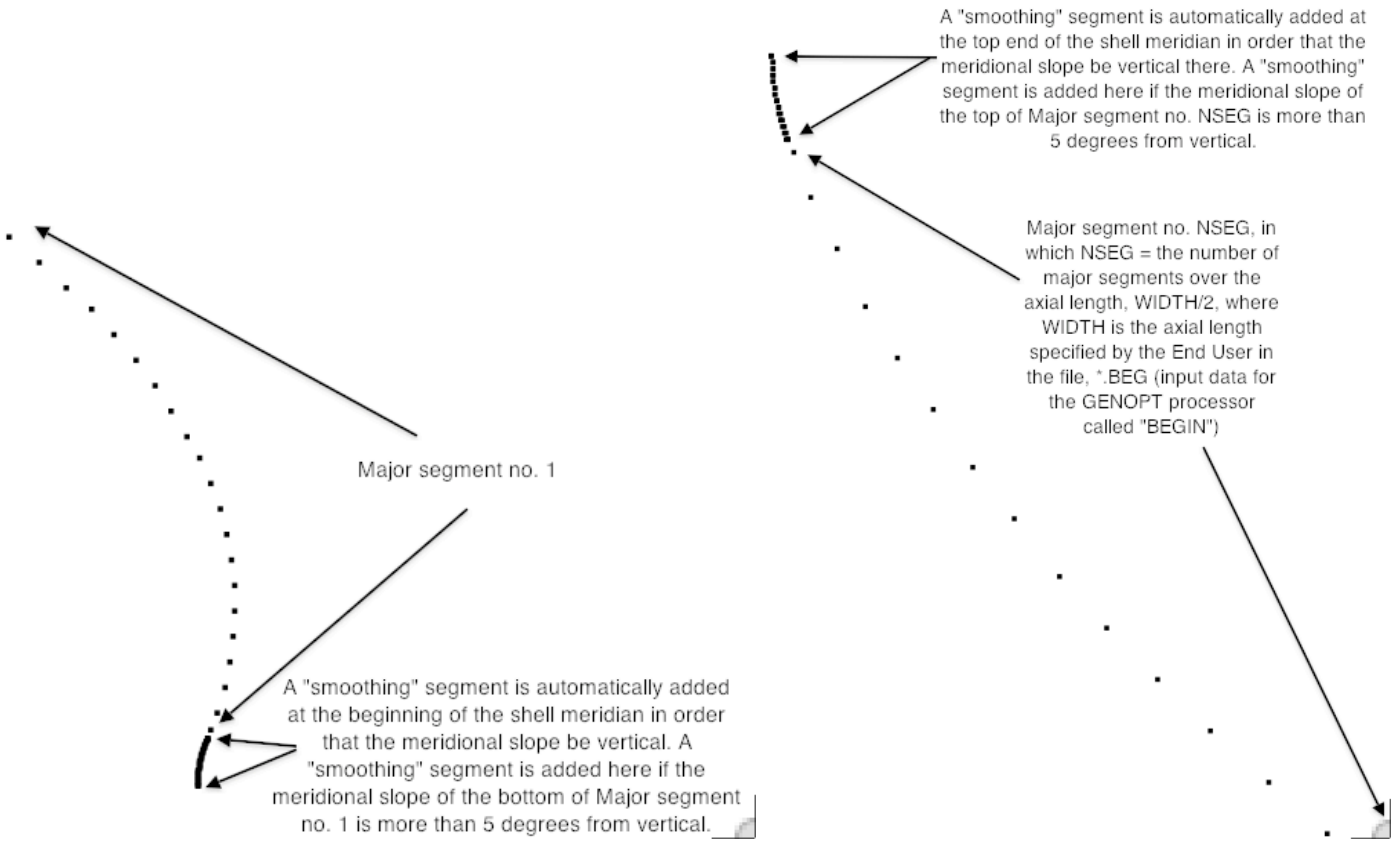

Fig. 9g **"Zoomed" views** of the bottom of the nonlinearly optimized BIGBOSOR4 model (left-hand side) and the top of the nonlinearly optimized BIGBOSOR4 model (right-hand side) shown in the previous figure. The meridional radius of curvature of the "smoothing" segments, RSMOOTH = 1.0 inch at both locations. A "smoothing" segment is introduced at an end of a circumferentially corrugated shell of revolution if the meridional slope there deviates from vertical by more than 5 degrees.

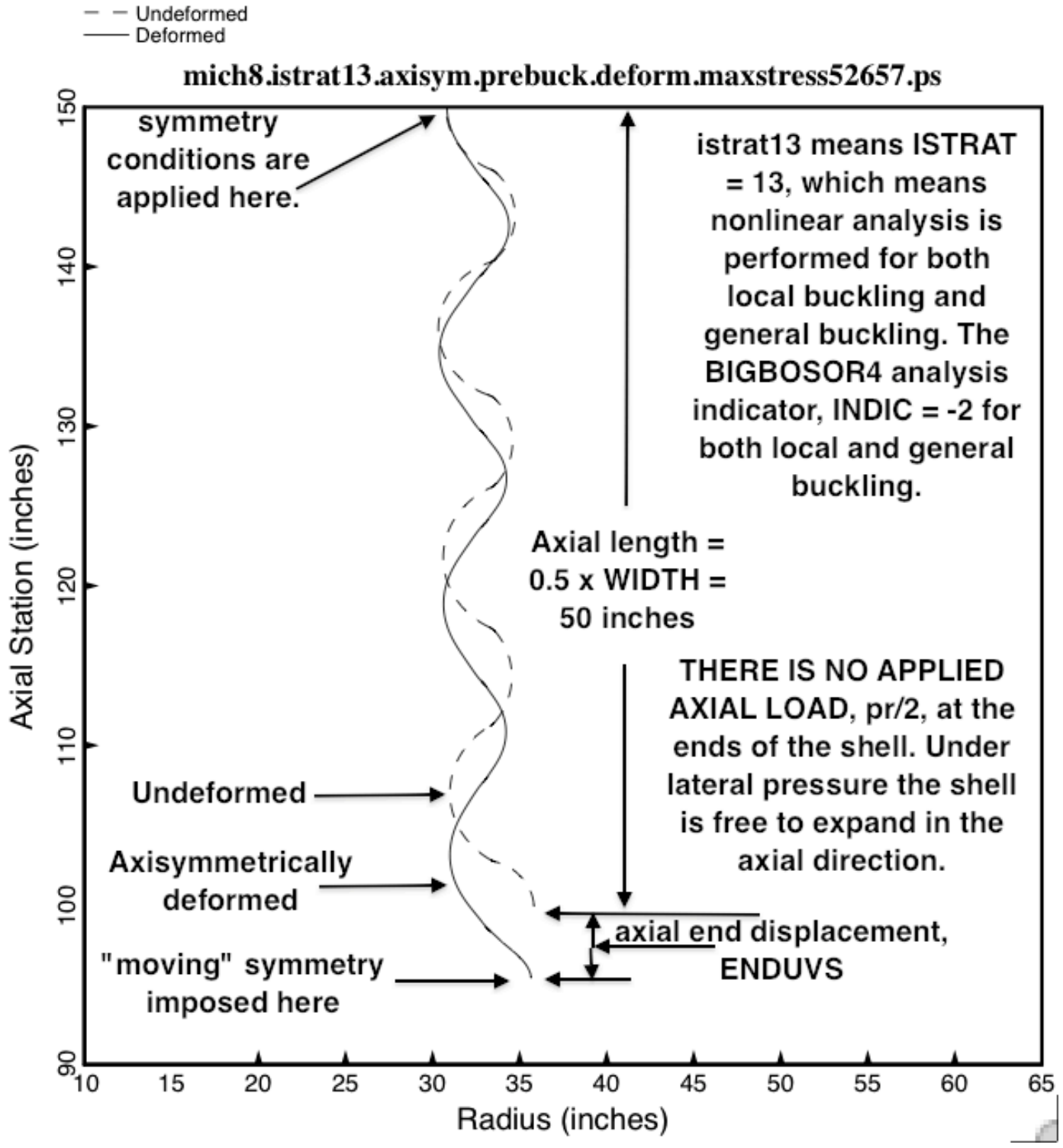

Fig. 10 **Axisymmetric pre-buckling deformation from BIGBOSOR4 of the nonlinearly optimized "mich8" configuration** shown in Fig. 9f. The optimized dimensions, the local and general buckling load factors, and the maximum effective stress, 52657 psi, for this optimized shell wall profile are listed in Table 2.

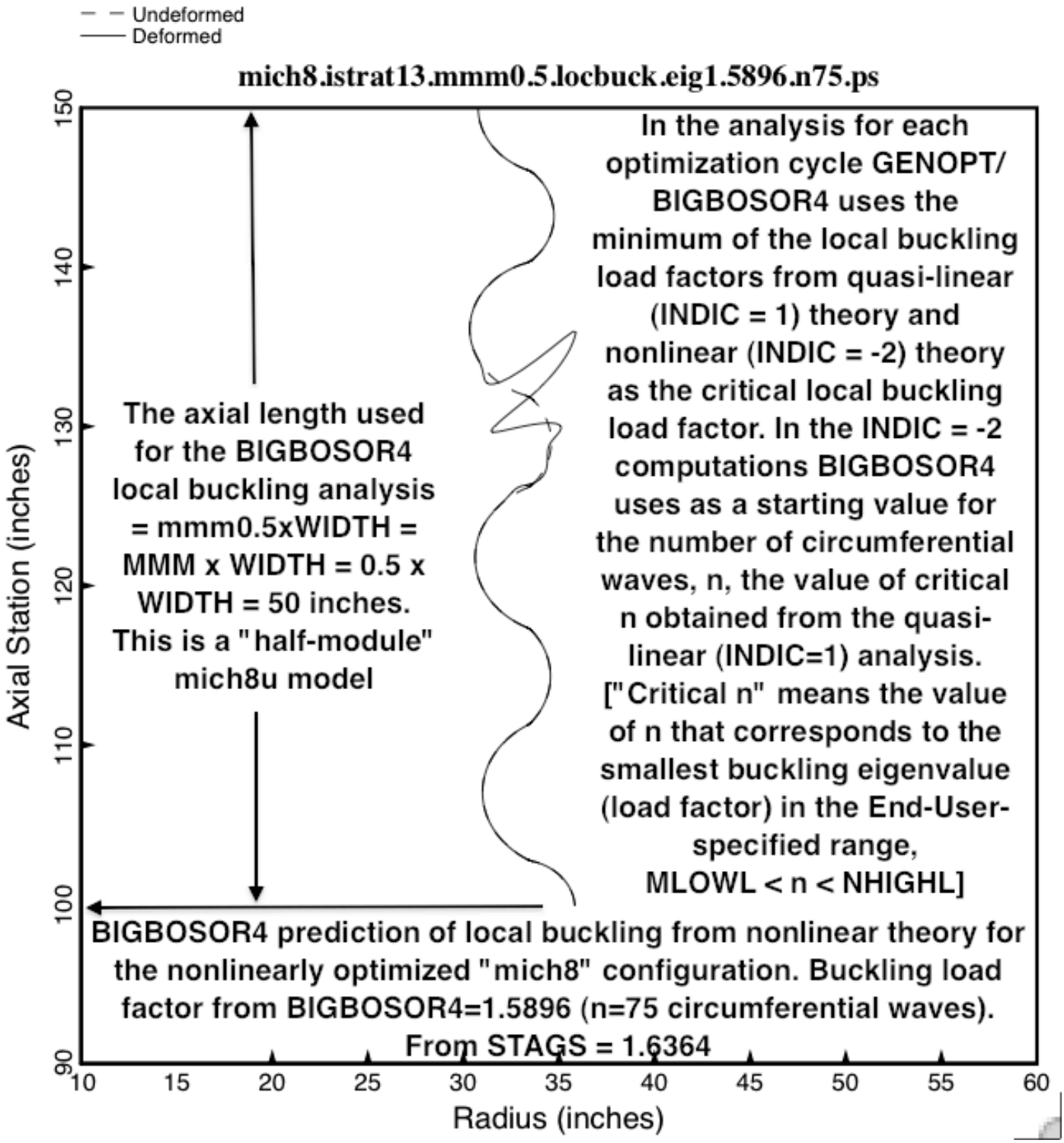

Fig. 11 **The nonlinear, non-axisymmetric local buckling mode and load factor from BIGBOSOR4 of the nonlinearly optimized "mich8" configuration** shown in the previous figure. The optimized dimensions, the local and general buckling load factors, and the maximum effective stress for this optimized shell wall profile are listed in Table 2. The local buckling mode predicted by STAGS is shown in the next figure.

Fig. 12 **STAGS model of nonlinear local buckling of the nonlinearly optimized specific case called "mich8"**. (See Table 2.) There is good agreement between the predictions of STAGS and BIGBOSOR4 both with respect to the critical nonlinear local buckling load factor and the nonlinear local buckling mode shape.

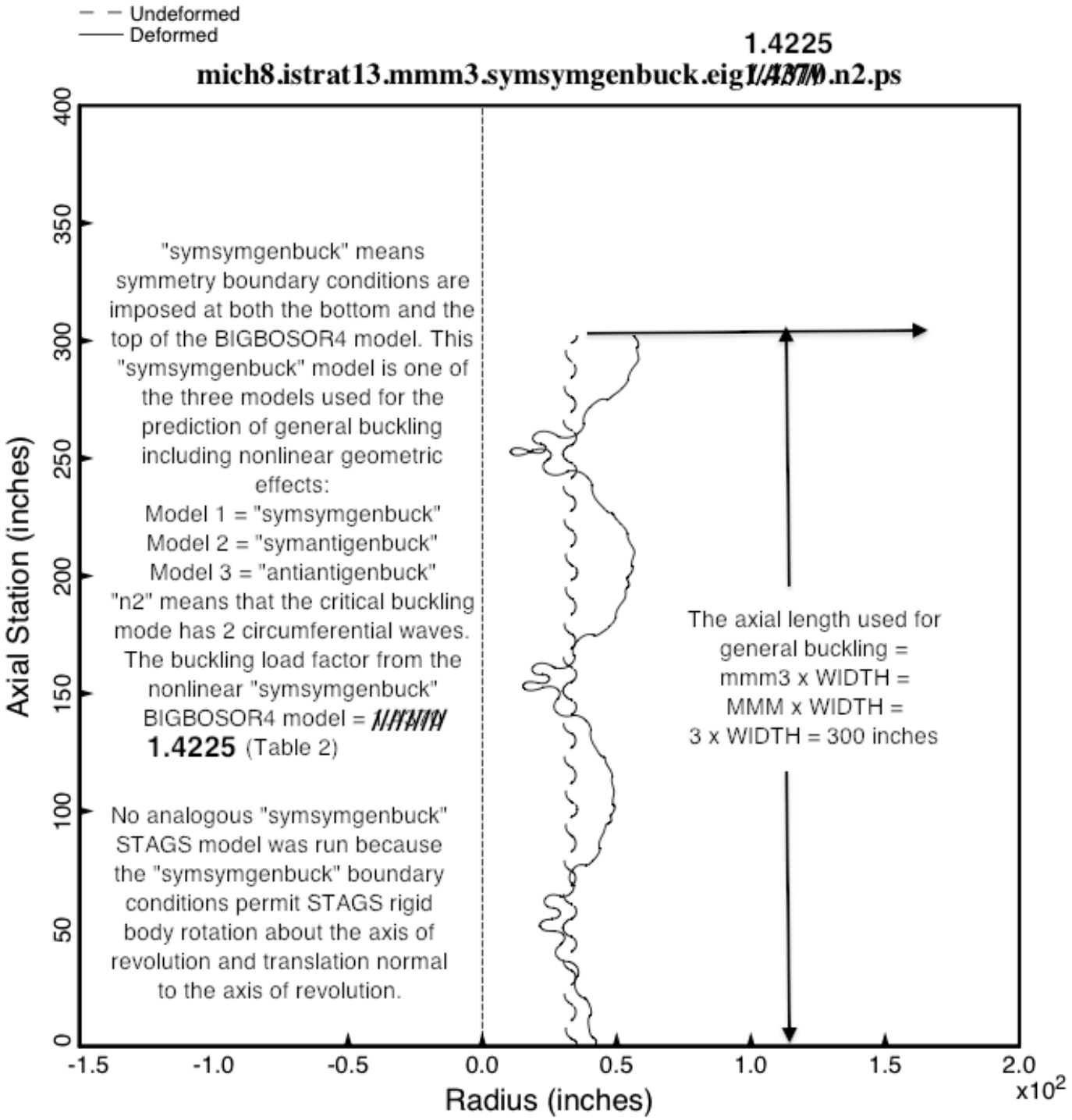

Fig. 13a **Symmetric nonlinear general buckling ("symsymgenbuck") from BIGBOSOR4 of the nonlinearly optimized specific case called "mich8"**. The length of circumferentially corrugated shell displayed here (300 inches) is six times that included in Figs. 10 and 11. This 300-inch-long shell is one of the three BIGBOSOR4 models ("symsymgenbuck", "symantigenbuck" and "antiantigenbuck") used during nonlinear optimization cycles for the prediction of nonlinear general buckling.

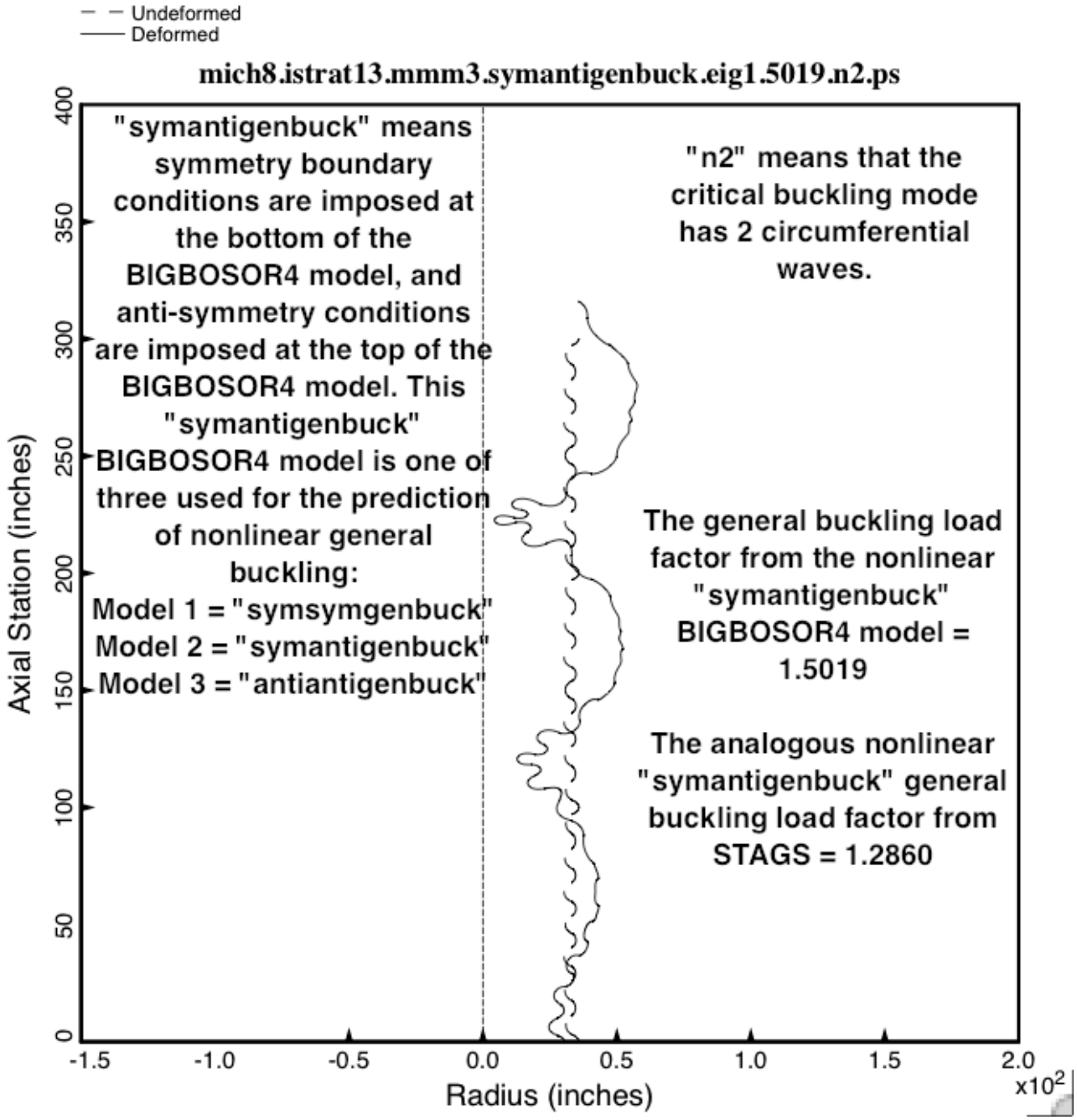

Fig. 13b **Symmetric-antisymmetric nonlinear general buckling ("symantigenbuck") from BIGBOSOR4 of the nonlinearly optimized specific case called "mich8"**. "Symantigenbuck" is the first type of general buckling computed in SUBROUTINE BEHX3, which is part of the behavior.michelin library. SUBROUTINE BEHX3 generates the general buckling load factor called "BUKASY" in Table 2. "BUKASY" is the more critical (lowest) of the two general buckling load factors computed in SUBROUTINE BEHX3: that from the "symantigenbuck" model displayed here and that from the "antiantigenbuck" model displayed in the next figure. Notice that in the case of nonlinear general buckling there is only fair agreement with the prediction from STAGS.

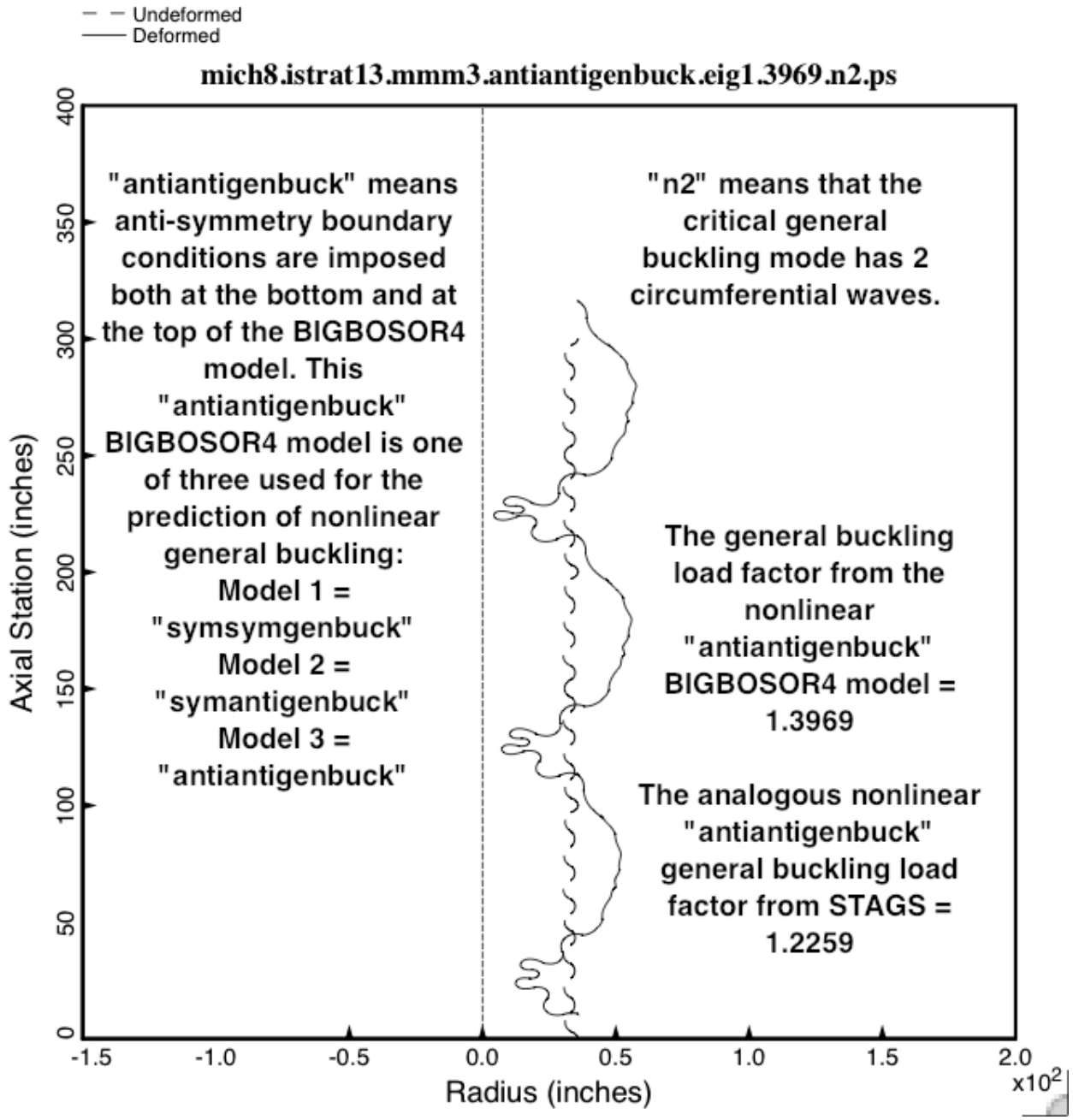

Fig. 13c **Antisymmetric-antisymmetric nonlinear general buckling ("antiantigenbuck") from BIGBOSOR4 of the nonlinearly optimized specific case called "mich8"**. "Antiantigenbuck" is the second type of general buckling computed in SUBROUTINE BEHX3, which is part of the behavior.michelin library. SUBROUTINE BEHX3 generates the general buckling load factor called "BUKASY" in Table 2. "BUKASY" is the more critical (lowest) of the two general buckling load factors computed in SUBROUTINE BEHX3: that from the "symantigenbuck" model displayed in the previous figure and that from the "antiantigenbuck" model displayed here. In this particular case the "antiantigenbuck" buckling mode is associated with the lowest general buckling load factor. Therefore, in Table 2 BUKASY has the value, 1.3969. Notice that in the case of nonlinear general buckling there is only fair agreement with the prediction from STAGS.

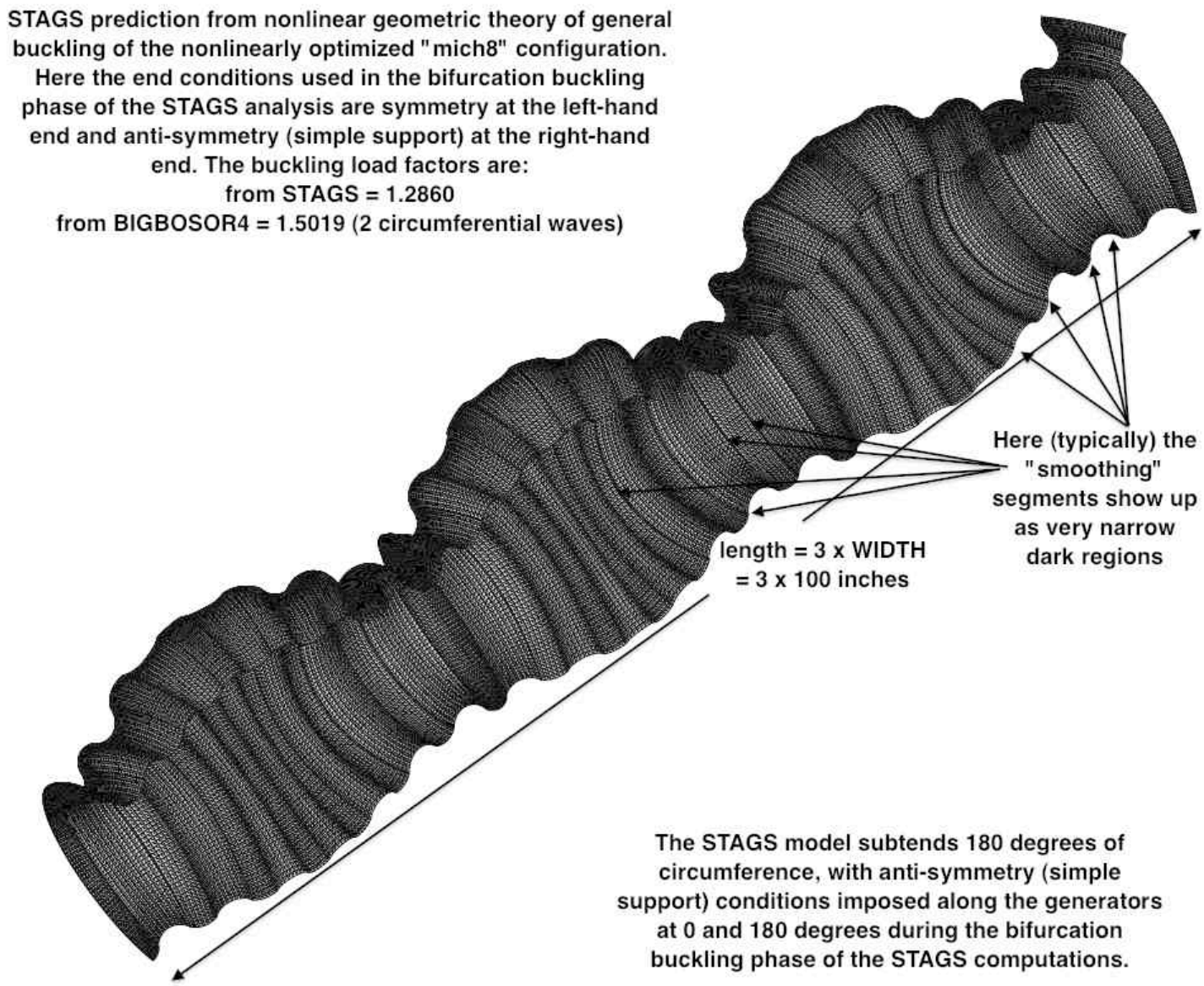

Fig. 14a **The prediction from STAGS of nonlinear general buckling for the nonlinearly optimized specific case called "mich8"**. Two nonlinear STAGS "mich8" models were analyzed: "symantigenbuck" (shown here) and "antiantigenbuck" (shown in the next figure). In this particular case the nonlinear "antiantigenbuck" STAGS model yields the more critical (lowest) nonlinear general buckling load factor. There is only fair agreement with the prediction of nonlinear "symantigenbuck" general buckling obtained from BIGBOSOR4, and the STAG prediction is significantly lower than the BIGBOSOR4 prediction. It is proposed that the discrepancy arises because BIGBOSOR4 is based on an approximate "classical" (legacy) "moderately large" meridional rotation theory (sine and cosine of the meridional rotation replaced, respectively, by the meridional rotation and unity), whereas STAGS is based on an exact "co-rotational" theory [41] in which the rigid body component of a large displacement stores no energy.

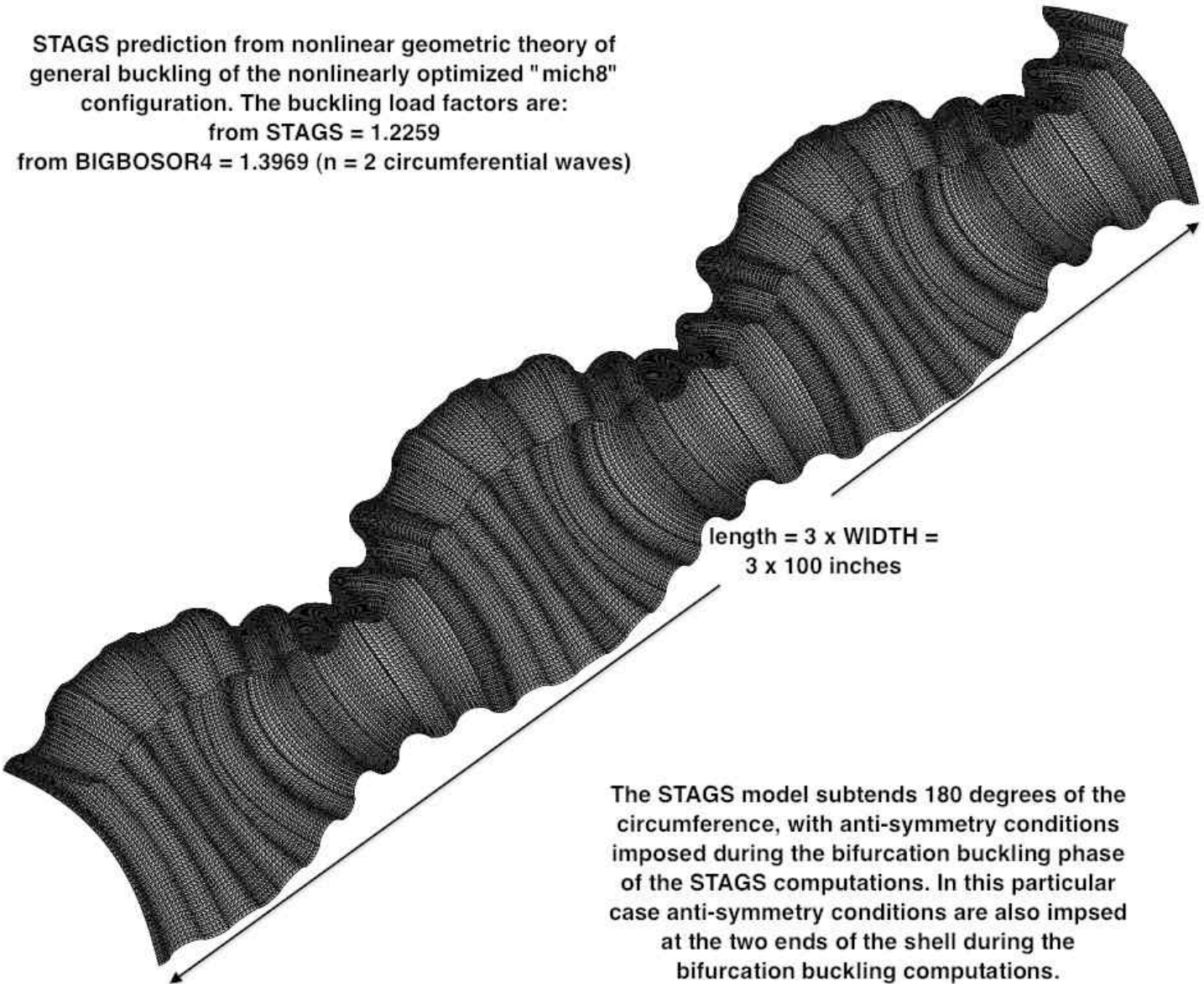

Fig. 14b **The prediction from STAGS of nonlinear general buckling for the nonlinearly optimized specific case called "mich8"**. Two nonlinear STAGS "mich8" models were analyzed: "symantigenbuck" (shown in the previous figure) and "antiantigenbuck" (shown here). In this particular case the nonlinear "antiantigenbuck" STAGS model yields the more critical (lowest) nonlinear general buckling load factor. There is only fair agreement with the prediction of nonlinear "antiantigenbuck" general buckling obtained from BIGBOSOR4.

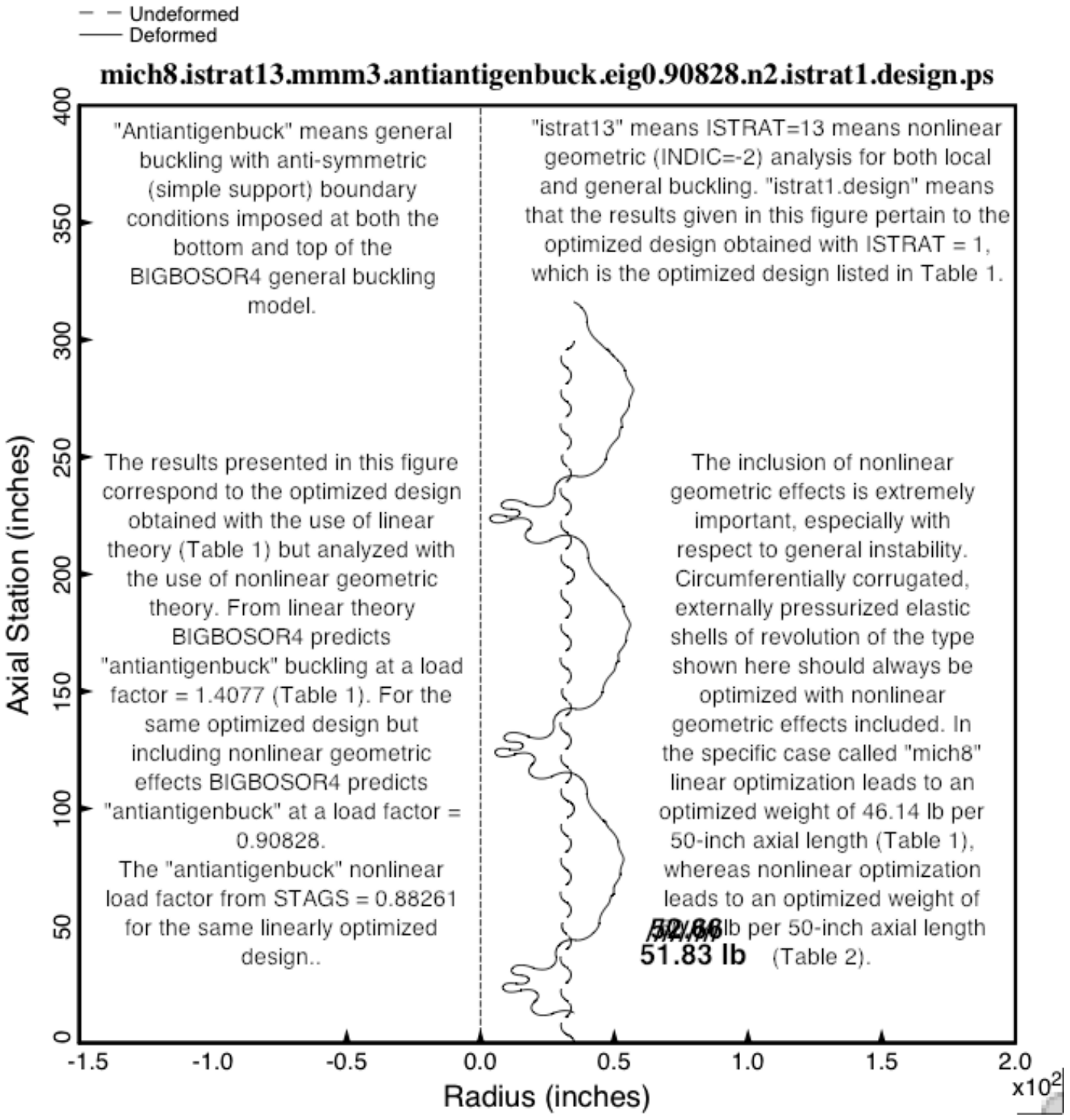

Fig. 15 **Nonlinear general buckling from the BIGBOSOR4 "antiantigenbuck" general buckling model of the optimized "mich8" design obtained with the use of linear theory**, that is, the optimized design listed in Table 1. The introduction of nonlinear geometric effects dramatically reduces the general buckling load factor.

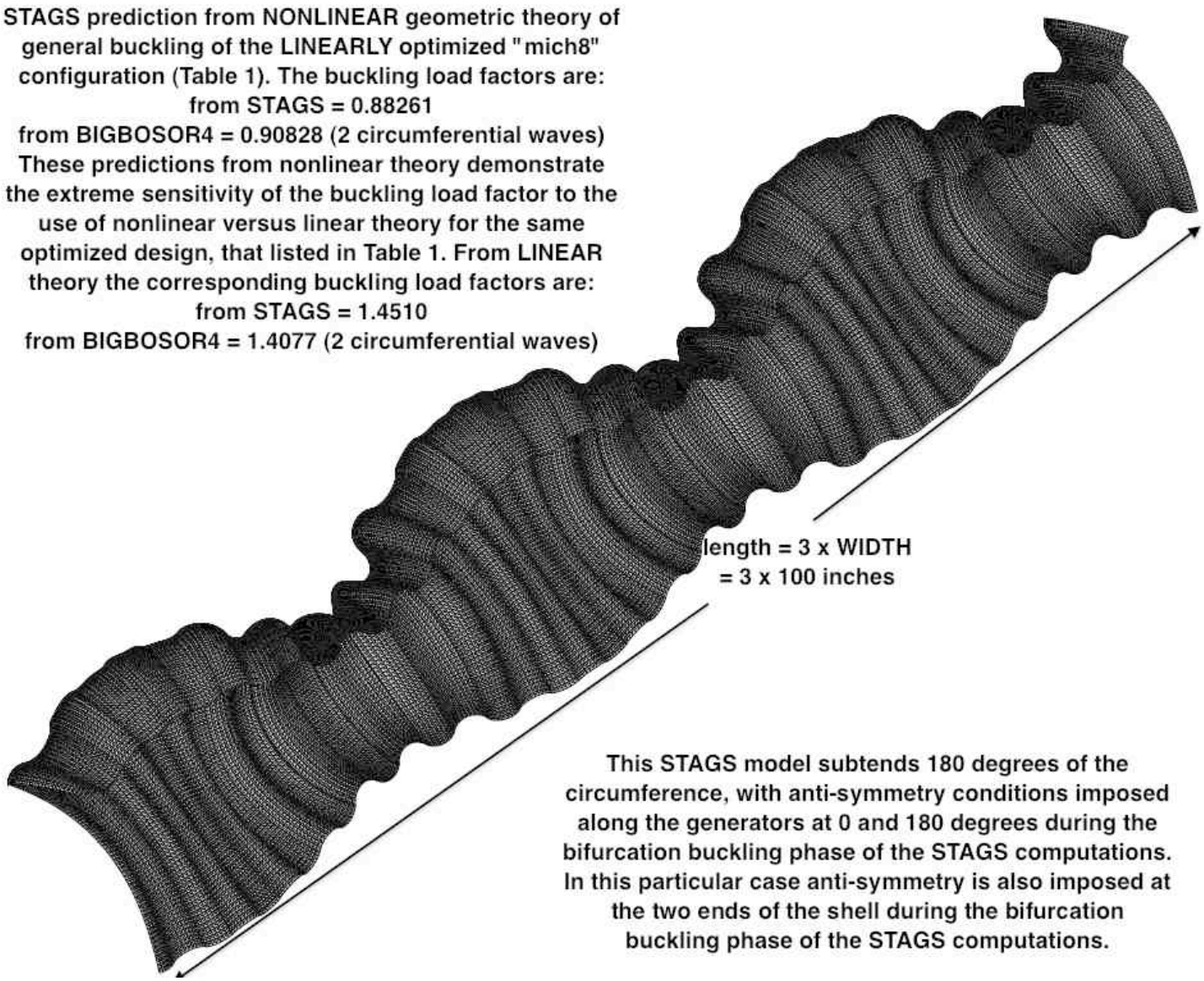

Fig. 16 **Nonlinear general buckling from the STAGS "antiantigenbuck" general buckling model of the optimized "mich8" design obtained with the use of linear theory**, that is, the optimized design listed in Table 1. The introduction of nonlinear geometric effects dramatically reduces the general buckling load factor predicted by STAGS. In this case there is reasonably good agreement between the predictions of STAGS and BIGBOSOR4, even though nonlinear geometric theory is used for these predictions. However, it is emphasized that this is the optimized design obtained with the use of LINEAR theory, not the optimized design obtained with the use of NONLINEAR theory, predictions for which appear in Figs. 13a,b,c and 14a,b.

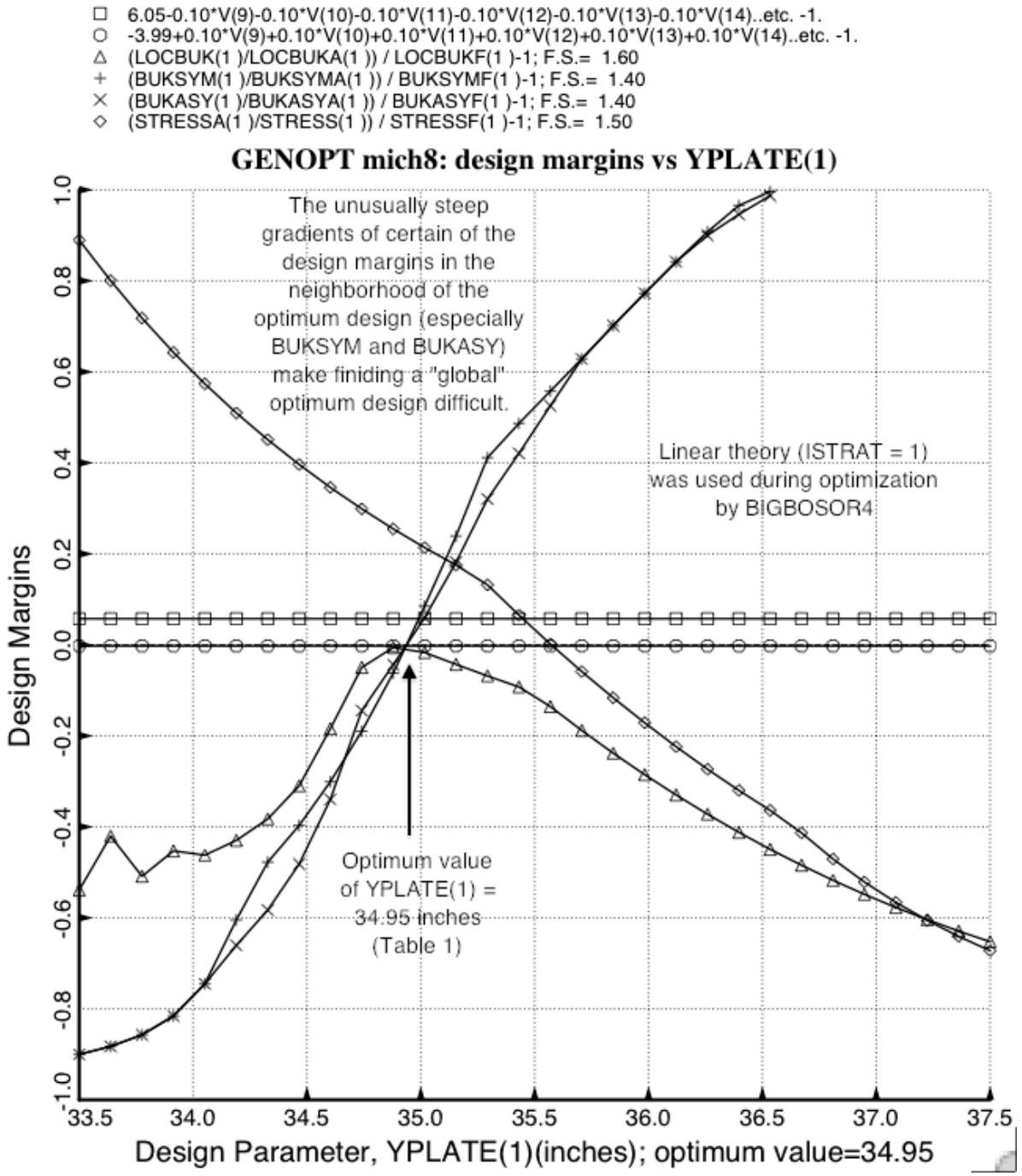

Fig. 17 **Design sensitivity from GENOPT/BIGBOSOR4 with respect to the decision variable, YPLATE(1), of the LINEARLY optimized specific case called "mich8"**. YPLATE(1) is the radius from the axis of revolution to the shell reference surface at the bottom of the BIGBOSOR4 model shown in Figs. A2b, 20 and 27. Notice the very fine scale on the horizontal axis. This extreme design sensitivity leads to very large behavioral constraint gradients, especially those for general buckling (BUKSYM and BUKASY; See Table6 for very high constraint gradients from the optimized design of a different specific case: "mich1".). Large behavioral constraint gradients cause difficulty in the search for a "global" optimum design.

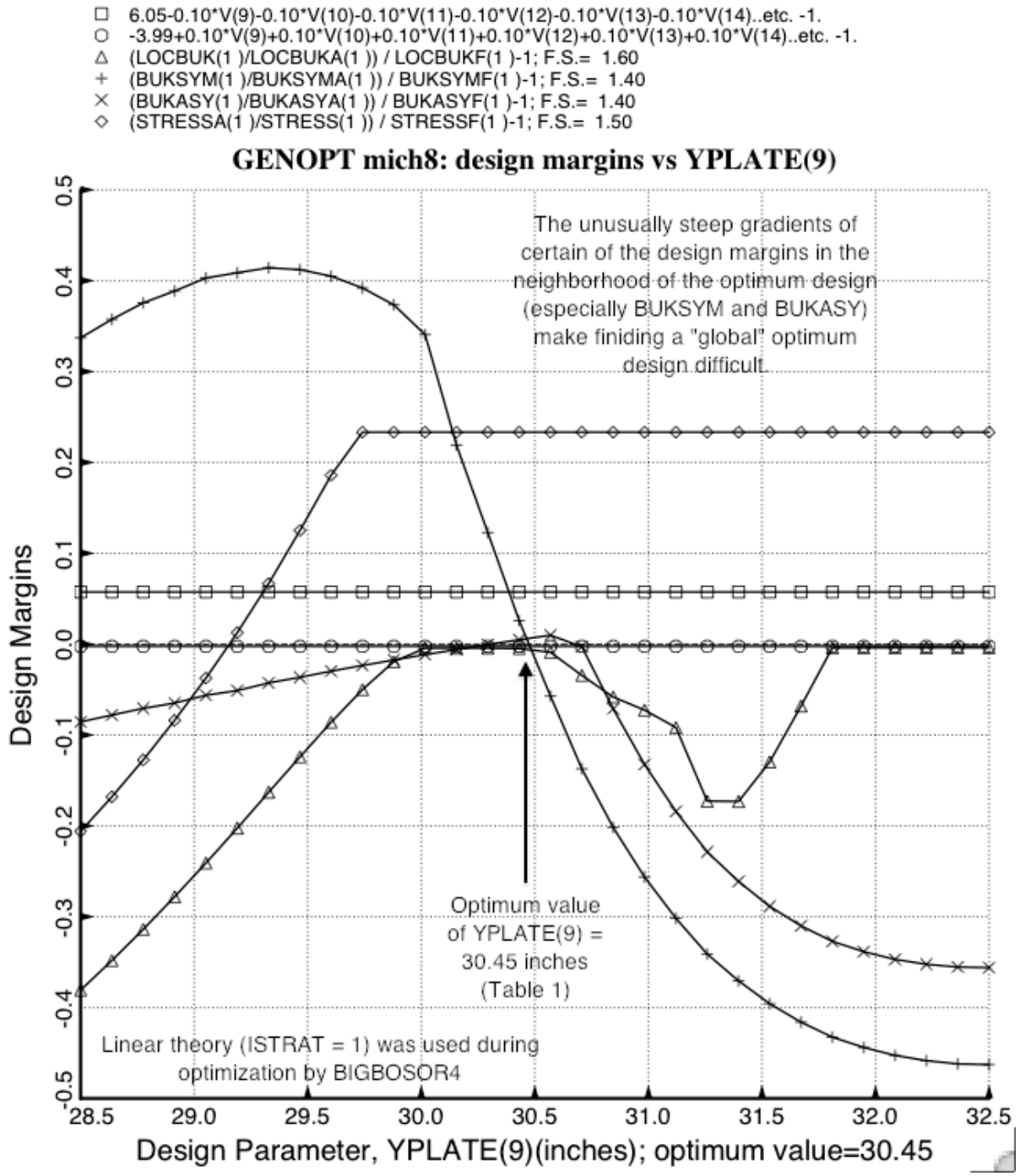

Fig. 18 **Design sensitivity from GENOPT/BIGBOSOR4 with respect to the decision variable, YPLATE(9), of the linearly optimized specific case called "mich8"**. YPLATE(9) is the radius from the axis of revolution to the shell reference surface at the top of the BIGBOSOR4 model shown in Figs. A2b, 20 and 27. Notice the very fine scale on the horizontal axis. This extreme design sensitivity leads to very large behavioral constraint gradients, especially those for general buckling (BUKSYM and BUKASY). Large behavioral constraint gradients cause difficulty in the search for a "global" optimum design.

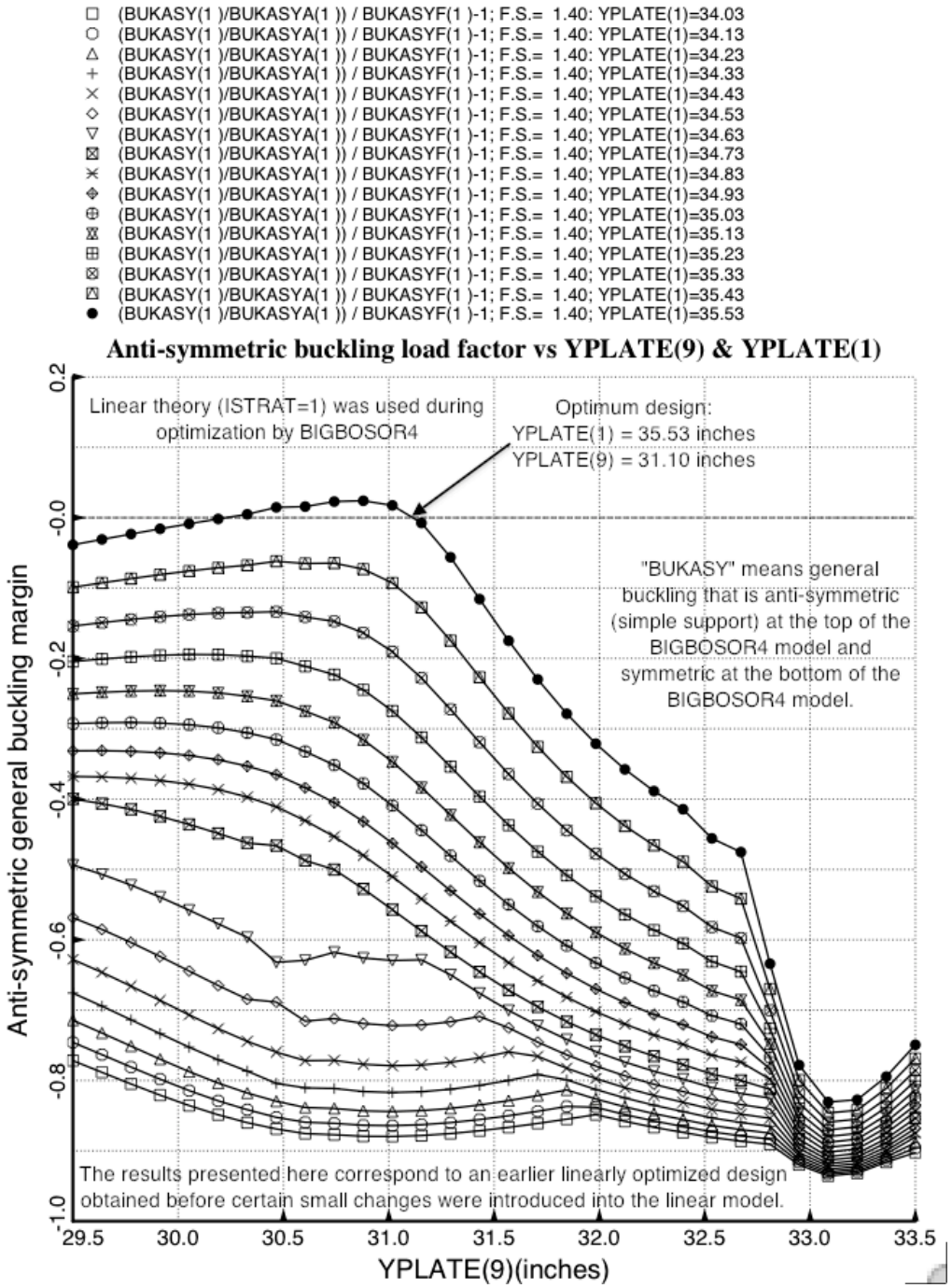

Fig. 19 **Design sensitivity "surface" from GENOPT/BIGBOSOR4 with respect to the decision variables, YPLATE(1) and YPLATE(9), of the linearly optimized specific case called "mich8"**. YPLATE(1) and YPLATE(9) are the radii from the axis of revolution to the shell reference surface at the bottom and top, respectively, of the BIGBOSOR4 model shown in Figs. A2b, 20 and 27. Notice the fine scale on the horizontal axis and the small range of YPLATE(1) explored for the production of this chart. (This chart corresponds to a somewhat different linearly optimized design than that listed in Table 1 because it was created before certain small changes were introduced into the linear model.)

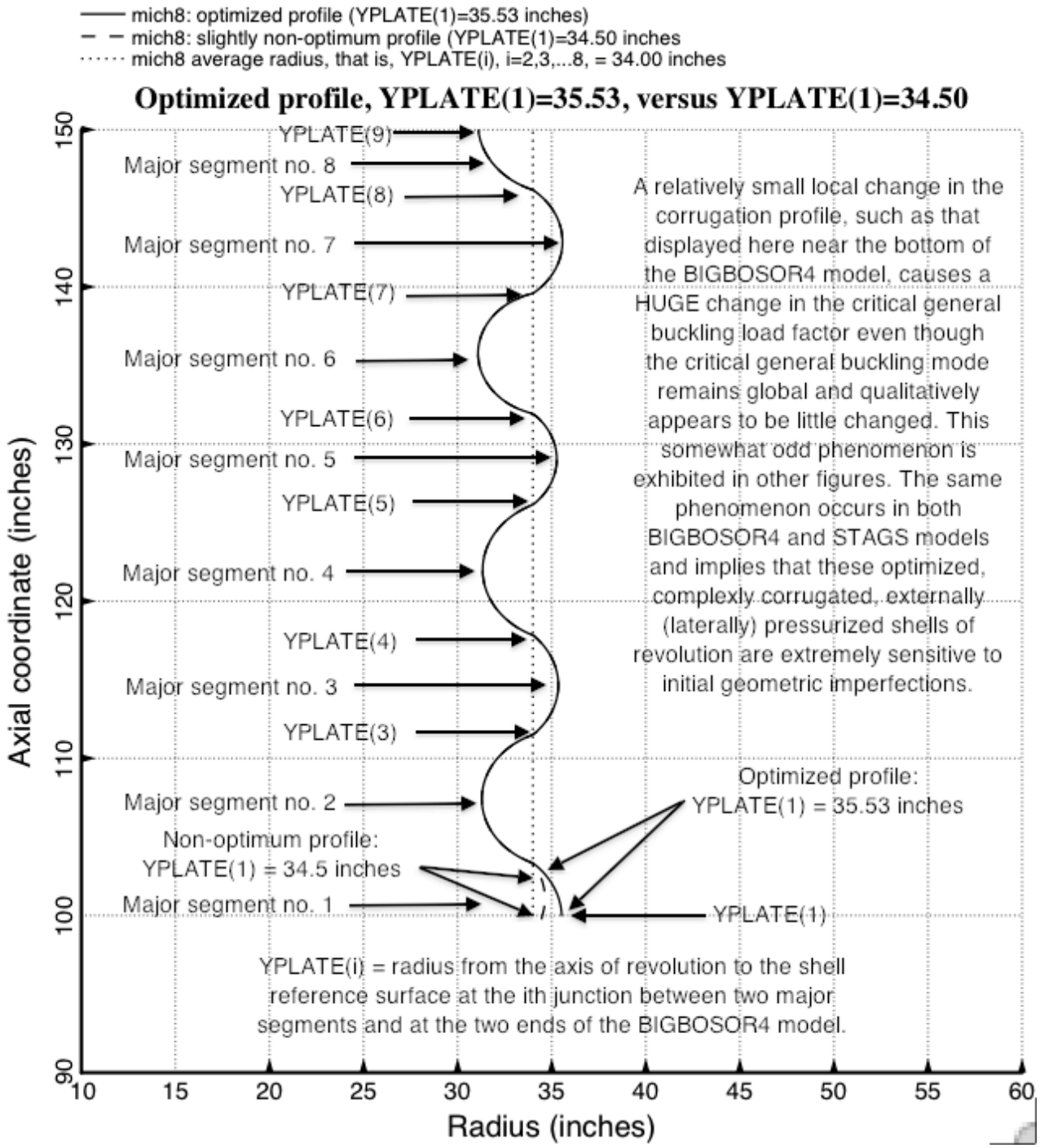

Fig. 20 **Linearly optimized and slightly non-optimum profiles of the specific case called "mich8"**. A rather small change in YPLATE(1) from its optimized value to a slightly lower value causes a huge decrease in the general buckling load factors obtained with the use of linear theory, as has been demonstrated in Fig. 17 and as will be further demonstrated in the next figure. (This figure corresponds to a somewhat different linearly optimized design than that listed in Table 1 because it was created before certain small changes were introduced into the linear model.)

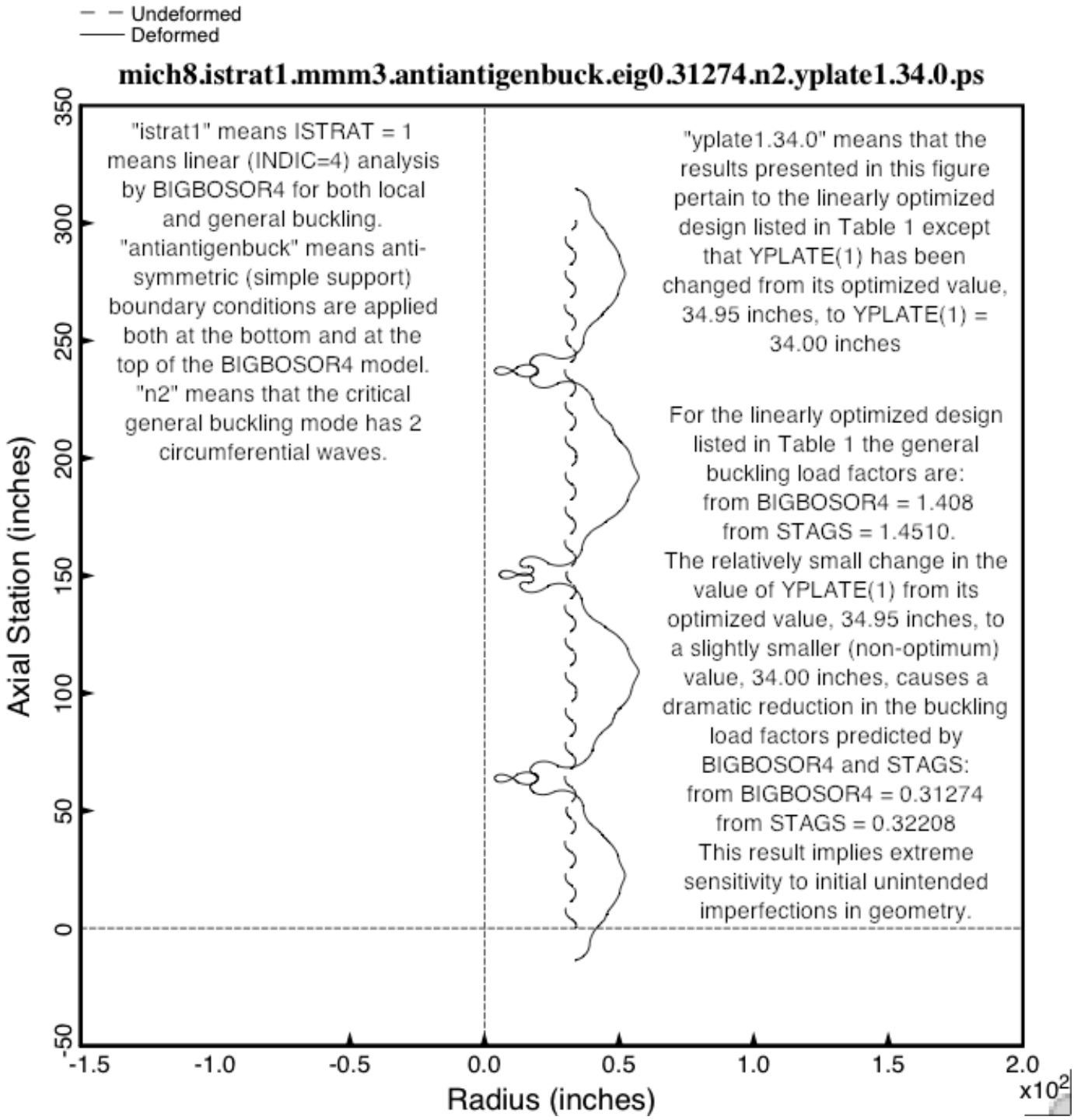

Fig. 21 **"Antiantigenbuck" linear general buckling mode and load factor from BIGBOSOR4 for a linearly optimized specific case called "mich8"** with one of the decision variables, YPLATE(1), reduced from its optimum value by about 3 per cent. (See the previous figure.) This relatively small change in the design causes a huge reduction of the critical linear general buckling load factor: from about 1.4 to about 0.3. The STAGS prediction shown in the next figure demonstrates the same extreme sensitivity.

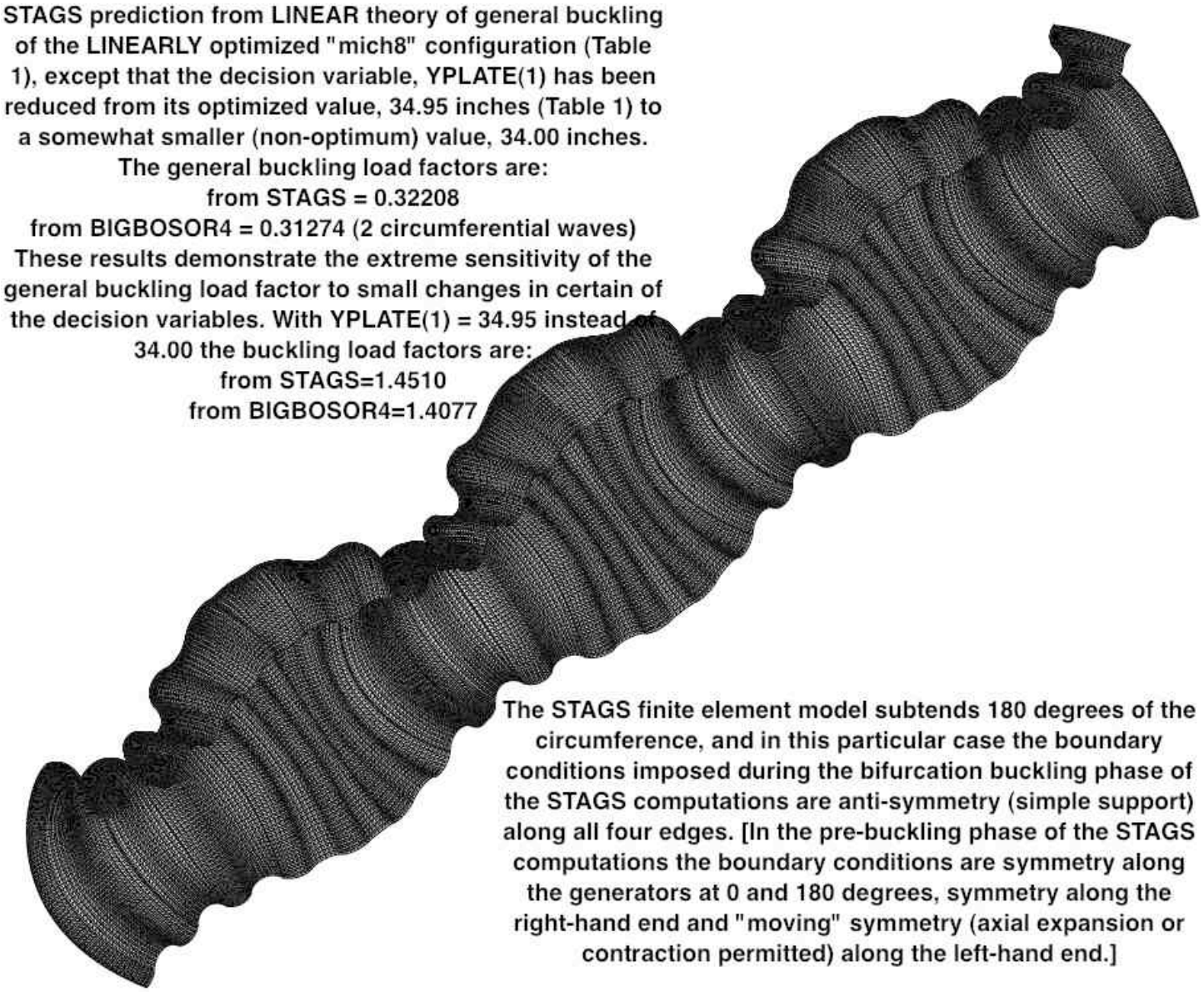

Fig. 22 **STAGS prediction of linear general "antiantigenbuck" buckling analogous to that predicted by BIGBOSOR4 shown in the previous figure for the specific case called "mich8"**. The STAGS model and the BIGBOSOR4 model exhibit essentially the same sensitivity of the critical general buckling load factor to the small reduction in YPLATE(1). (Also see Fig. 17.)

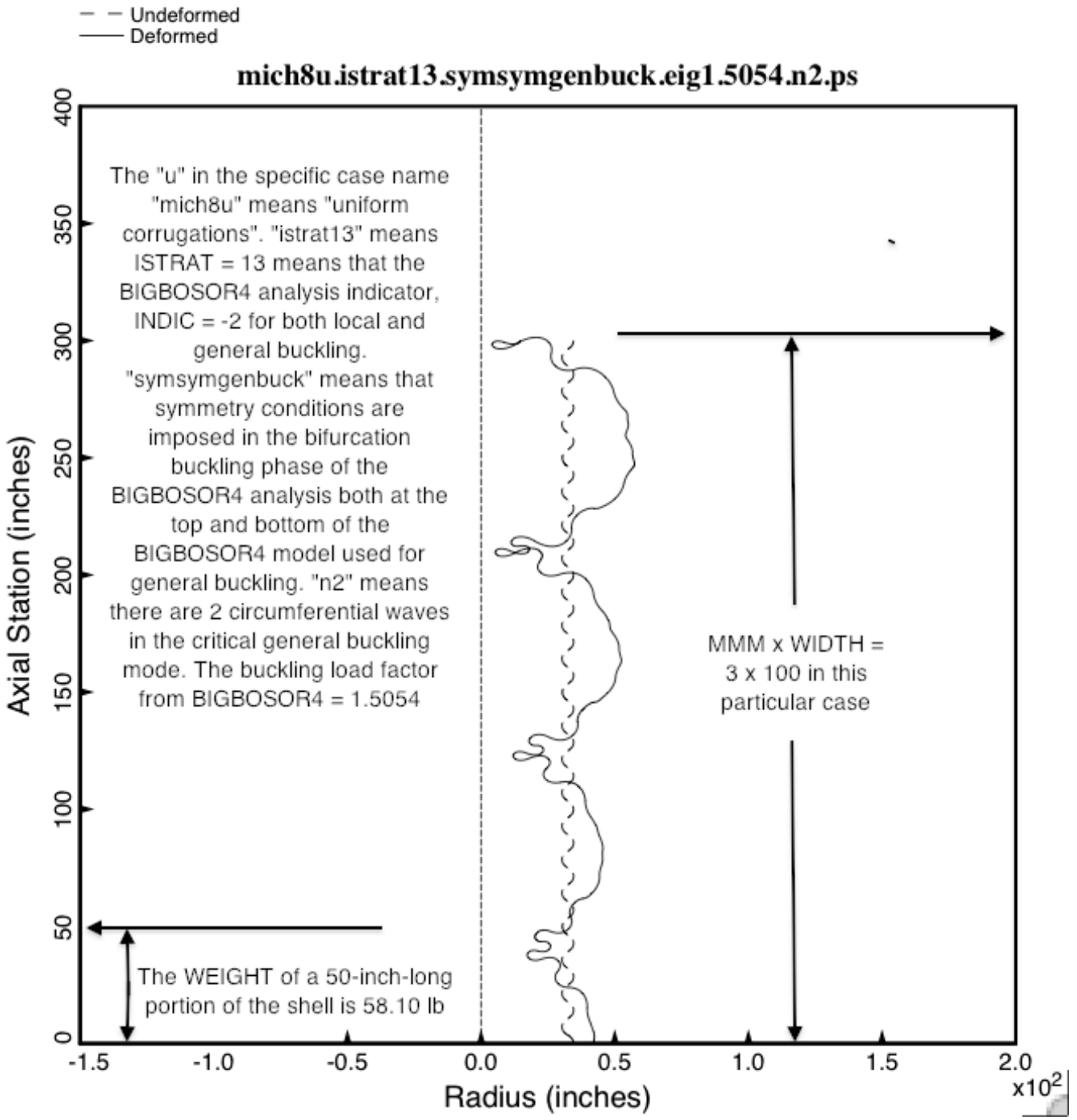

Fig. 23a **"Symsymgenbuck" nonlinear general buckling from BIGBOSOR4 of the nonlinearly optimized specific case called "mich8u" (uniformly corrugated shell)**. This figure is analogous to Fig. 13a, which pertains to the nonlinearly optimized complexly corrugated shell called "mich8". As with the specific case called "mich8", this 300-inch-long "mich8u" "symsymgenbuck" shell is one of the three BIGBOSOR4 nonlinear models ("symsymgenbuck", "symantigenbuck" and "antiantigenbuck") used during nonlinear optimization cycles for the prediction of nonlinear general buckling.

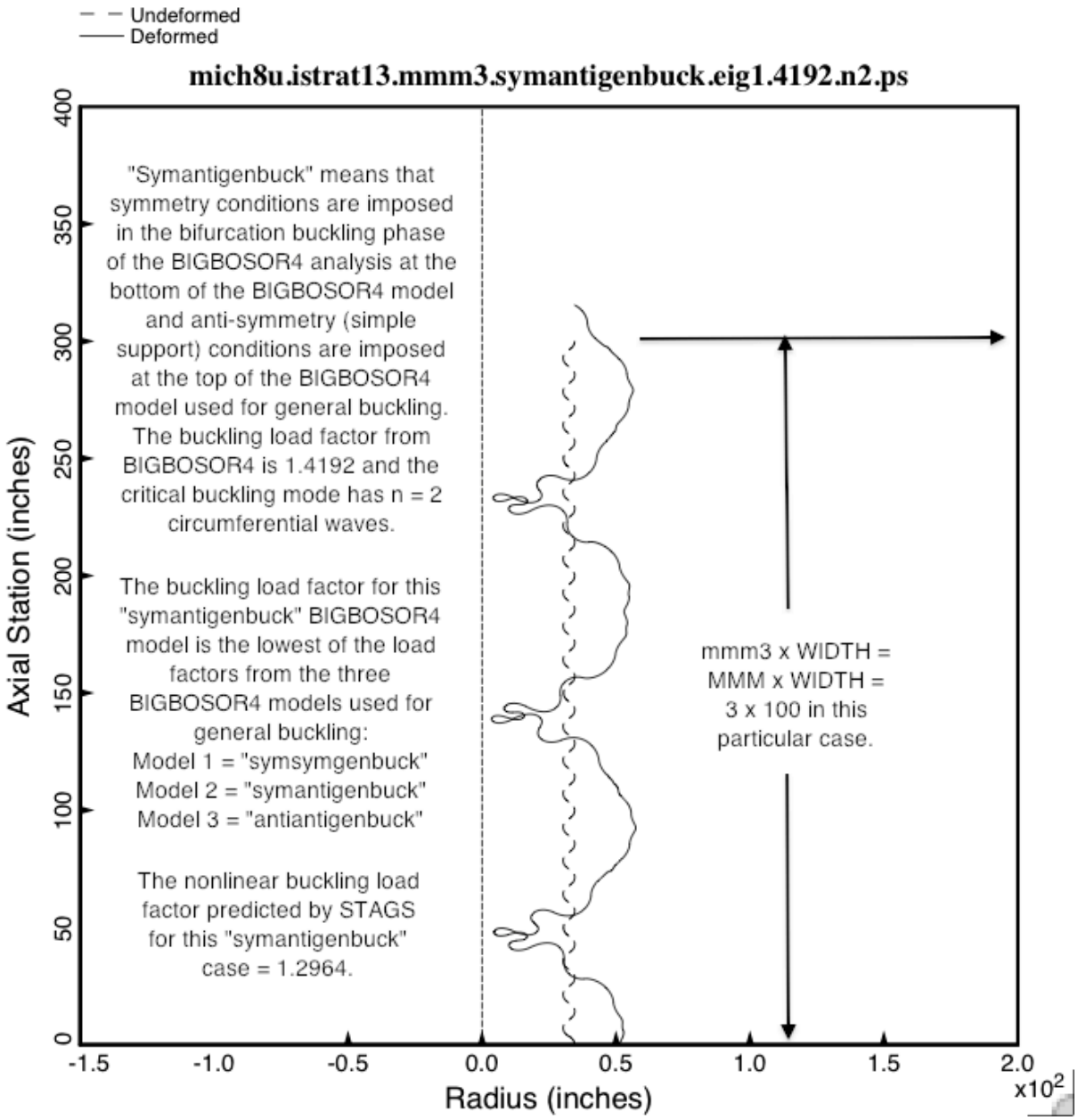

Fig. 23b **"Symantigenbuck" nonlinear general buckling from BIGBOSOR4 of the nonlinearly optimized specific case called "mich8u" (uniformly corrugated shell)**. This figure is analogous to Fig. 13b, which pertains to the nonlinearly optimized complexly corrugated shell called "mich8". As with the specific case called "mich8", this 300-inch-long "mich8u" "symantigenbuck" shell is one of the three BIGBOSOR4 nonlinear models ("symsymgenbuck", "symantigenbuck" and "antiantigenbuck") used during nonlinear optimization cycles for the prediction of nonlinear general buckling. It is this "symantigenbuck" general buckling mode that is associated with the more critical of the two general buckling modes: "symantigenbuck" and "antiantigenbuck". Therefore, the buckling load factor, 1.419, associated with the "symantigenbuck" general buckling mode is listed as the value of the third "behavior" in Table 3b: "antisymmetric general buckling: BUKASY(1)", For nonlinear general buckling there is only fair agreement with STAGS.

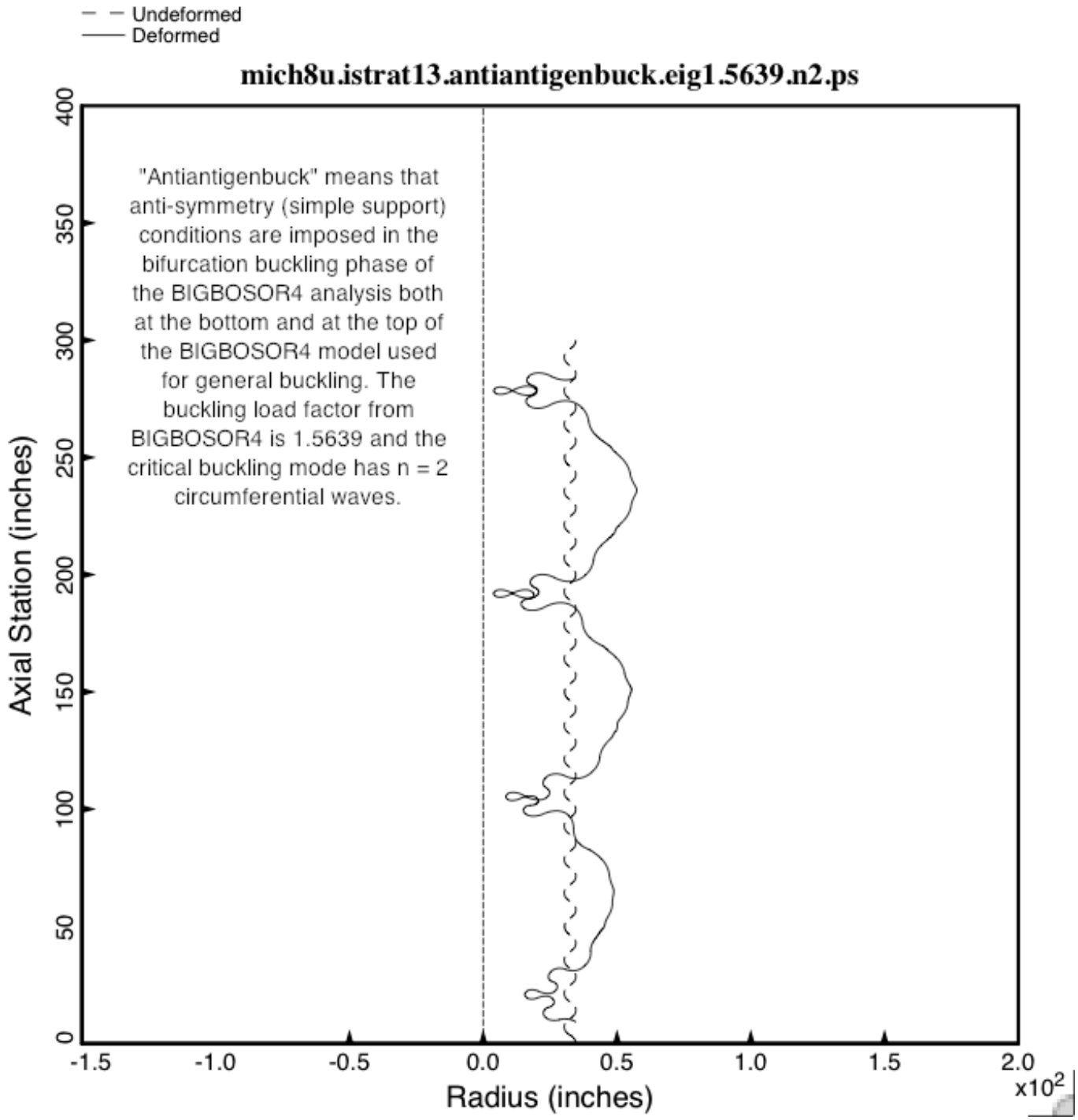

Fig. 23c **"antiantigenbuck" nonlinear general buckling from BIGBOSOR4 of the nonlinearly optimized specific case called "mich8u" (uniformly corrugated shell)**. This figure is analogous to Fig. 13c, which pertains to the nonlinearly optimized complexly corrugated shell called "mich8". As with the specific case called "mich8", this 300-inch-long "mich8u" "antiantigenbuck" shell is one of the three BIGBOSOR4 nonlinear models ("symsymgenbuck", "symantigenbuck" and "antiantigenbuck") used during nonlinear optimization cycles for the prediction of nonlinear general buckling.

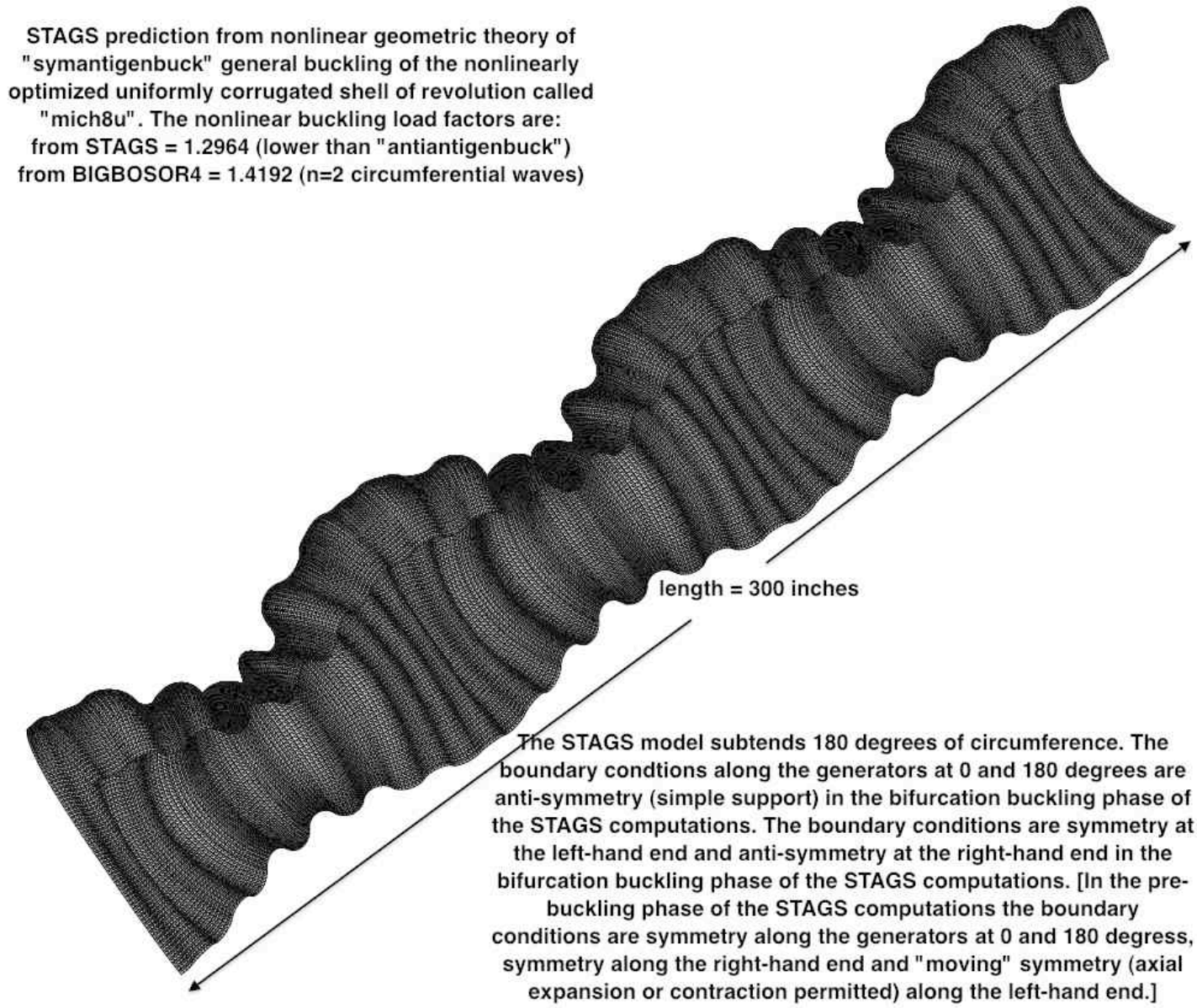

Fig. 24 **The prediction from STAGS of nonlinear general buckling for the nonlinearly optimized specific case called "mich8u" (uniformly corrugated shell)**. Two nonlinear STAGS "mich8u" models were analyzed: "symantigenbuck" (shown here) and "antiantigenbuck" (not included as a figure in this already very long paper). In this particular case the nonlinear "symantigenbuck" STAGS model yields the more critical (lowest) nonlinear general buckling load factor. There is only fair agreement with the prediction of nonlinear "symantigenbuck" general buckling obtained from BIGBOSOR4. (See Fig. 23b.)

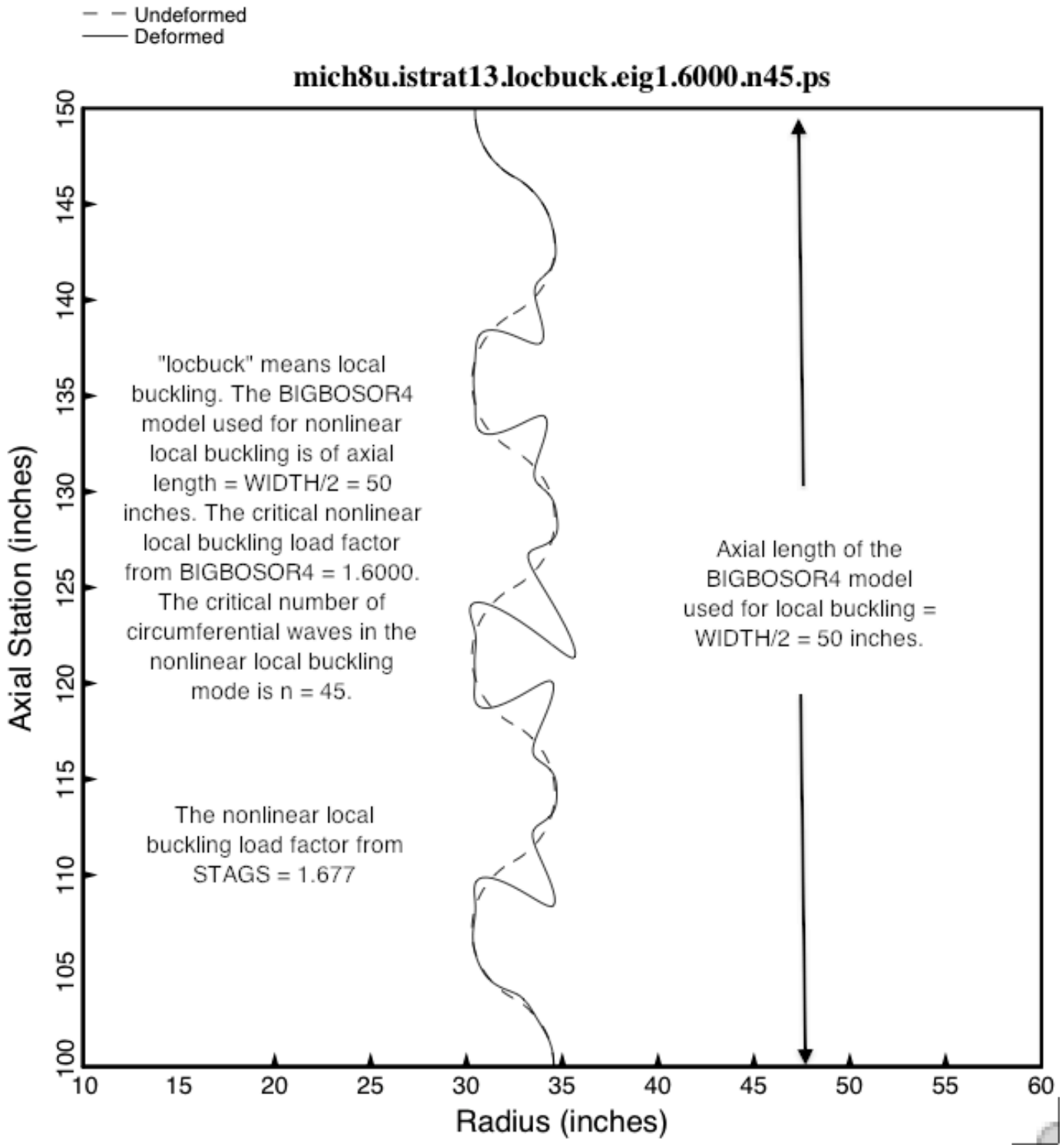

Fig. 25 **Nonlinear local buckling from BIGBOSOR4 of the nonlinearly optimized specific case called "mich8u" (uniformly corrugated shell)**. This figure is analogous to Fig 11, which pertains to nonlinear local buckling of the nonlinearly optimized complexly corrugated shell called "mich8". There is good agreement with the prediction from STAGS, both with respect to the nonlinear local buckling load factor and the mode shape.

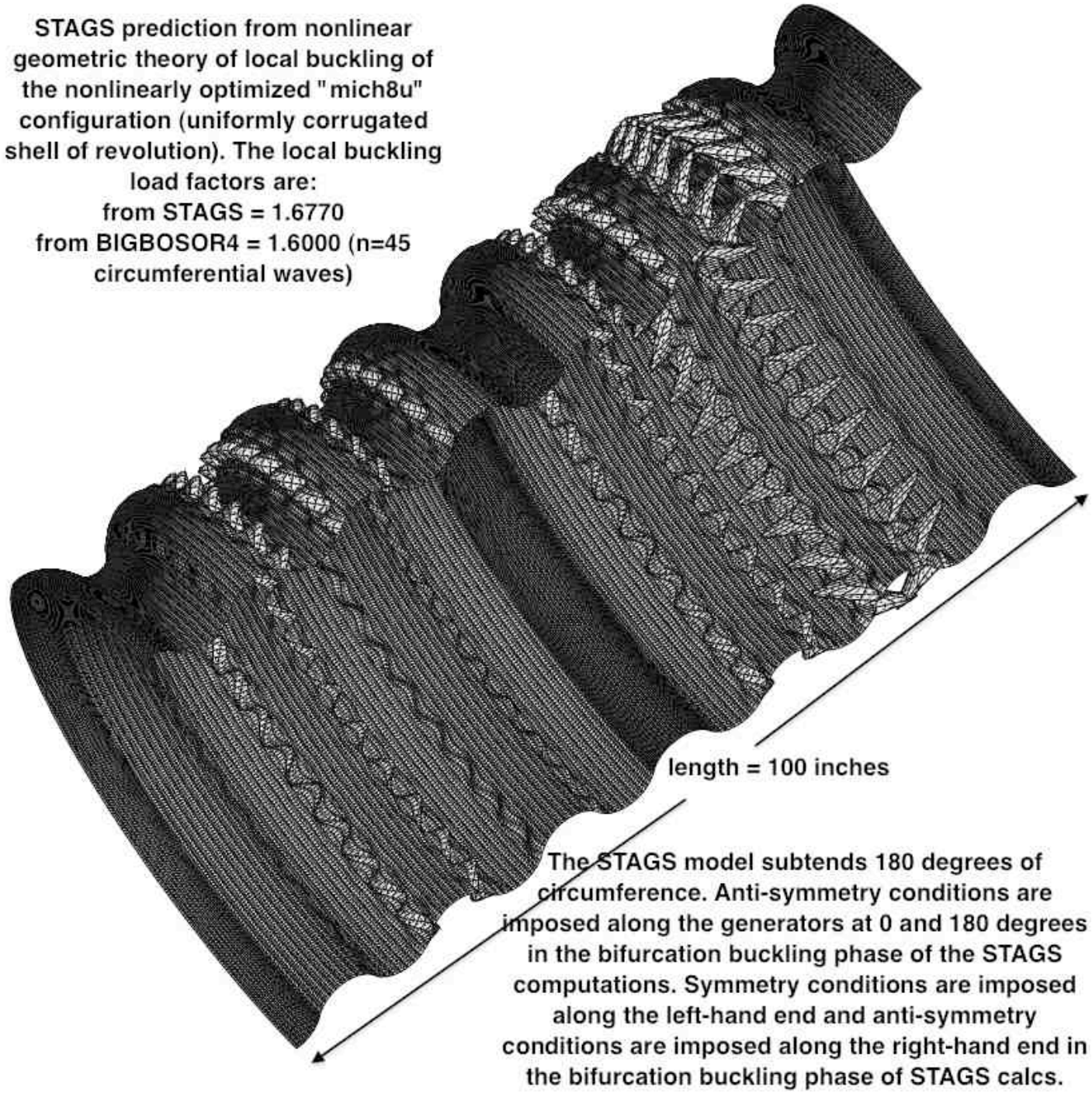

Fig. 26 **Nonlinear local buckling from STAGS of the nonlinearly optimized specific case called "mich8u" (uniformly corrugated shell)**. This figure is analogous to Fig 12, which pertains to nonlinear local buckling of the nonlinearly optimized complexly corrugated shell called "mich8". There is good agreement with the prediction from BIGBOSOR4, both with respect to the nonlinear local buckling load factor and the mode shape.

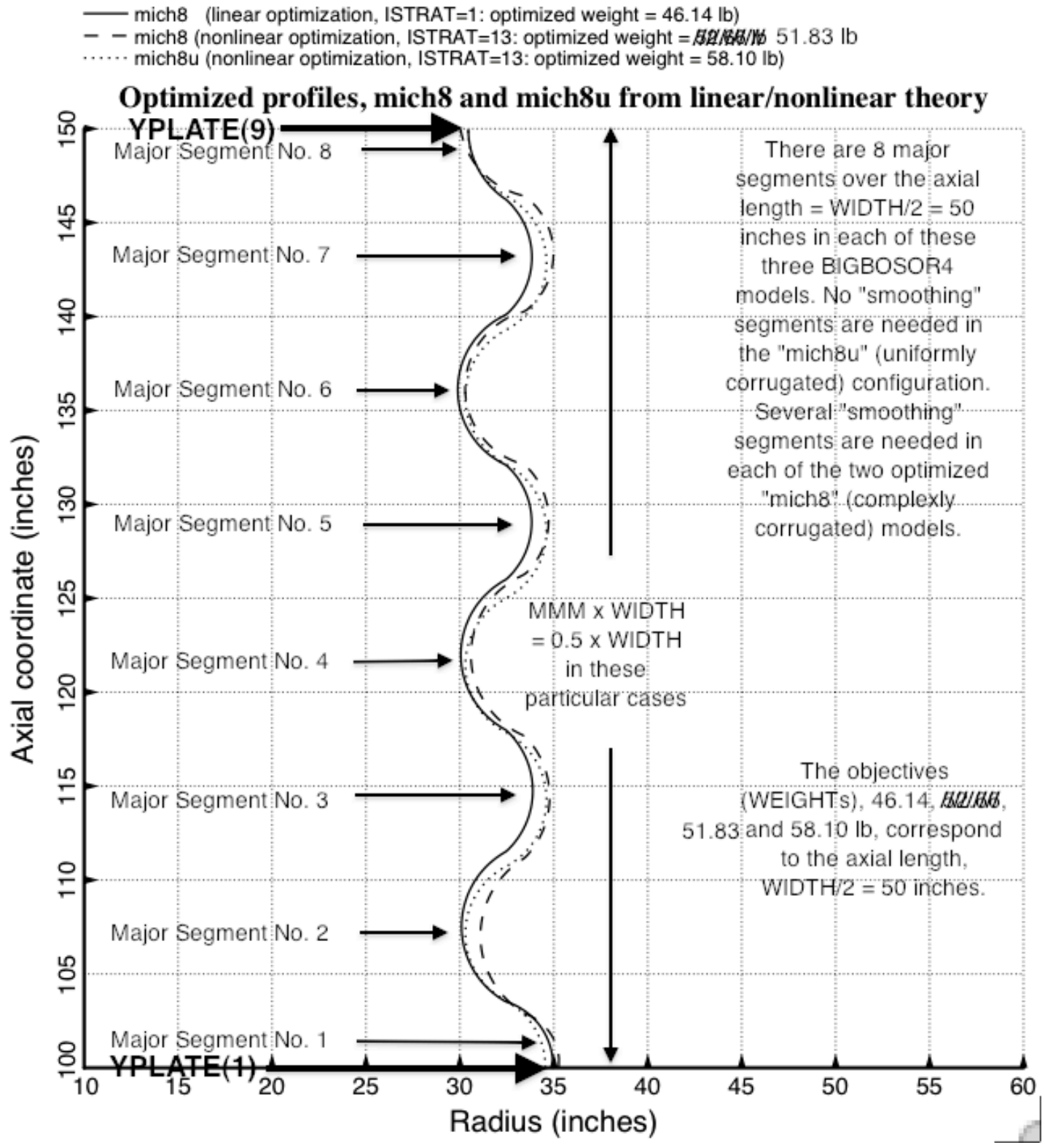

Fig. 27 **Optimized profiles of the specific cases, "mich8" (Tables 1 and 2) and "mich8u" (Table 3b)**

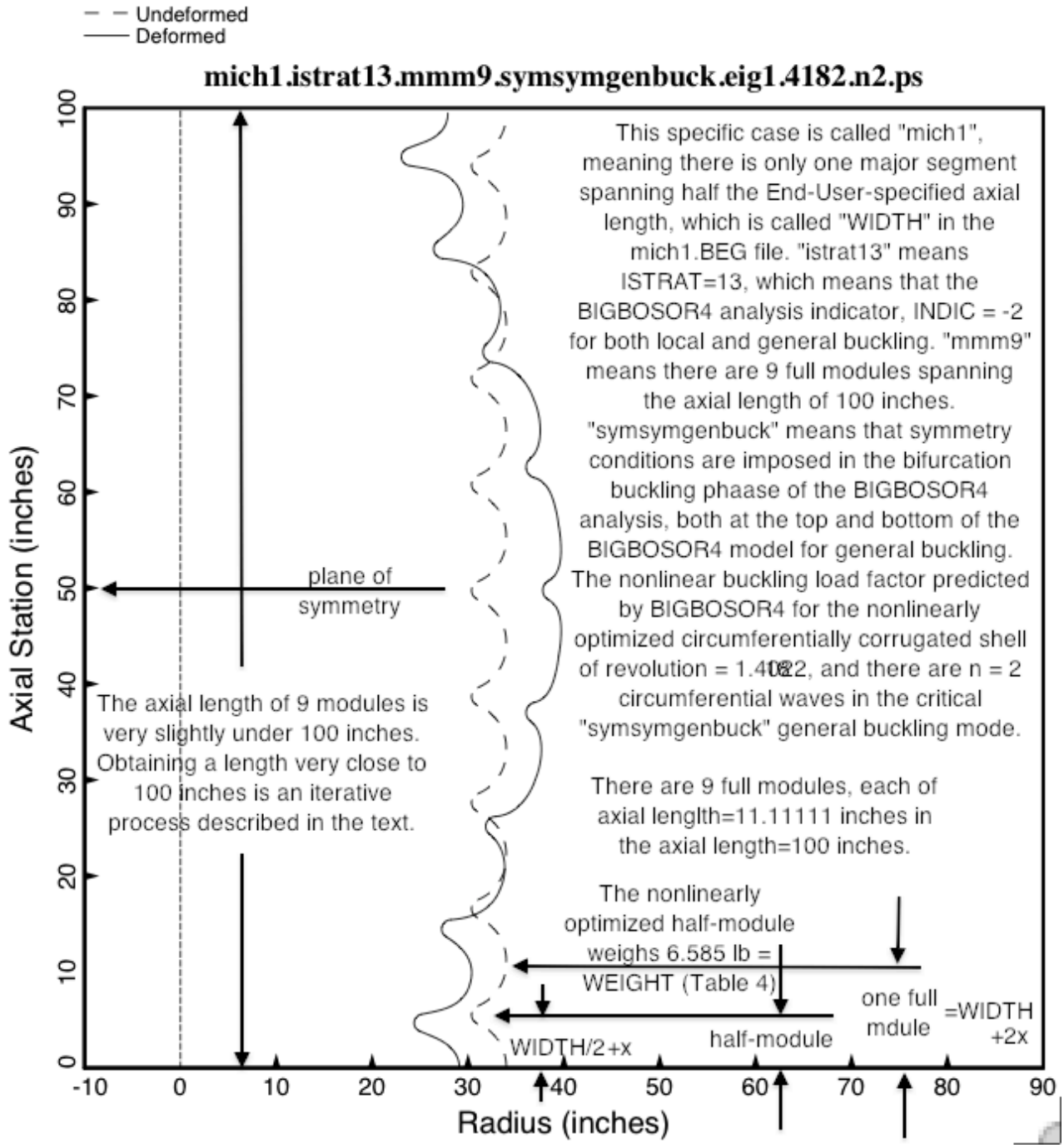

Fig. 28a **"Symsymgenbuck" nonlinear general buckling from BIGBOSOR4 of the nonlinearly optimized specific case called "mich1"**. This figure is analogous to Fig. 13a, which pertains to the nonlinearly optimized complexly corrugated shell called "mich8" and to Fig. 23a, which pertains to the nonlinearly optimized uniformly corrugated shell called "mich8u. As with the specific cases called "mich8" and "mich8u", this 100-inch-long "mich1" "symsymgenbuck" shell is one of the three BIGBOSOR4 nonlinear models ("symsymgenbuck", "symantigenbuck" and "antiantigenbuck") used during nonlinear optimization cycles for the prediction of nonlinear general buckling.

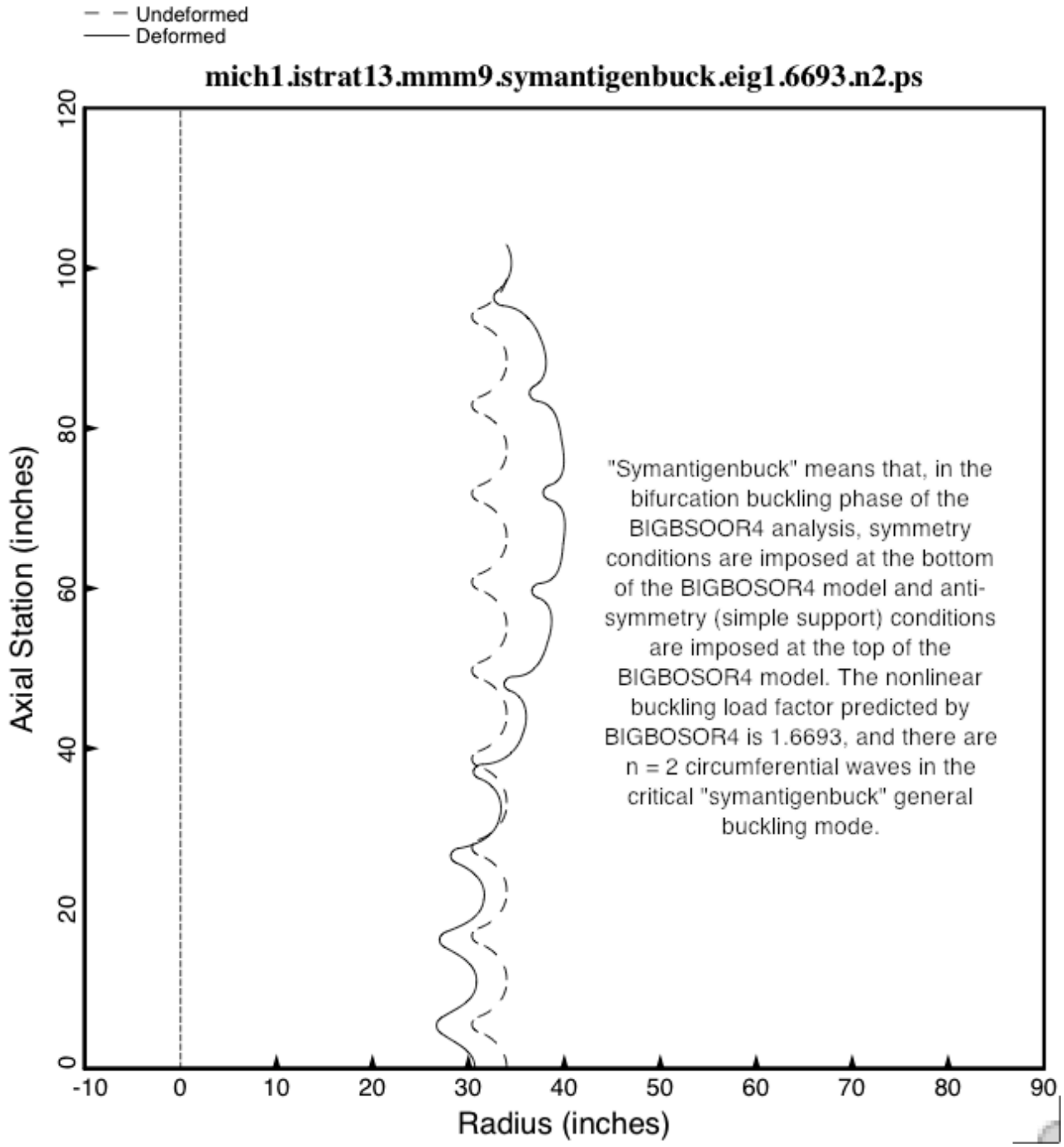

Fig. 28b **"Symantigenbuck" nonlinear general buckling from BIGBOSOR4 of the nonlinearly optimized specific case called "mich1"**. This figure is analogous to Fig. 13b, which pertains to the nonlinearly optimized complexly corrugated shell called "mich8" and to Fig. 23b, which pertains to the nonlinearly optimized uniformly corrugated shell called "mich8u. As with the specific cases called "mich8" and "mich8u", this 100-inch-long "mich1" "symantigenbuck" shell is one of the three BIGBOSOR4 nonlinear models ("symsymgenbuck", "symantigenbuck" and "antiantigenbuck") used during nonlinear optimization cycles for the prediction of nonlinear general buckling.

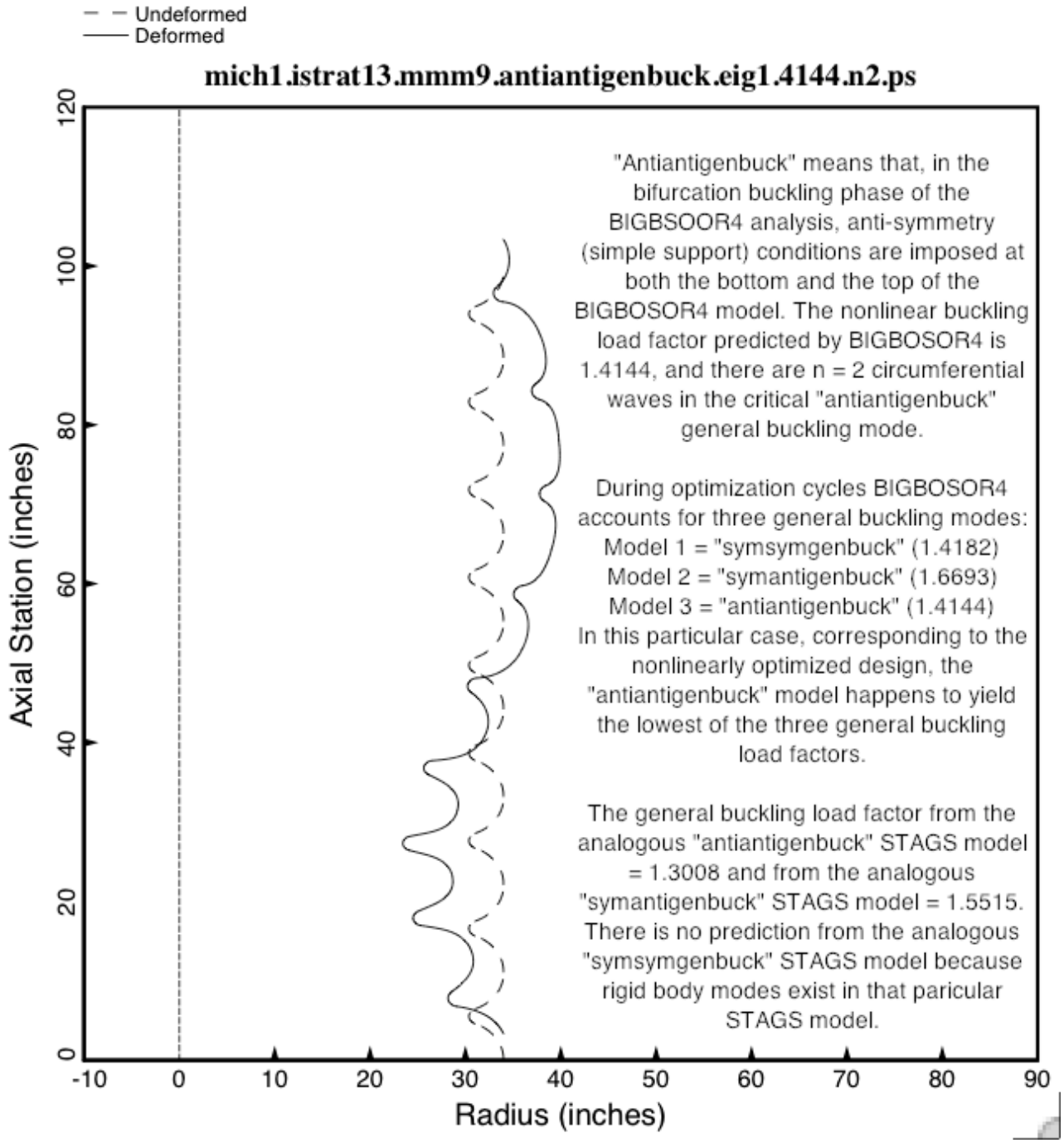

Fig. 28c **"Antiantigenbuck" nonlinear general buckling from BIGBOSOR4 of the nonlinearly optimized specific case called "mich1"**. This figure is analogous to Fig. 13c, which pertains to the nonlinearly optimized complexly corrugated shell called "mich8" and to Fig. 23c, which pertains to the nonlinearly optimized uniformly corrugated shell called "mich8u. As with the specific cases called "mich8" and "mich8u", this 100-inch-long "mich1" "antiantigenbuck" shell is one of the three BIGBOSOR4 nonlinear models ("symsymgenbuck", "symantigenbuck" and "antiantigenbuck") used during nonlinear optimization cycles for the prediction of nonlinear general buckling. There is fair agreement between BIGBOSOR4 and STAGS.

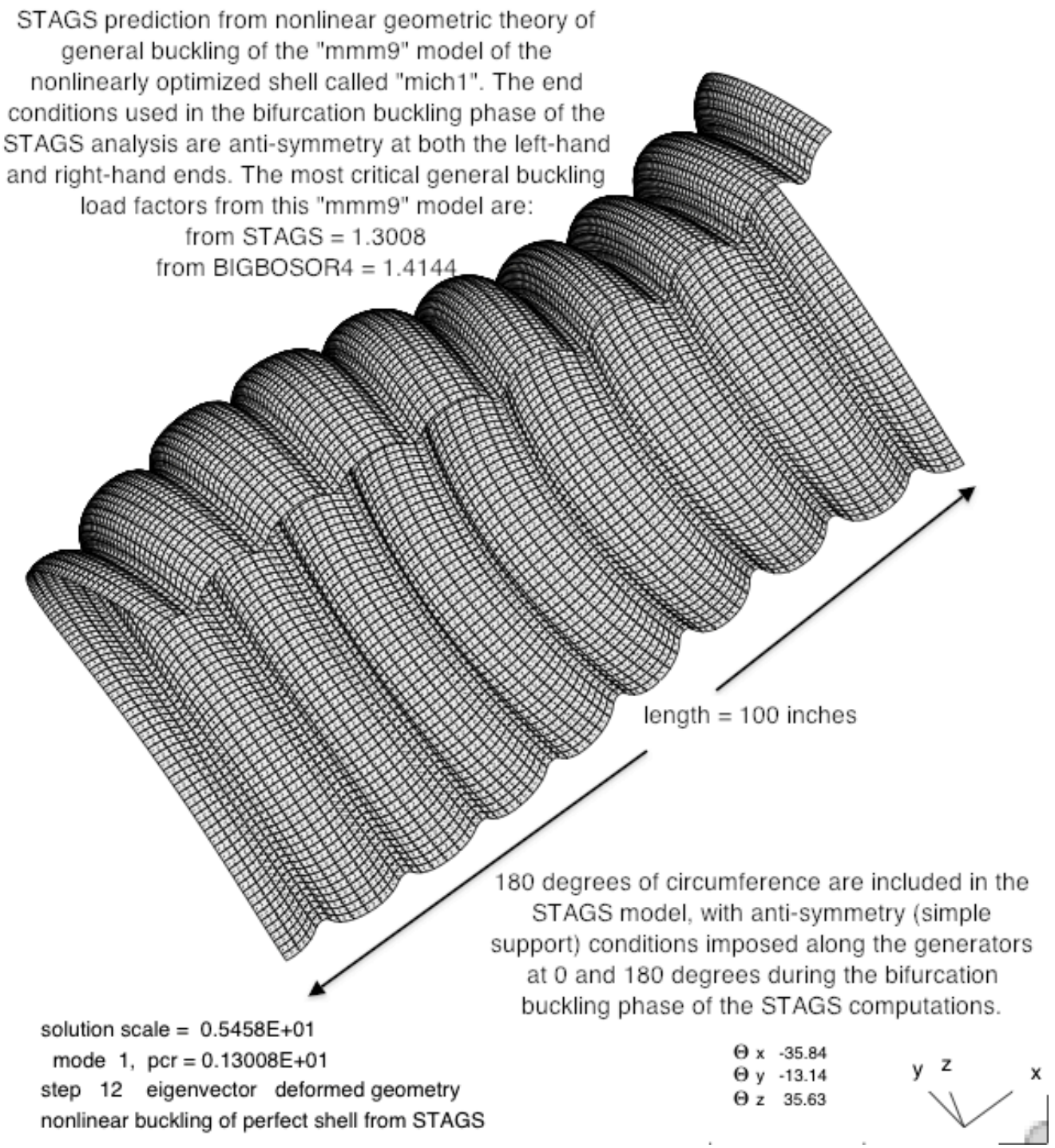

Fig. 29 **The prediction from STAGS of nonlinear general buckling for the nonlinearly optimized specific case called "mich1"**. Two nonlinear STAGS "mich1" models were analyzed: "symantigenbuck" (not included as a figure in this already very long paper) and "antiantigenbuck" (shown here). In this particular case the nonlinear "antiantigenbuck" STAGS model yields the more critical (lowest) nonlinear general buckling load factor. There is only fair agreement with the prediction of nonlinear "antiantigenbuck" general buckling obtained from BIGBOSOR4. (See Fig. 28c.)

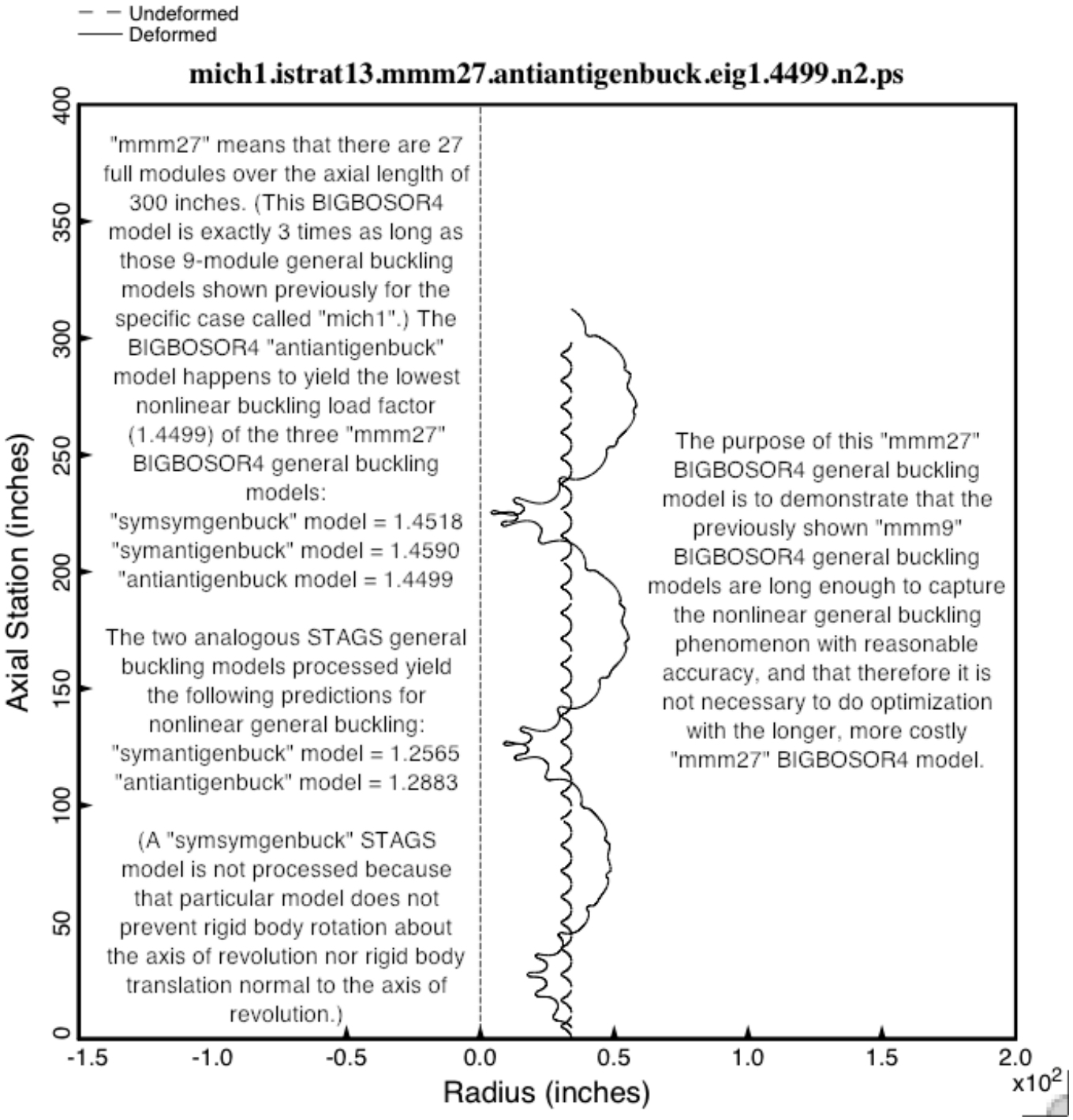

Fig. 30 **"Antiantigenbuck" from BIGBOSOR4 of the nonlinearly optimized specific case called "mich1"**. The purpose of this much longer "mmm27" "mich1" general buckling BIGBOSOR4 model is to prove that the much shorter "mmm9" "mich1" BIGBOSOR4 model displayed in Fig. 28c is long enough to predict with reasonable accuracy general buckling of the nonlinearly optimized "mich1" configuration, and that therefore it is not necessary to use such a long BIGBOSOR4 "mmm27" "mich1" model for optimization. There is only fair agreement between the predictions of BIGBOSOR4 and STAGS for nonlinear general buckling of "mich1".

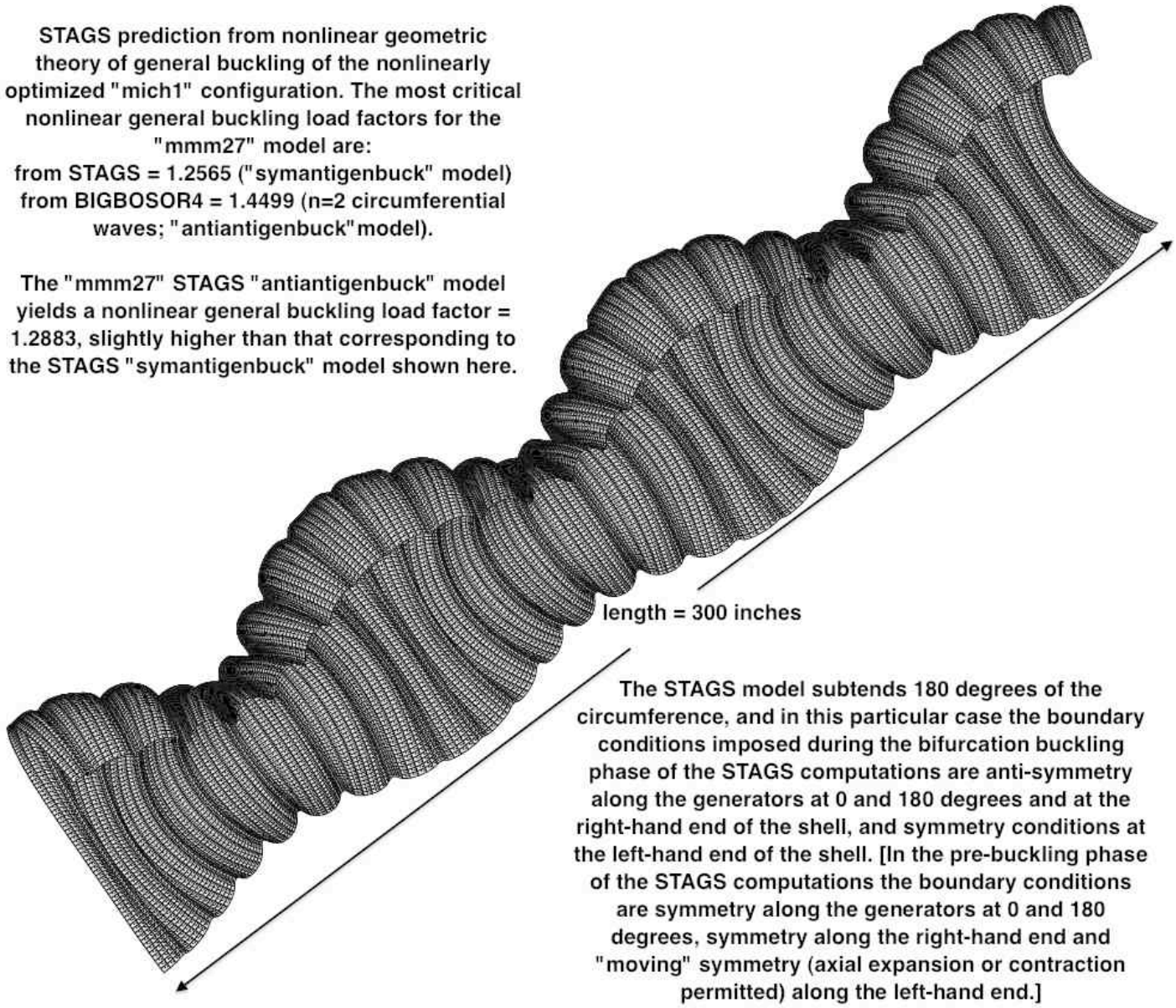

Fig. 31 **The prediction from STAGS of nonlinear general buckling for the nonlinearly optimized specific case called "mich1"** Two "mmm27" "mich1" nonlinear STAGS models were analyzed: "symantigenbuck" (shown here) and "antiantigenbuck" (not included as a figure in this already very long paper). In this particular case the nonlinear "symantigenbuck" STAGS model yields the more critical (lowest) nonlinear general buckling load factor. There is only fair agreement with the prediction of nonlinear general buckling obtained from the long "mmm27" "mich1" BIGBOSOR4 model. (See the previous figure.) It is proposed that the discrepancy arises because BIGBOSOR4 is based on an approximate "classical" (legacy) "moderately large" meridional rotation theory (sine and cosine of the meridional rotation replaced, respectively, by the meridional rotation and unity), whereas STAGS is based on an exact "co-rotational" theory [41] in which the rigid body component of a large displacement stores no energy.

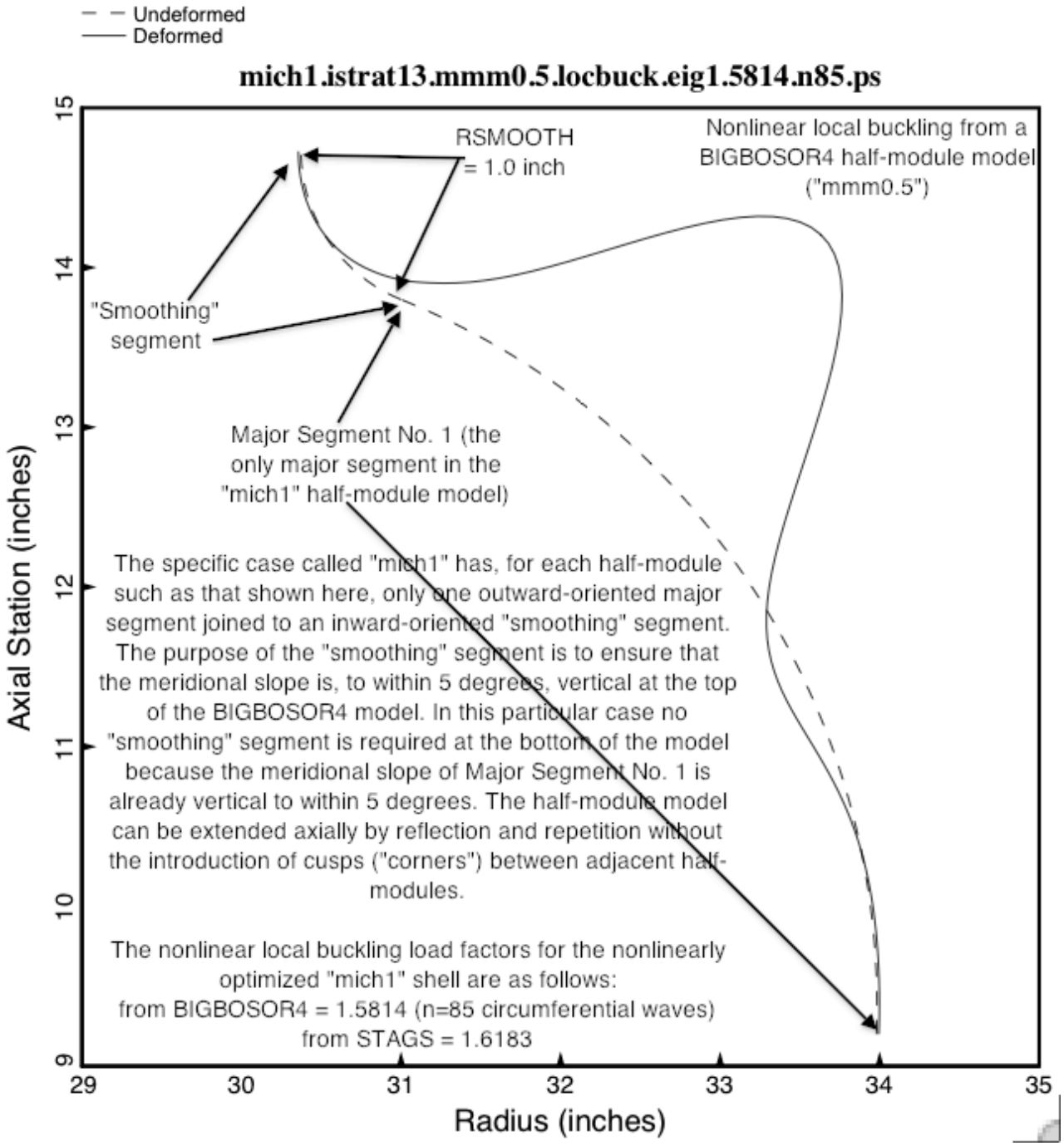

Fig. 32 **Nonlinear local buckling from BIGBOSOR4 of the nonlinearly optimized specific case called "mich1"**. This figure is analogous to Fig 11, which pertains to nonlinear local buckling of the nonlinearly optimized complexly corrugated shell called "mich8" and Fig. 25, which pertains to nonlinear local buckling of the nonlinearly optimized uniformly corrugated shell called "mich8u". Local buckling is computed with use of the so-called "**half-module**" model displayed here. The relationship between a "**half-module**" model and a model of the entire shell is demonstrated at the bottom of Fig. 28a. There is good agreement with the prediction from STAGS, both with respect to the nonlinear local buckling load factor and the local buckling mode shape.

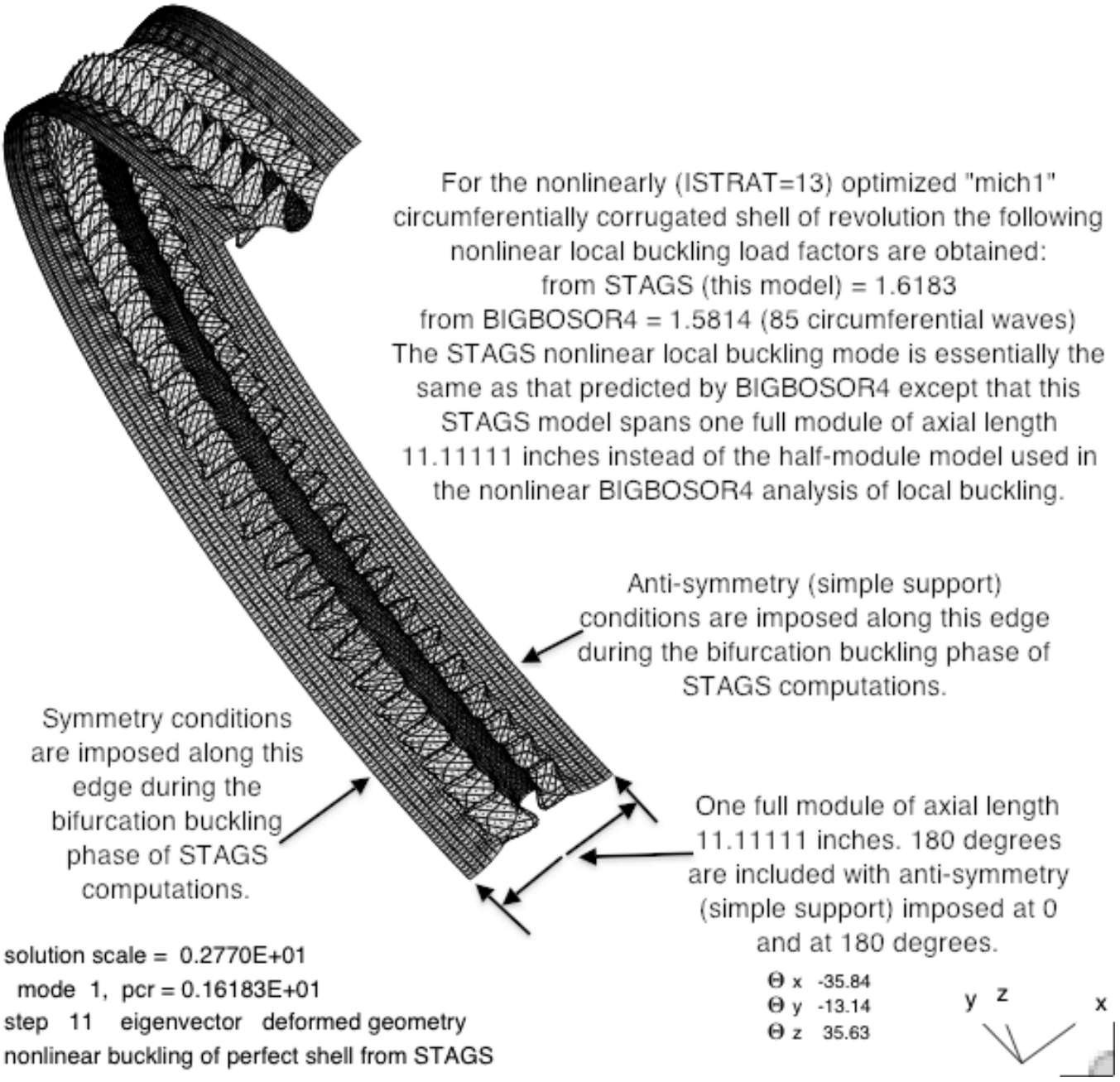

Fig. 33 **Nonlinear local buckling from STAGS of the nonlinearly optimized specific case called "mich1"**. This figure is analogous to Fig 12, which pertains to nonlinear local buckling of the nonlinearly optimized complexly corrugated shell called "mich8" and to Fig. 26, which pertains to nonlinear local buckling of the nonlinearly optimized uniformly corrugated shell called "mich8u". The relationship between a "full-module" model and a model of the entire shell is demonstrated at the bottom of Fig. 28a. There is good agreement with the prediction from BIGBOSOR4, both with respect to the nonlinear local buckling load factor and the mode shape.

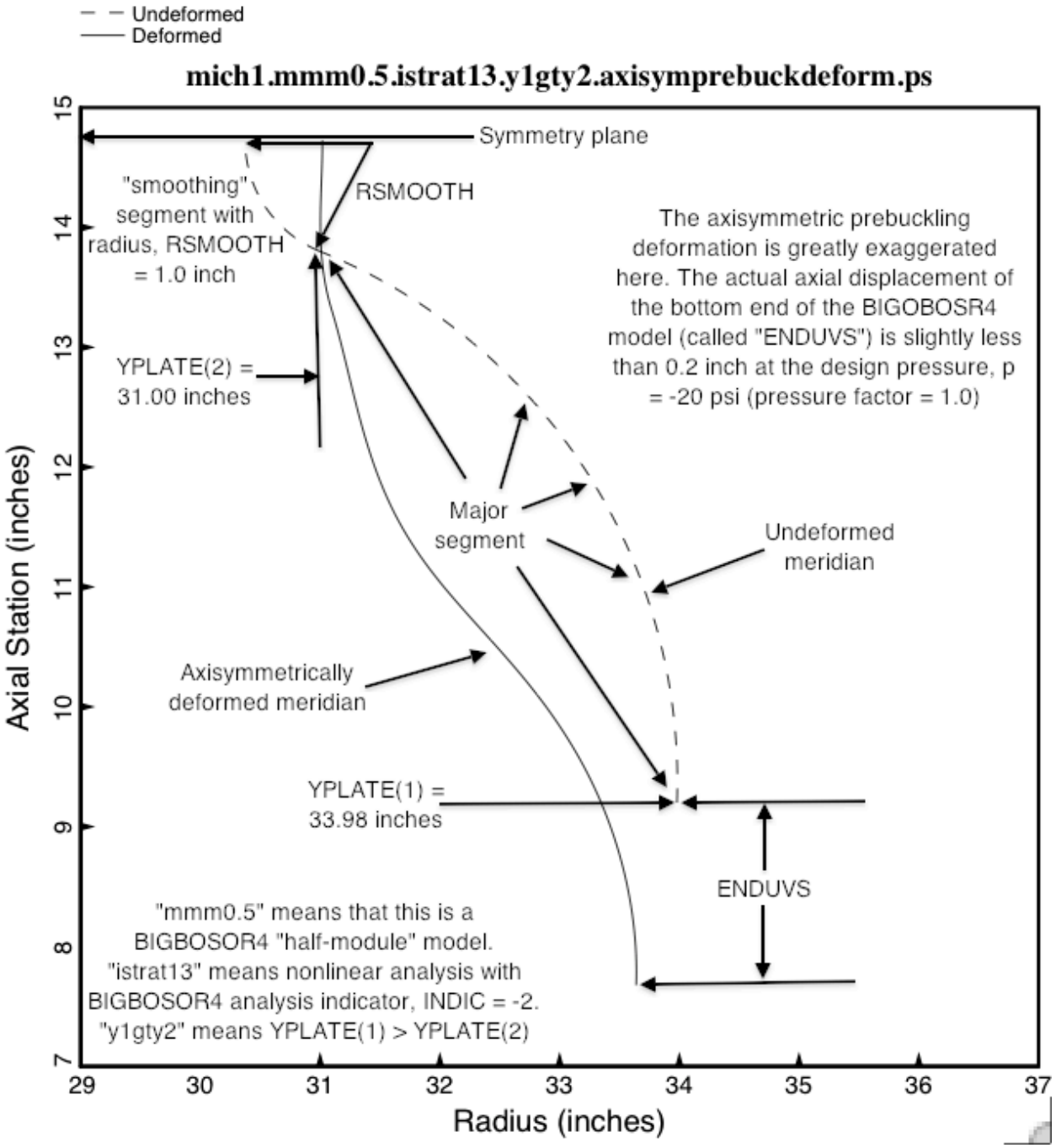

Fig. 34 **Axisymmetric pre-buckling deformation from BIGBOSOR4 of the nonlinearly optimized "mich1" configuration**. The optimized dimensions, the local and general buckling load factors, and the maximum effective stress for this nonlinearly optimized "mich1" shell wall profile are listed in Table 4. This figure is analogous to Fig. 10, which pertains to the nonlinearly optimized complexly corrugated specific case called "mich8". This configuration in which YPLATE(1) > YPLATE(2) expands in the axial direction under the applied uniform external lateral normal pressure, and the nonlinear load-ENDUVS curve exhibits a stiffening characteristic with increasing pressure, as shown in Fig. 36.

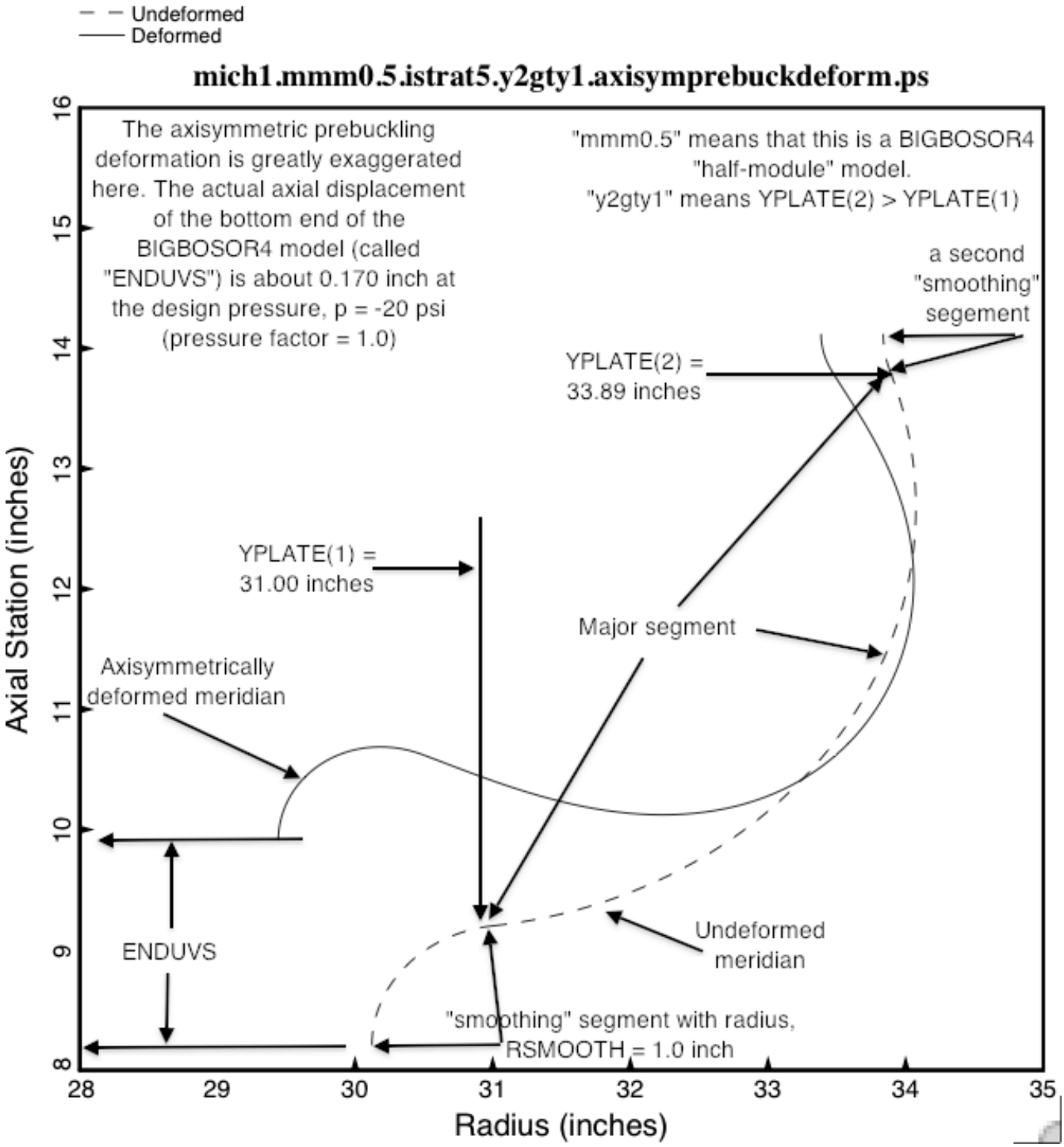

Fig. 35 **Axisymmetric pre-buckling deformation from BIGBOSOR4 of a nonlinearly optimized configuration analogous to the "mich1" configuration except that YPLATE(1) < YPLATE(2)**. This configuration in which YPLATE(1) < YPLATE(2) contracts in the axial direction under the applied uniform external lateral normal pressure, and the nonlinear load-ENDUVS curve exhibits a softening characteristic with increasing pressure, as shown in Fig. 36.

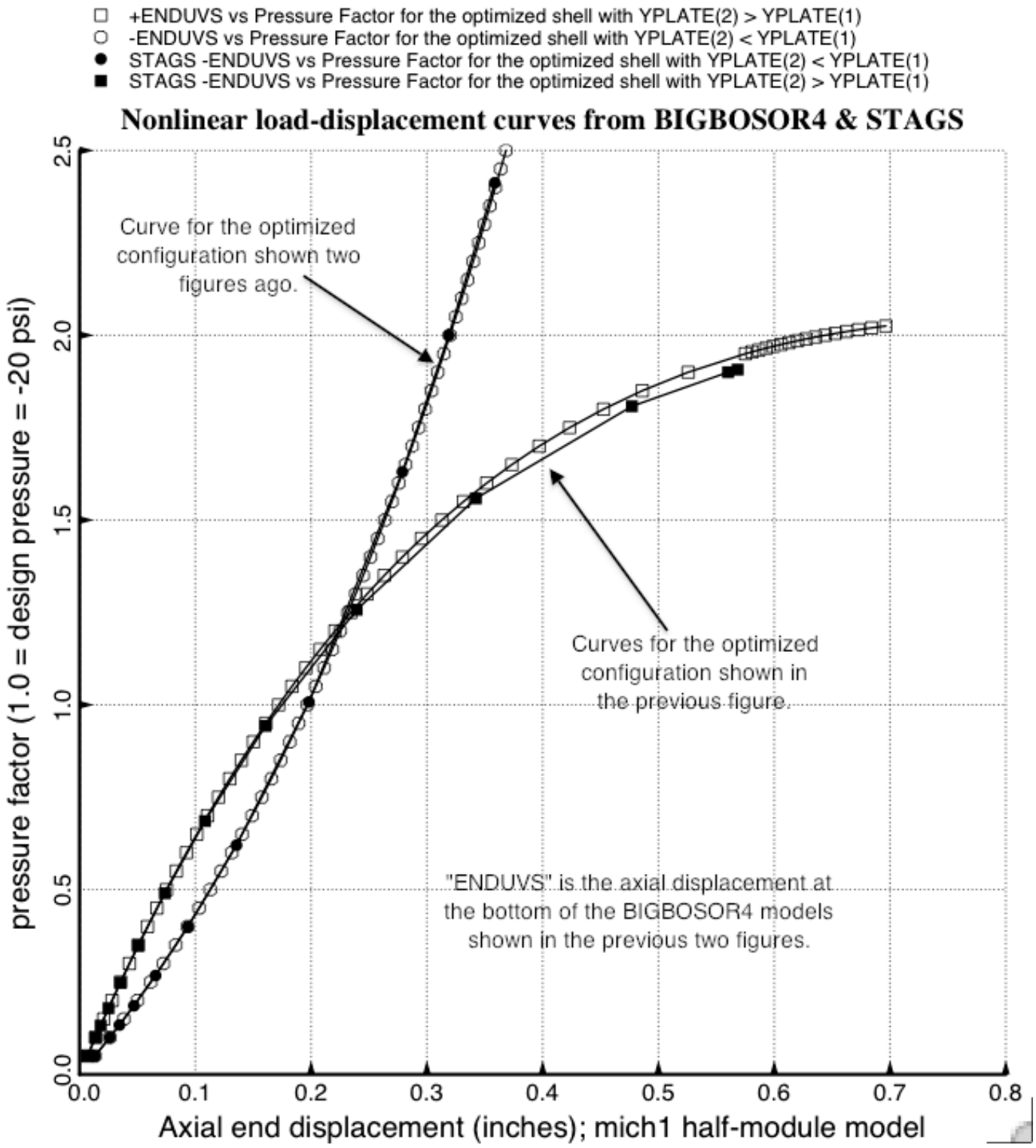

Fig. 36 **Pre-buckling nonlinear Load-ENDUVS curves for the configurations shown in the previous two figures**. There is good agreement between the axisymmetric pre-buckling predictions of BIGBOSOR4 and STAGS.

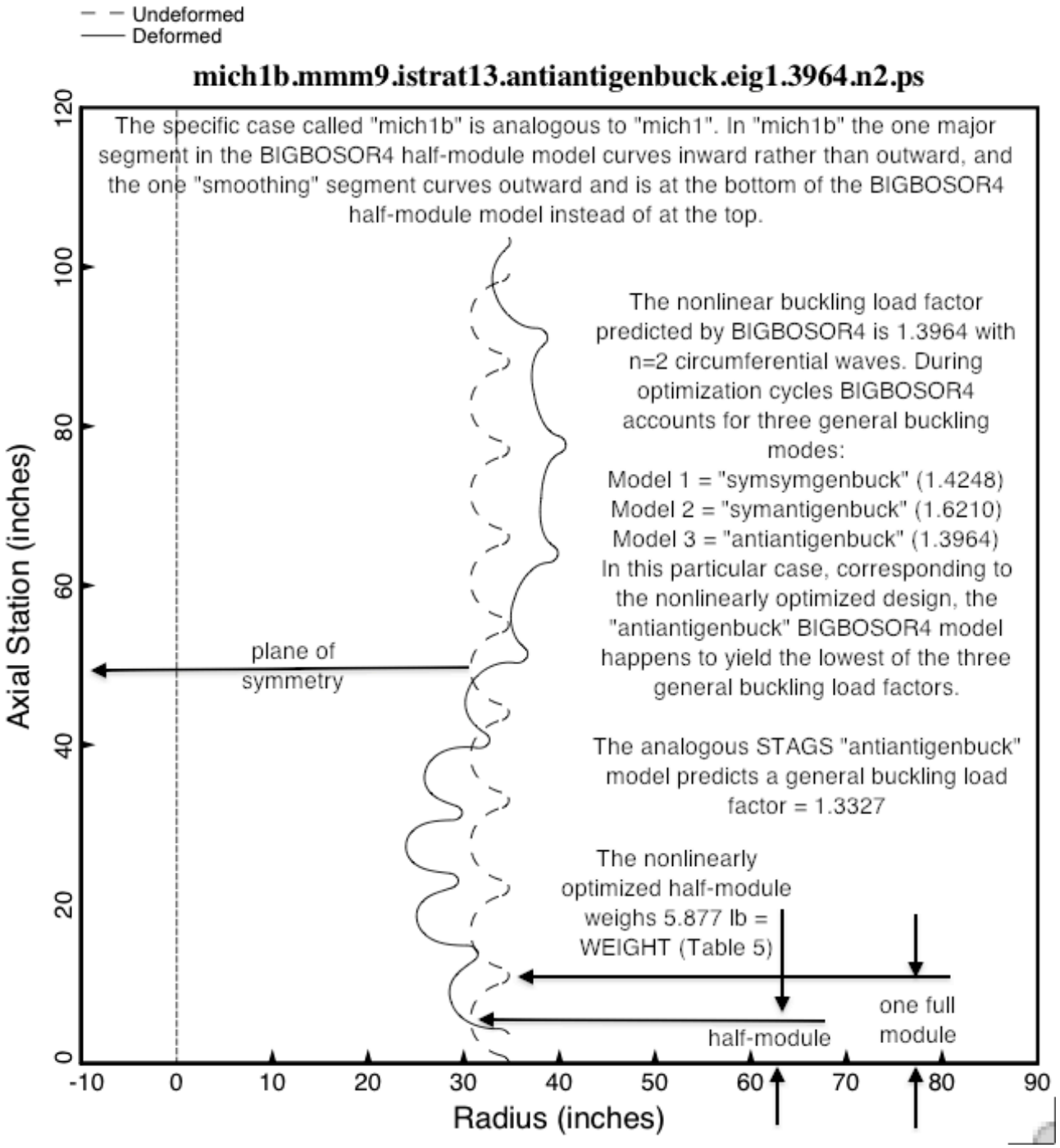

Fig. 37 **"Antiantigenbuck" nonlinear general buckling from BIGBOSOR4 of the nonlinearly optimized specific case called "mich1b"**. This figure is analogous to Fig. 28c, which pertains to the nonlinearly optimized shell called "mich1". As with the specific case called "mich1", this 100-inch-long "mich1b" "antiantigenbuck" shell is one of the three BIGBOSOR4 nonlinear models ("symsymgenbuck", "symantigenbuck" and "antiantigenbuck") used during nonlinear optimization cycles for the prediction of nonlinear general buckling. There is fair agreement between BIGBOSOR4 and STAGS.

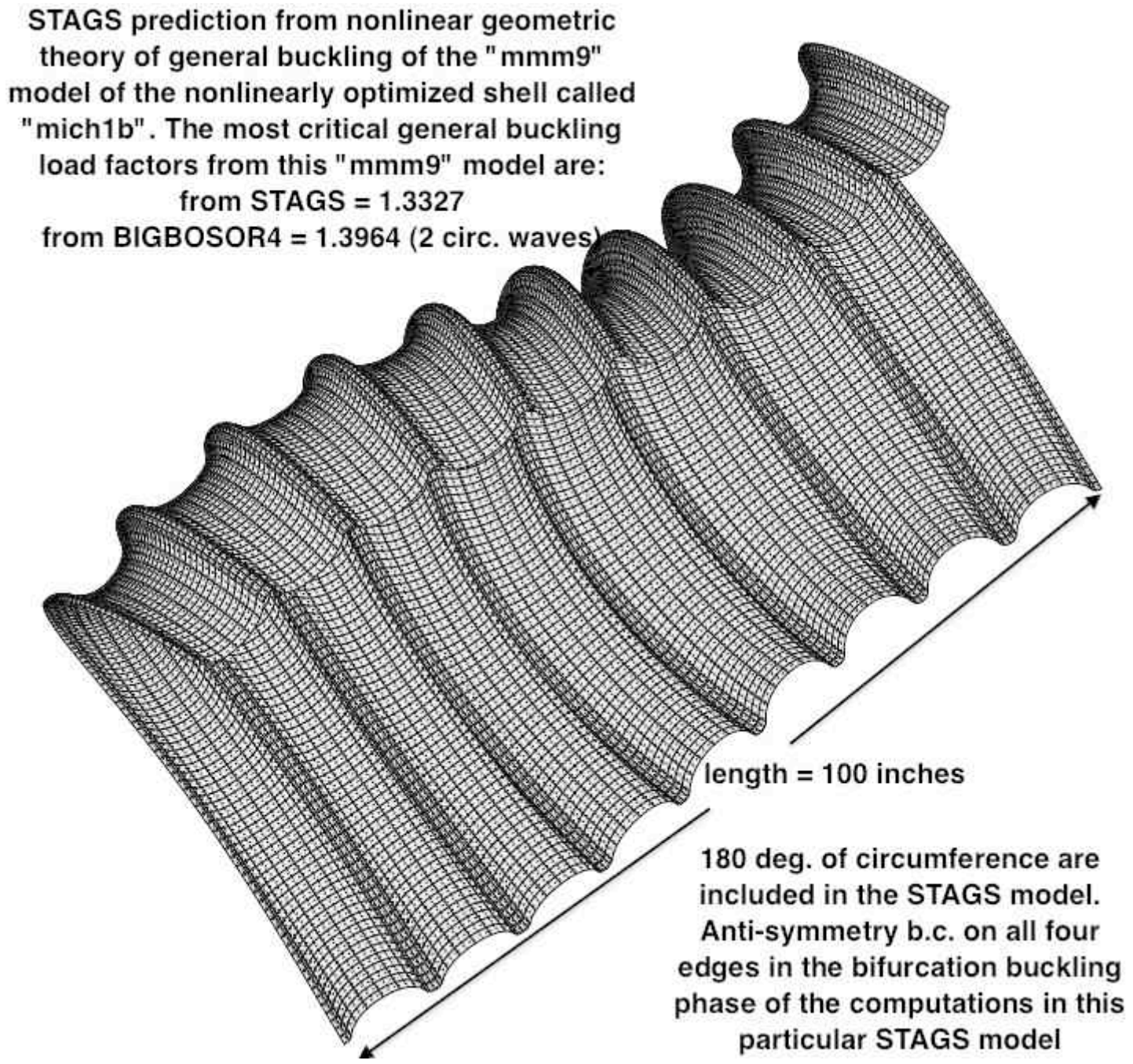

Fig. 38 **The prediction from STAGS of nonlinear general buckling for the nonlinearly optimized specific case called "mich1b"**. This figure is analogous to Fig. 29, which pertains to the nonlinearly optimized "mich1" configuration. Two nonlinear STAGS "mich1b" models were analyzed: "symantigenbuck" (not included as a figure in this already very long paper) and "antiantigenbuck" (shown here). In this particular case the nonlinear "antiantigenbuck" STAGS model yields the more critical (lowest) nonlinear general buckling load factor. There is fair agreement with the prediction of nonlinear "antiantigenbuck" general buckling obtained from BIGBOSOR4. (See Fig. 37.)

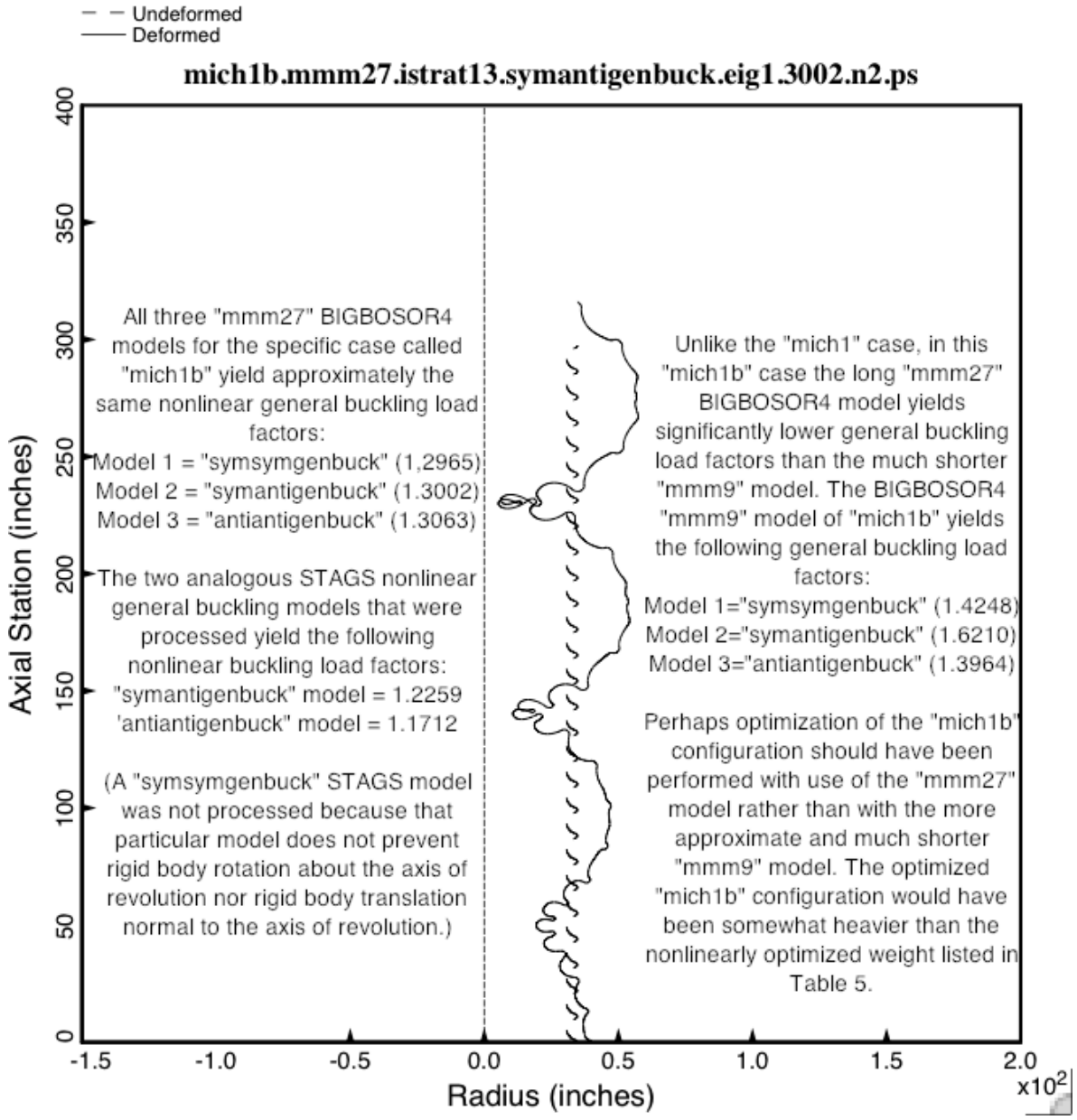

Fig. 39 **"Symantigenbuck" from BIGBOSOR4 of the nonlinearly optimized specific case called "mich1b"**. This figure is analogous to Fig. 30, which pertains to the specific case called "mich1". The purpose of this long "mmm27" "mich1b" general buckling BIGBOSOR4 model is to attempt to prove that the much shorter "mmm9" "mich1b" BIGBOSOR4 model displayed in Fig. 37 is long enough to predict with reasonable accuracy general buckling of the nonlinearly optimized "mich1b" configuration, as was done for the nonlinearly optimized "mich1" configuration, and that therefore it would not be necessary to use such a long BIGBOSOR4 "mmm27" "mich1b" model for optimization. However, as is seen from the BIGBOSOR4 predictions listed in this figure, there exist fairly significant differences between the three predictions from the "mmm9" model and those from the "mmm27" model. The "mich1b" shell was therefore re-optimized with use of the "mmm27" general buckling model in the optimization loop. Results are listed at the bottom of Table 5. There is only fair agreement between the predictions of BIGBOSOR4 and STAGS for nonlinear general buckling of "mich1b".

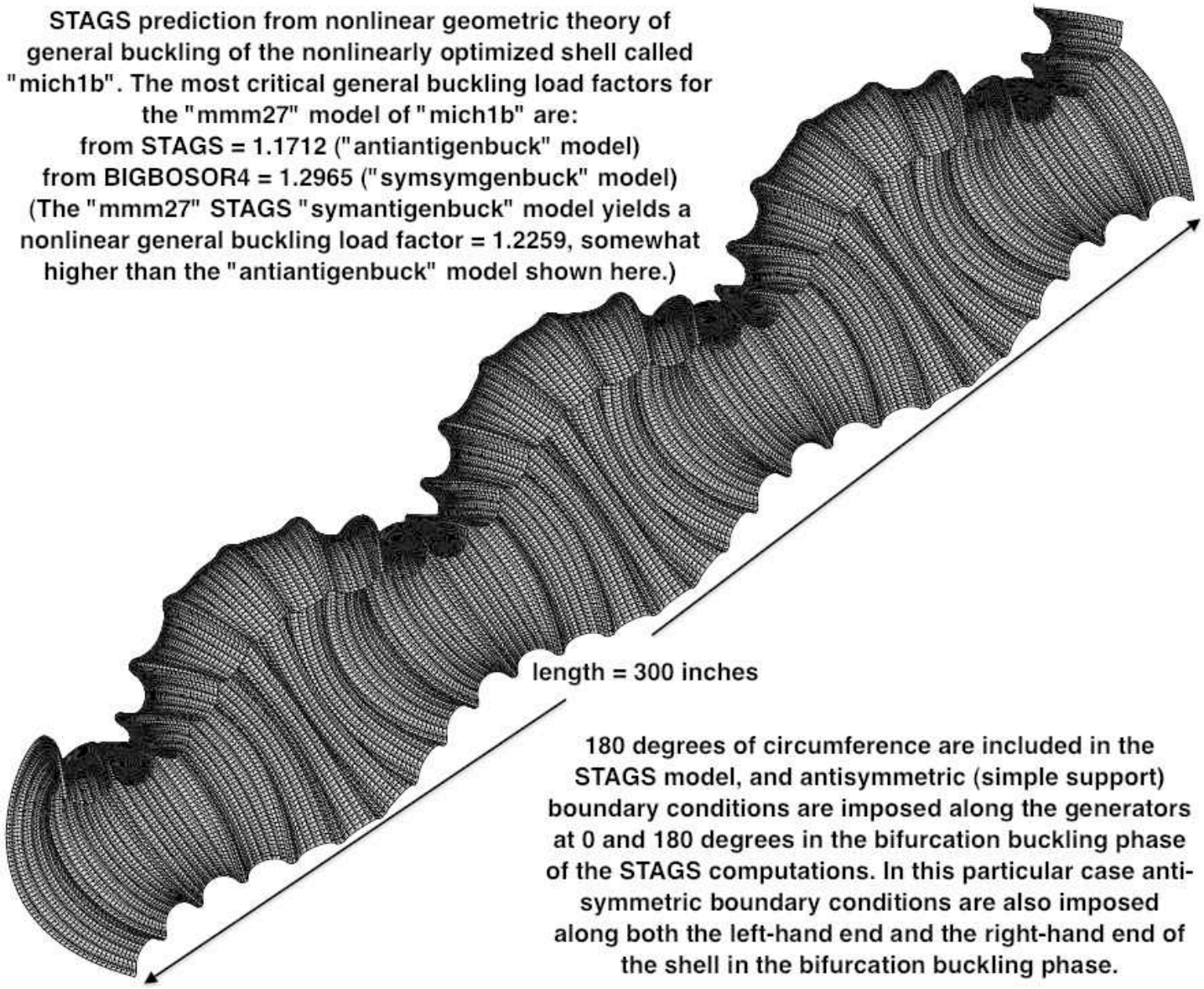

Fig. 40 **The prediction from STAGS of nonlinear general buckling for the nonlinearly optimized specific case called "mich1b".** This figure is analogous to Fig. 31, which pertains to the "mich1" configuration. Two "mmm27" "mich1b" nonlinear STAGS models were analyzed: "symantigenbuck" (not included as a figure in this already very long paper) and "antiantigenbuck" (shown here). In this particular case the nonlinear "antiantigenbuck" STAGS model yields the more critical (lowest) nonlinear general buckling load factor. There is only fair agreement with the prediction of nonlinear general buckling obtained from the long "mmm27" "mich1b" BIGBOSOR4 model. (See the previous figure.)

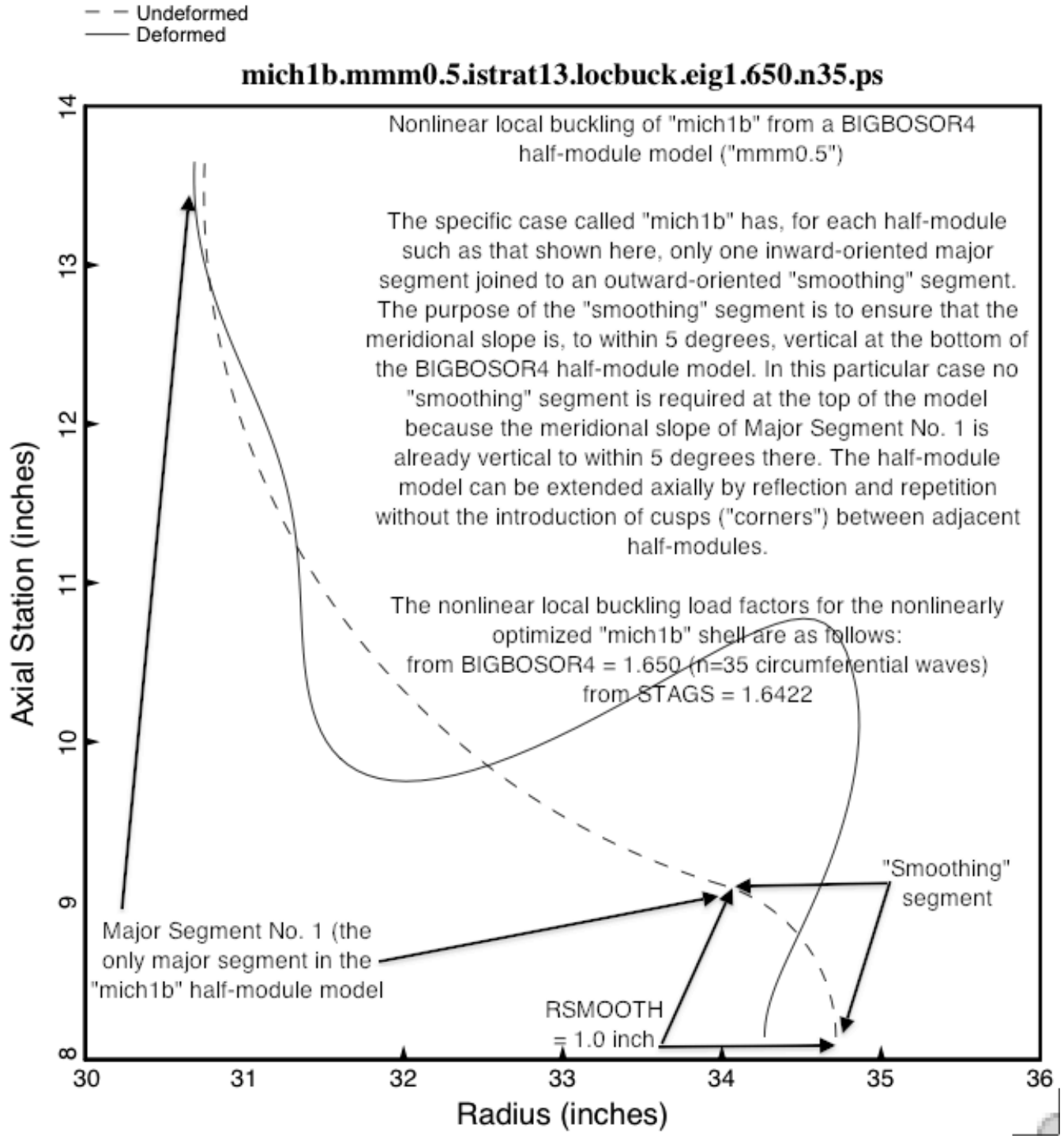

Fig. 41 **Nonlinear local buckling from BIGBOSOR4 of the nonlinearly optimized specific case called "mich1b"**. This figure is analogous to Fig 32, which pertains to nonlinear local buckling of the nonlinearly optimized shell called "mich1". The relationship between this "half-module" model and the complete "mich1b" shell is demonstrated at the bottom of Fig. 37. There is good agreement with the prediction from STAGS, both with respect to the nonlinear local buckling load factor and the mode shape.

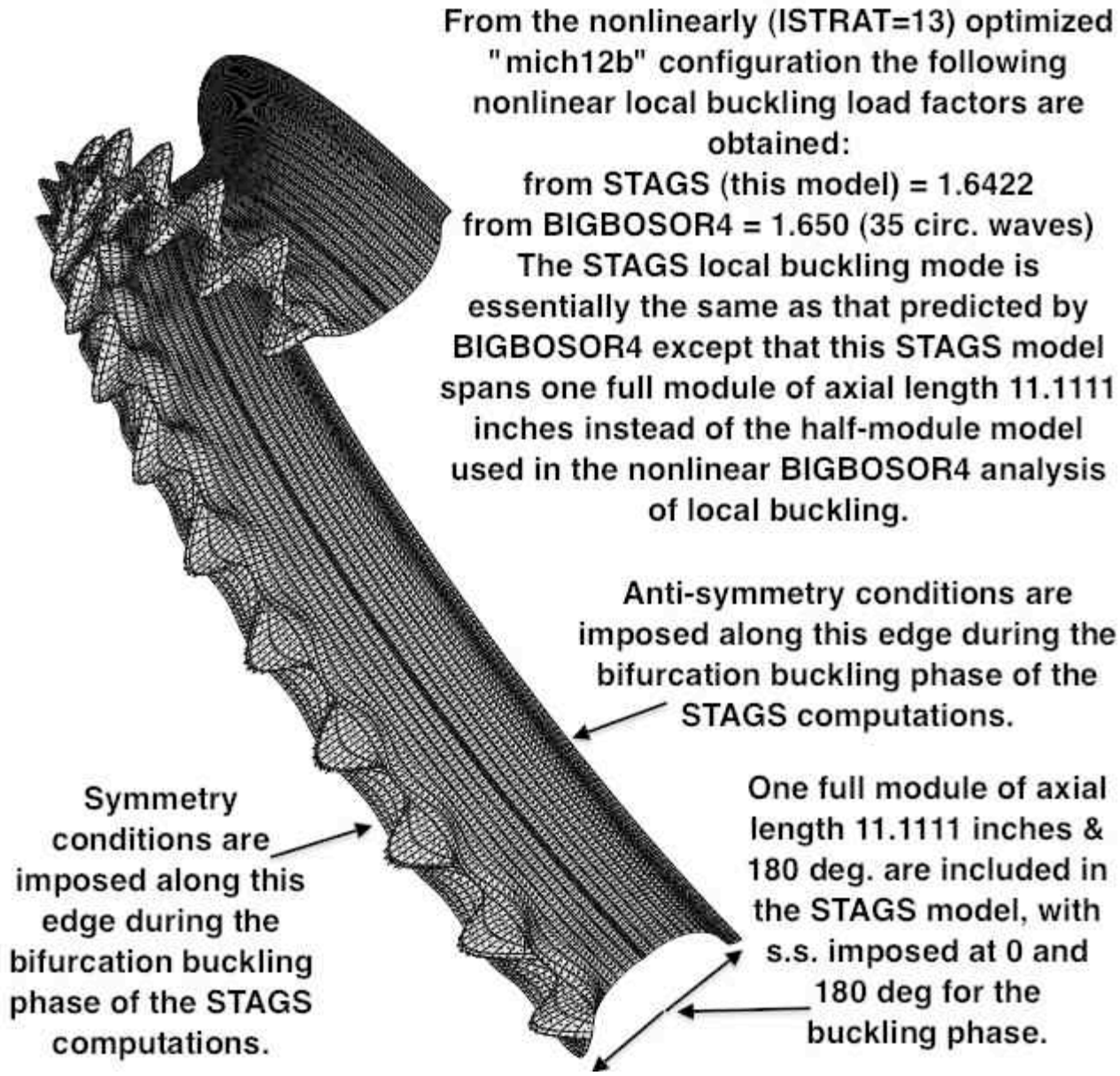

Fig. 42 **Nonlinear local buckling from STAGS of the nonlinearly optimized specific case called "mich1b"**. This figure is analogous to Fig. 33, which pertains to nonlinear local buckling of the nonlinearly optimized shell called "mich1". There is good agreement with the prediction from BIGBOSOR4, both with respect to the nonlinear local buckling load factor and the mode shape. (See Fig. 41.) The relationship between this "one-full-module" model and the complete "mich1b" shell is demonstrated at the bottom of Fig. 37.

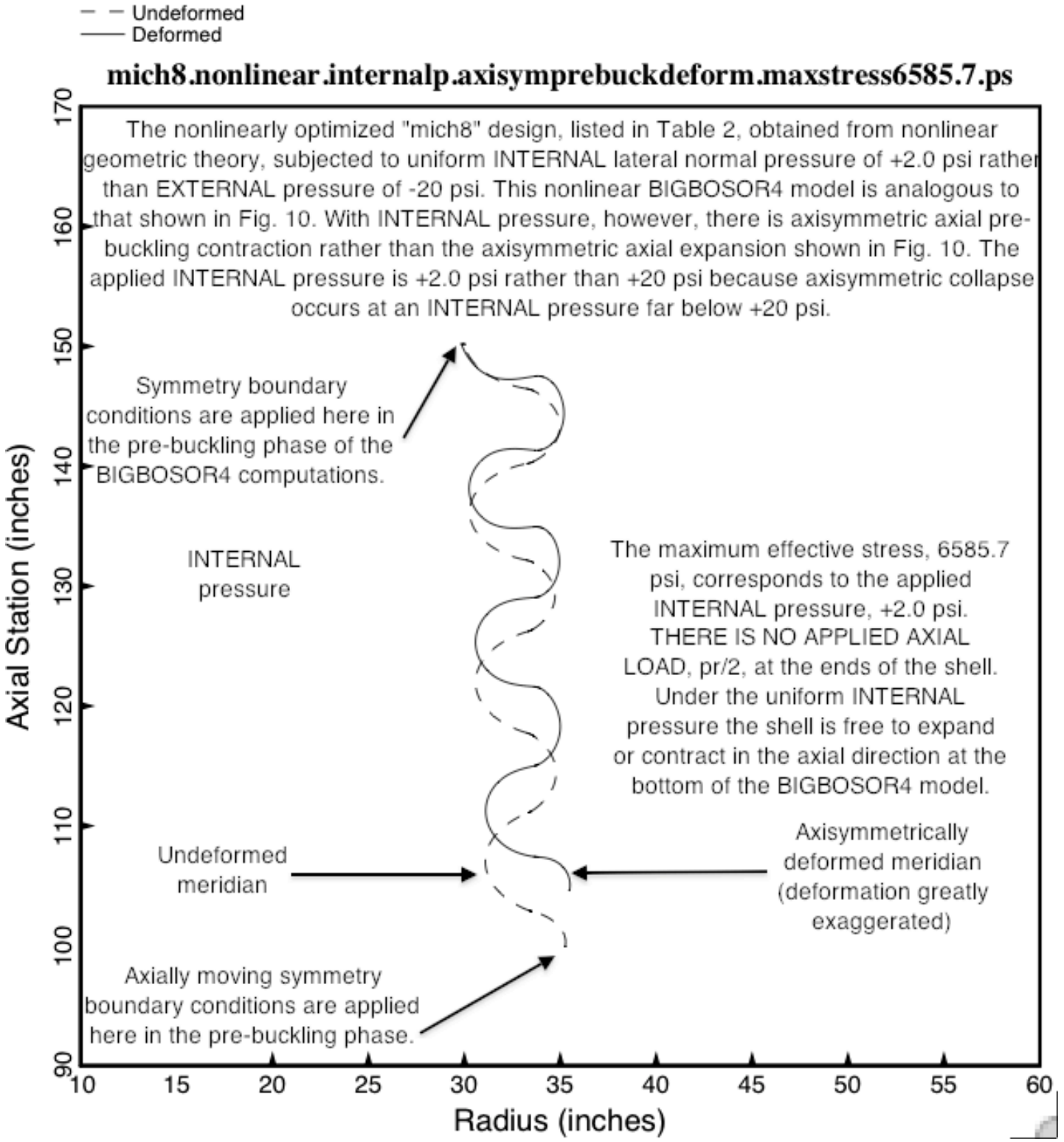

Fig. 43 **Axisymmetric prebuckling behavior of the INTERNALLY pressurized "mich8" shell**, the properties of which are listed in Table 2. Compare this figure with Fig. 10, for which the pressure is external.

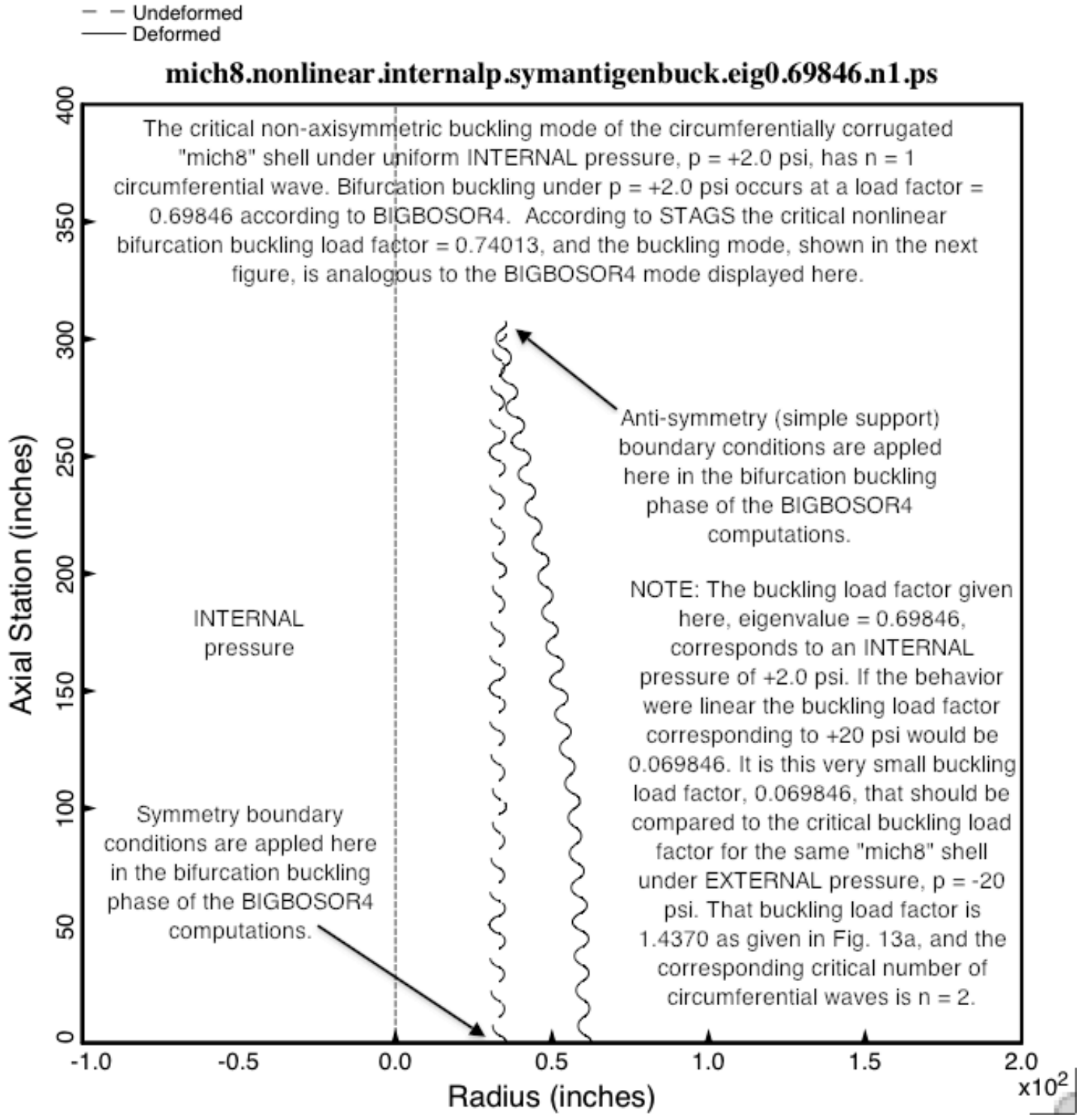

Fig. 44 **The critical buckling mode and load factor for the INTERNALLY pressurized "mich8" shell**, the properties of which are listed in Table 2. Compare the BIGBOSOR4 predictions give in this figure with those given in Figs. 13a,b,c for the same shell subjected to external pressure.

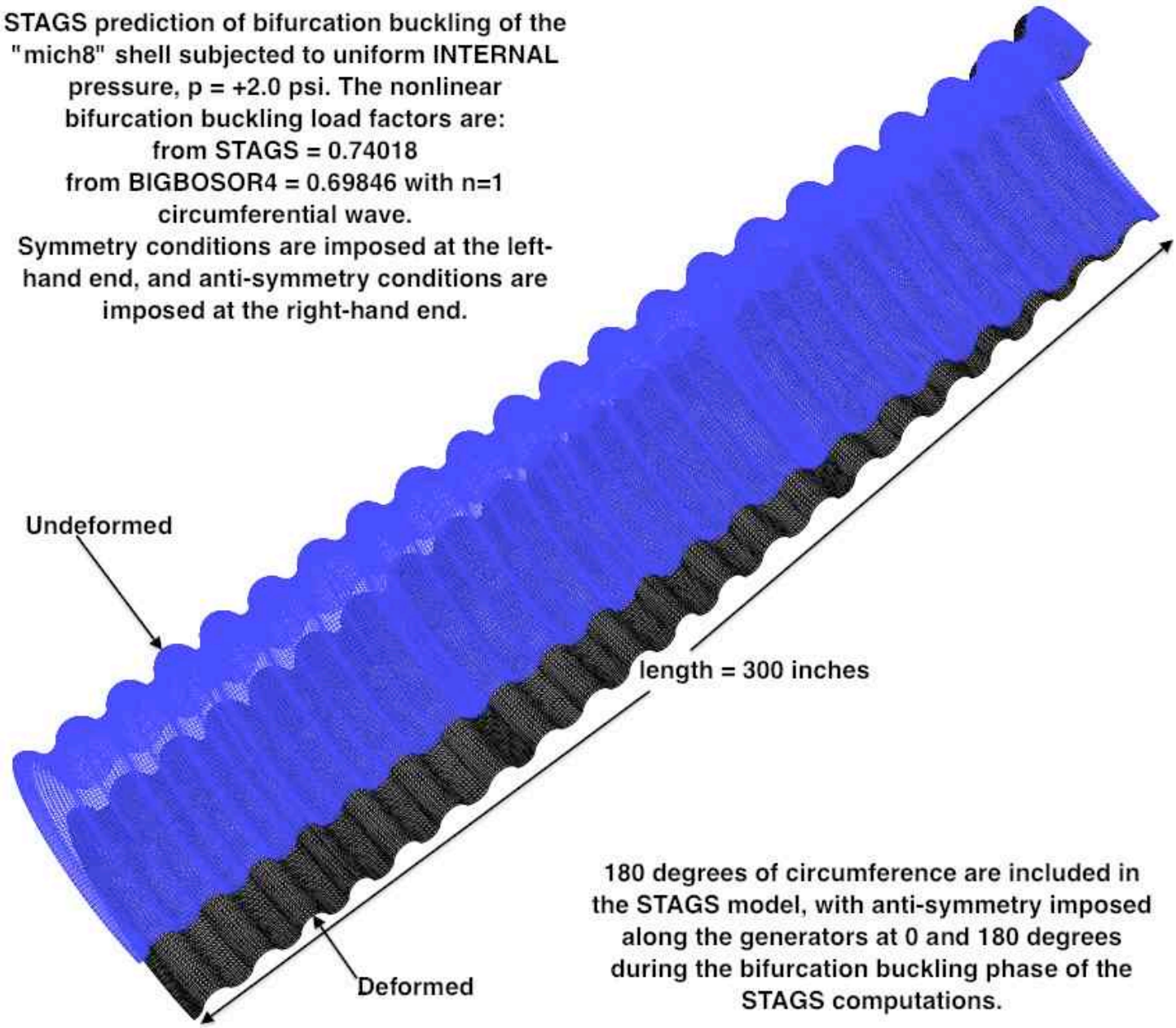

Fig. 45 **STAGS prediction of general buckling of the "mich8" shell under uniform INTERNAL pressure**. Compare with the BIGBOSOR4 prediction given in the previous figure.

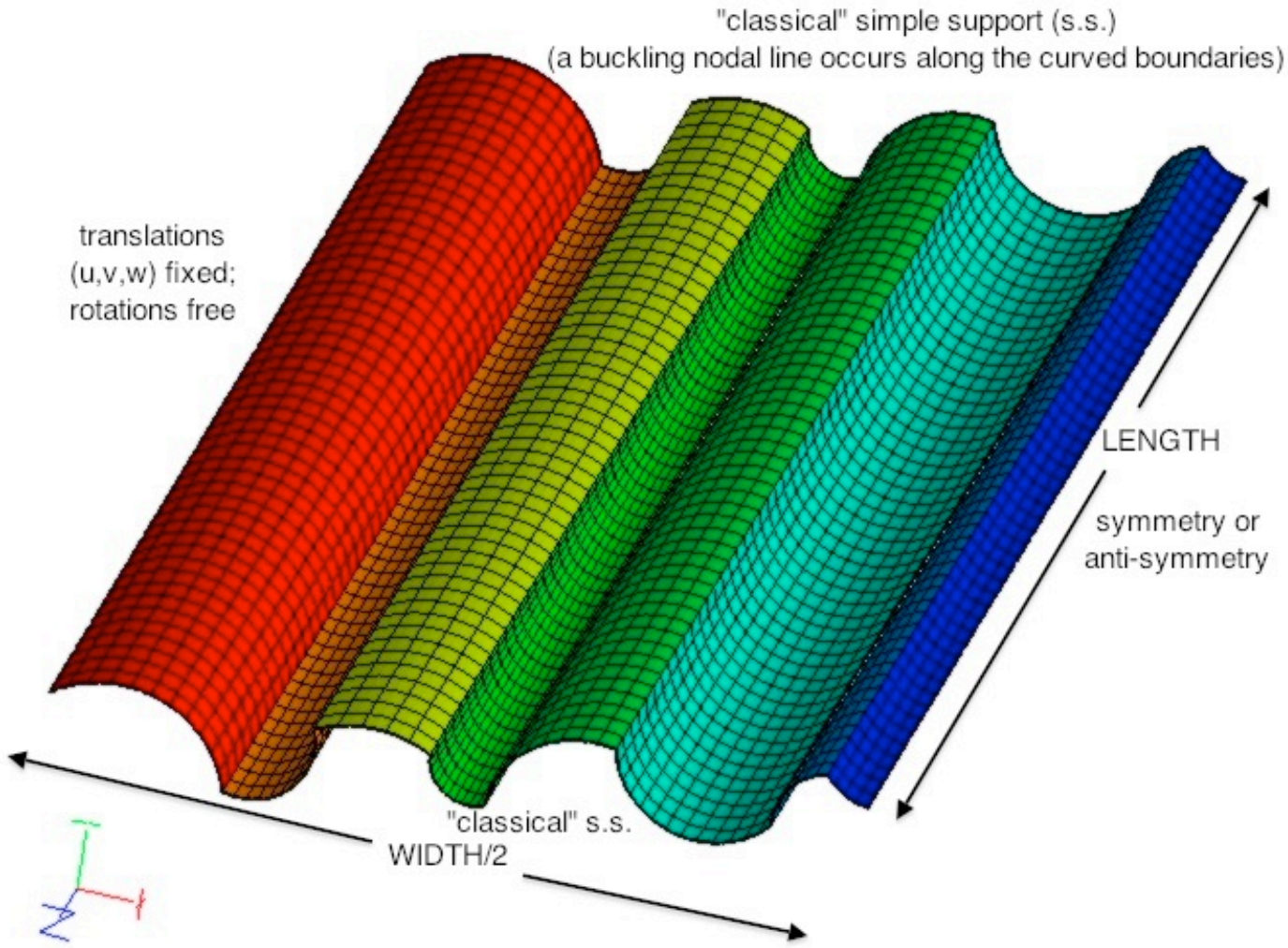

Fig A1 This figure is taken from [1], where it appears as Fig. 20a. Rather than longitudinally complexly corrugated prismatic panels, we study in the present paper circumferentially complexly corrugated shells of revolution such as that shown in Fig. 1.

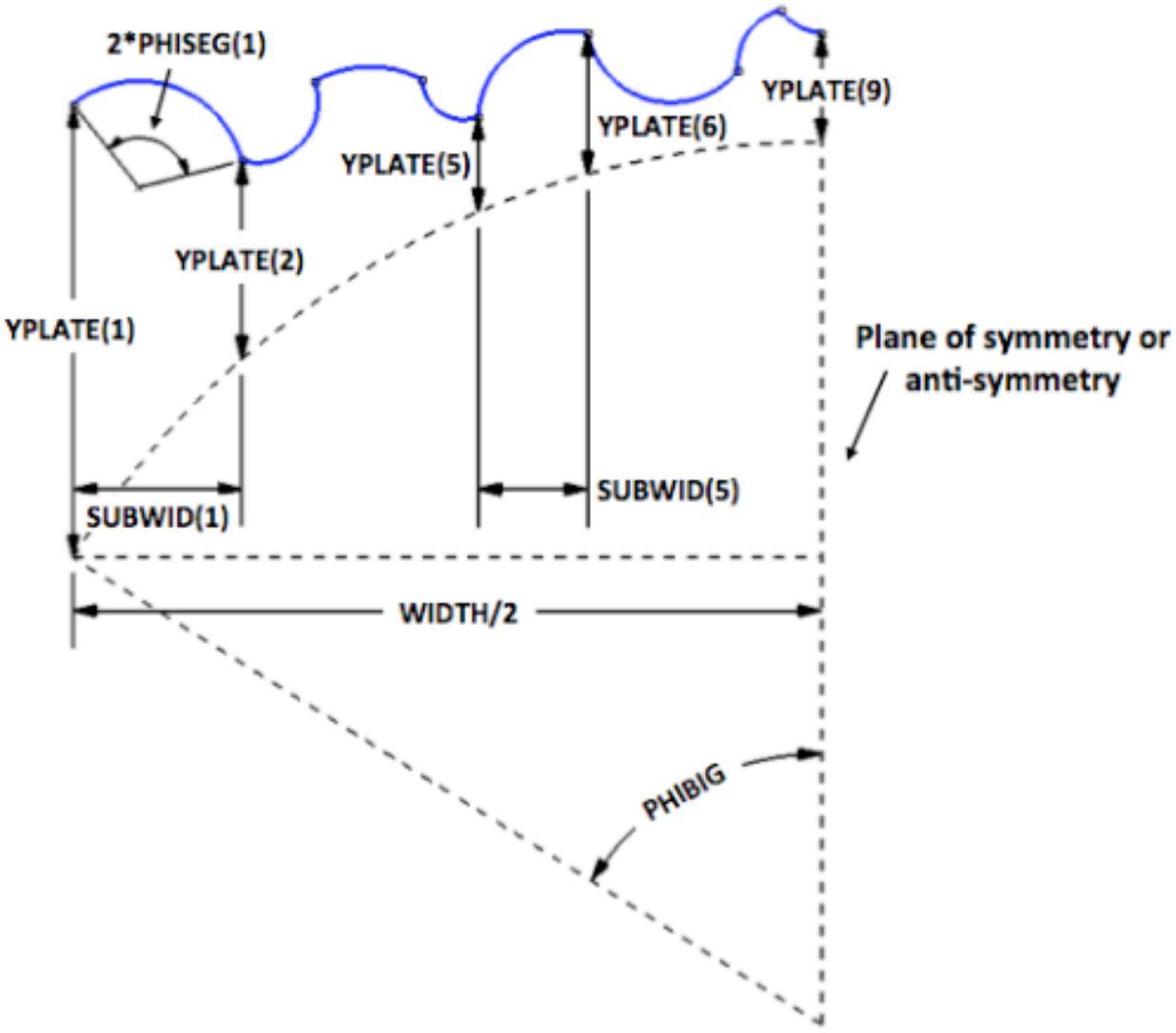

Fig. A2 This figure is taken from [1], where it is called Fig. 2. The decision variable candidates used in the present paper on circumferentially complexly corrugated shells of revolution have the same names as those given here, which apply to a longitudinally complexly corrugated prismatic panel. To convert the prismatic configuration shown here to the analogous circumferentially complexly corrugated shell of revolution, rotate the image in-plane clockwise by 90 degrees, then flip it over so that YPLATE(1) becomes the radius from the axis of revolution to the shell reference surface at the bottom of the transformed model and YPLATE(9) is the radius from the axis of revolution to the shell reference surface at the top of the transformed model (when the variable PHIBIG is zero or vanishingly small). (See Fig. A2b.) The horizontal dashed line of length WIDTH/2 becomes the axis of revolution in the transformed model. In the models treated in the present paper there is no overall arching created by a finite PHIBIG. PHIBIG is always set equal to a very small number (0.01 degrees). Therefore, the YPLATE(i), i=1, 2, …, NSEG+1 are the radii from the axis of revolution to the shell reference surface at the junctions between major segments and at the two ends (bottom and top) of the shell of revolution.

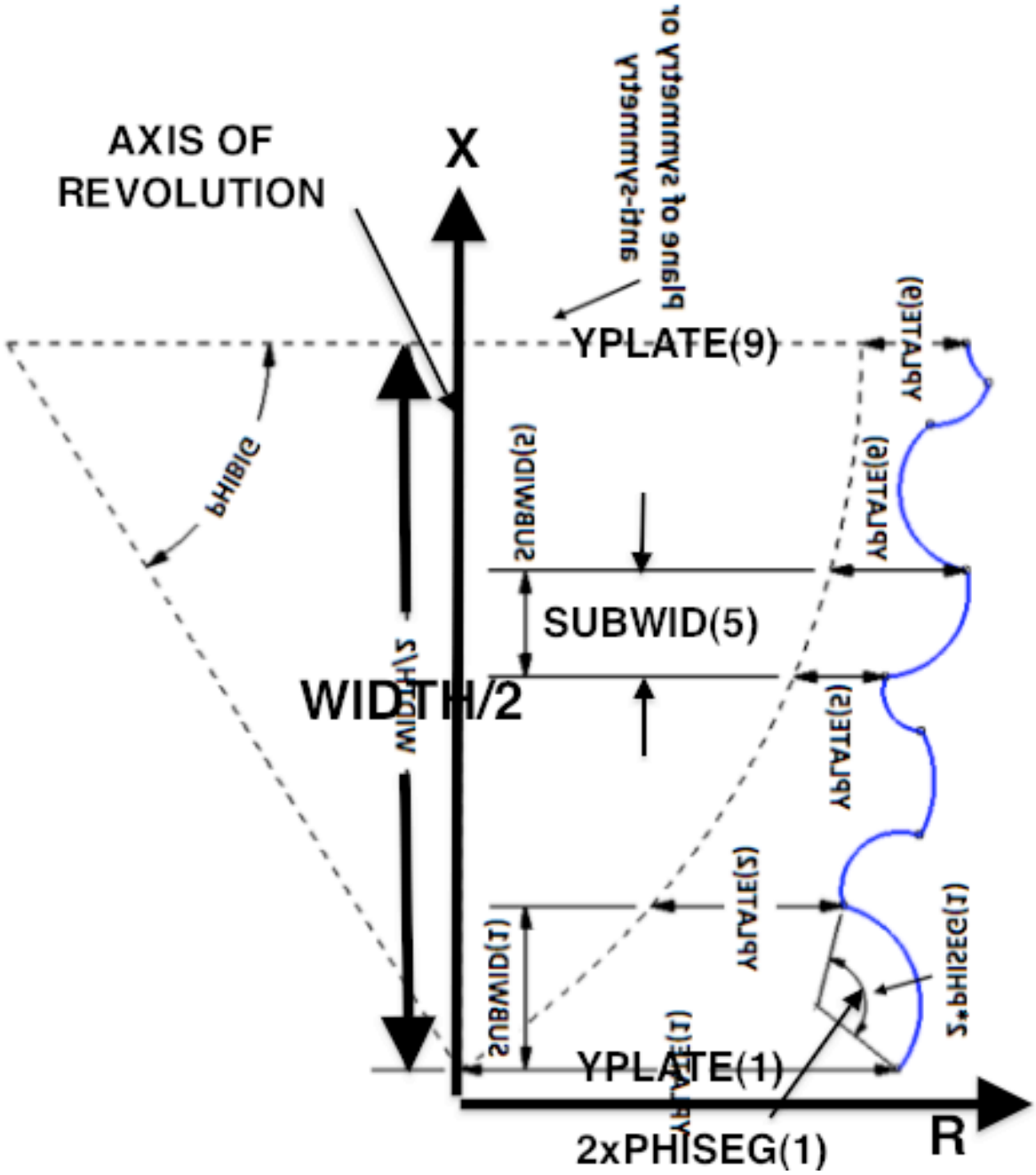

Fig. A2b The geometry displayed in the previous figure is rotated clockwise by 90 degrees, then flipped over vertically in order to transform the profile of the longitudinally complexly corrugated prismatic shell, which is the subject of [1], into the circumferentially complexly corrugated shell of revolution, which is the subject of this paper. In this paper the overall arching angle, called PHIBIG in the previous figure, is never chosen as a decision variable and is always set equal to a very small value: 0.01 degrees. Therefore, YPLATE(i), i=1, 2, … NSEG+1, are now the radii from the axis of revolution to the shell reference surface at the ends of the shell of revolution and at the junctions between major toroidal segments.

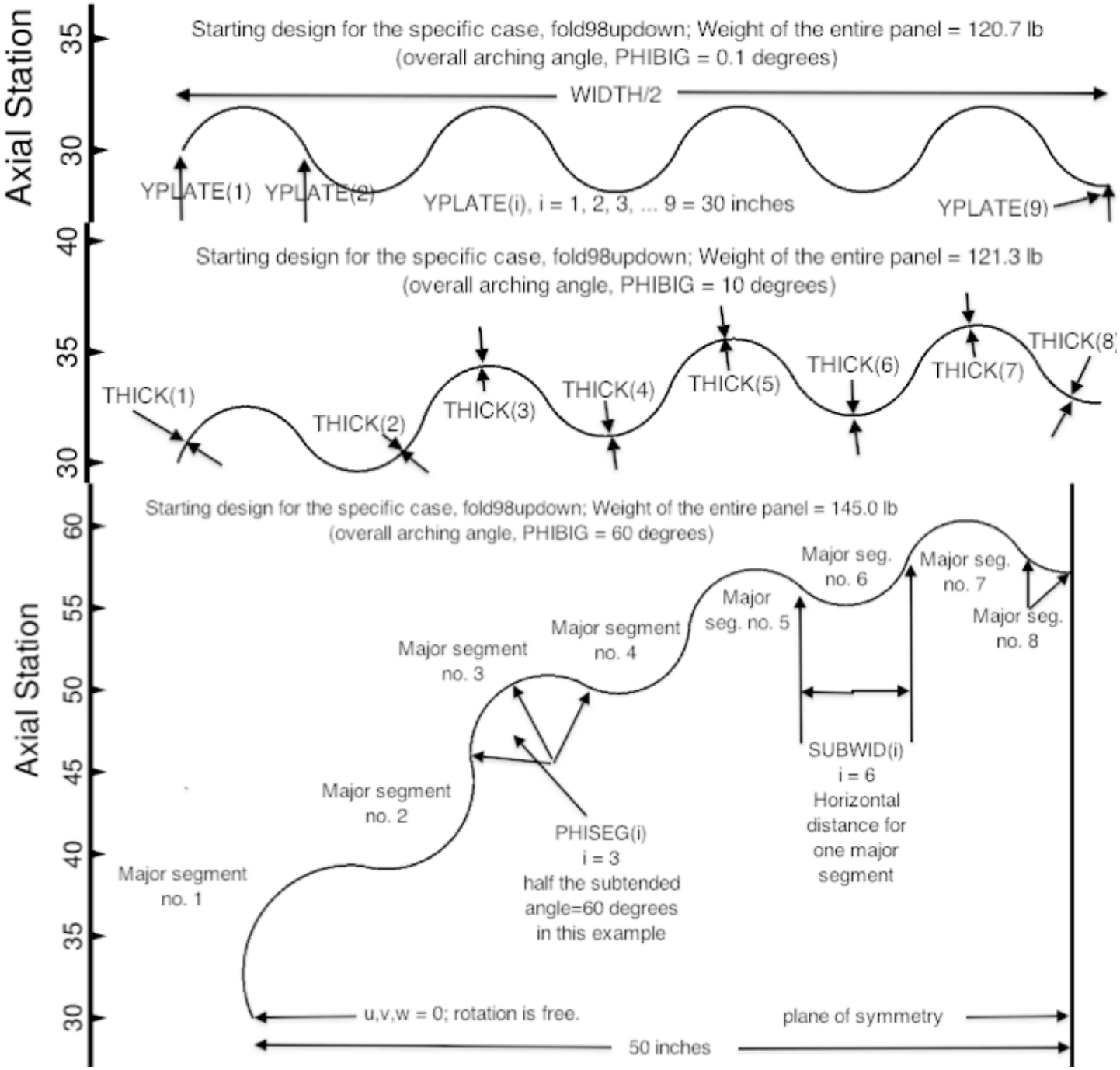

Fig. A3 This figure is taken from [1] where it is called Fig. 3. A longitudinally corrugated prismatic panel cross section is shown for three values of the overall arching variable called PHIBIG. In the present paper PHIBIG is always set to a very small number (0.01 degrees), and, with appropriate transformation of the model as described in the caption of the previous two figures, the decision variable candidates, YPLATE(i), i=1, 2, …, NSEG+1, become the radii from the axis of revolution to the shell reference surface at the junctions between major segments and at the two ends of the circumferentially complexly corrugated shell of revolution.

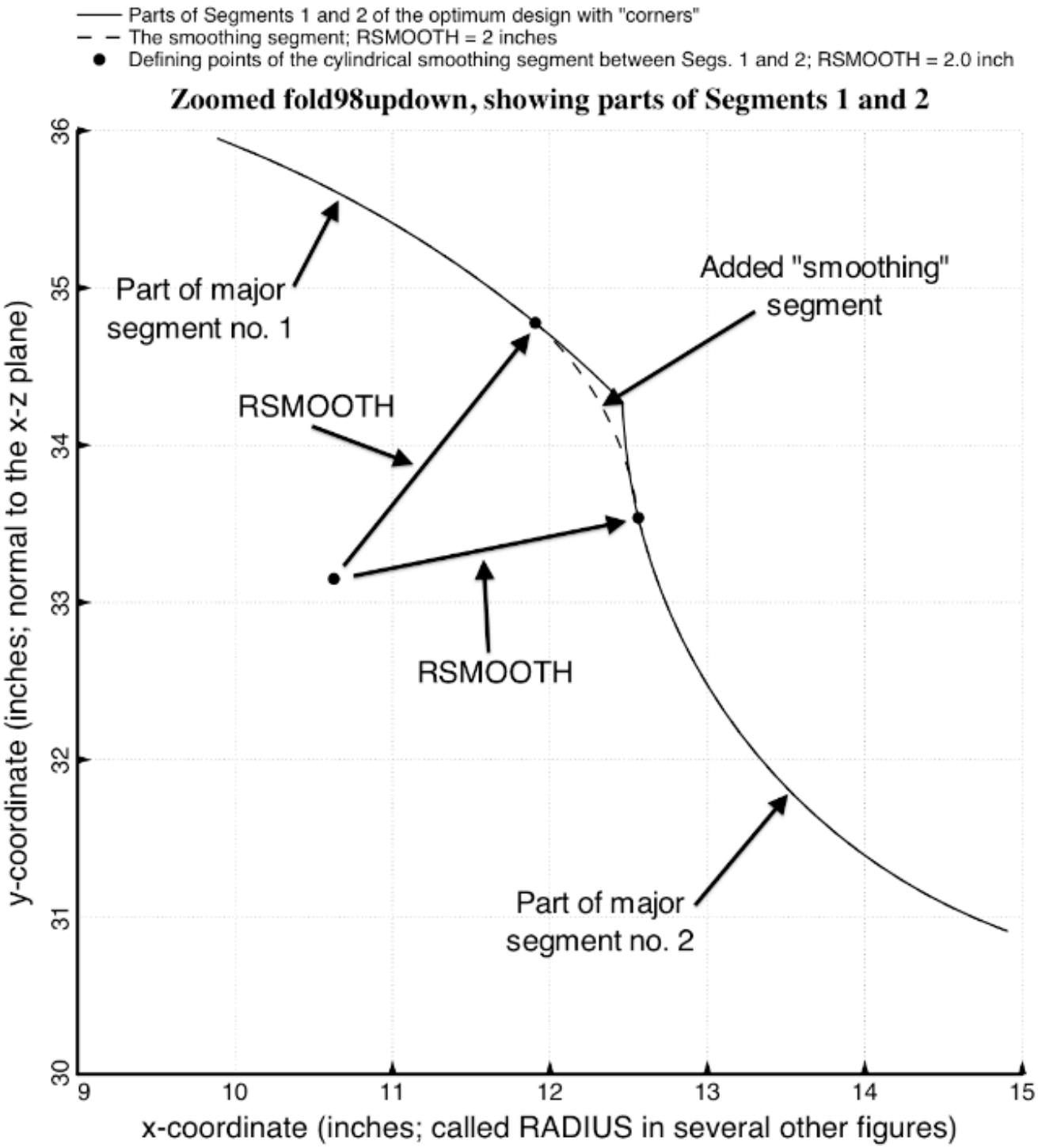

Fig. A4 This figure is taken from [1] where it is called Fig. 28. The meaning of a "smoothing" segment between two major segments is illustrated. "Smoothing" segments may also be added at the ends of the configuration in order to have the meridional slope be horizontal within 5 degrees (in this view) or vertical within 5 degrees (in the transformed shell-of-revolution model described in the captions of Figs. A2 and A2b).